A COMBINED FEEDBACK AND COMMAND SHAPING CONTROLLER FOR IMPROVING POSITIONING AND REDUCING CABLE SWAY IN CRANES

A Thesis
Presented to
The Academic Faculty

by

Khalid Lief Sorensen

In Partial Fulfillment
Of the Requirements for the Degree
Master of Science in Mechanical Engineering

School of Mechanical Engineering
Georgia Institute of Technology
February 2005

A COMBINED FEEDBACK AND COMMAND SHAPING CONTROLLER FOR IMPROVING POSITIONING AND REDUCING CABLE SWAY IN CRANES

Approved by:

Dr. William E. Singhose, Committee Chair
School of Mechanical Engineering
Georgia Institute of Technology

Dr. Stephen L. Dickerson, Committee Member
School of Mechanical Engineering
Georgia Institute of Technology

Aldo A. Ferri, Committee Member
School of Mechanical Engineering
Georgia Institute of Technology

Date Approved: February 22, 2005

ACKNOWLEDGEMENTS

I would like to thank my advisor, Dr. William Singhose, for his penetrating questions that drove this research toward the goal of further understanding. I am also extremely thankful for the generous support provided by Dr. Stephen Dickerson and CAMotion, Inc. that enabled the realization of the work presented in this thesis. I would also give my thanks to Dr. Aldo Ferri for the time and expertise that he provided throughout my time here.

I would also like to express a deep thanks to my parents, Lief and Silvia for their years of enduring love, encouragement, discipline, and support; and my wife, Tiffaney, for believing in me while also being the source of tremendous joy in my life.

Finally, I would like to thank my Lord and Savior Jesus Christ for His unending loving-kindness.

TABLE OF CONTENTS

LIST OF TABLES

LIST OF FIGURES

SUMMARY

Bridge and gantry cranes are crucially important elements in the industrial complex; they are used in many areas such as shipping, building construction, steel mills, and nuclear facilities, just to name a few.

These types of systems tend to be highly flexible in nature, generally responding to commanded motion with oscillations of the payload and hook. The response of these systems to external disturbances, such as wind, is also oscillatory in nature. Often, the oscillations of the hook and payload have undesirable consequences. For instance, precise manipulation of payloads is difficult when cable sway is present. Oscillation of the hook can also present a safety hazard. For these reasons, the ability to successfully negate these detrimental dynamics can result in improved positioning, quicker settling time, and improved safety.

This thesis addresses the dynamic properties of bridge and gantry cranes in an effort to develop a control scheme that enables strides to be made in the areas of positioning, efficiency, and safety.

The fundamental advancement arising from this thesis is the development of a control scheme that enables precise positioning of the payload while motion and disturbance-induced oscillations are eliminated. A command generation technique uniquely suited for reducing oscillation in low-frequency flexible systems is examined and utilized in the control. The control scheme is implemented on a 10-ton bridge crane for validation purposes.

CHAPTER 1

INTRODUCTION

Systems that exhibit flexible dynamics are widespread in every facet of industry. A particularly challenging class of systems is the low-frequency, crane-type systems that play a fundamental role in today's industrial and global society. Large cranes are the centerpieces of hundreds of shipping yards around the world that enable the throughput of vast quantities of imported and exported goods. The timeliness and effectiveness of this transportation venue are critical in some circumstances. During wartime, the effectiveness of the United States Military and its allies depends on supplies such as food, fuel, and ammunition reaching their destinations as needed. Cranes are also crucial in the construction industry where they are used not only for assembling components of immense structures, but more frequently for the movement of construction materials, such as concrete, rebar, and cement forms. At the Hanford Site in Washington State, part of the nuclear cleanup effort involves over 150 bridge and gantry cranes used to transport radiological packages. Cranes are also routinely employed in warehouses and steel mills. Clearly, it is difficult to overestimate the necessity and usefulness of cranes throughout the modern world.

Different crane applications present different challenges to crane operators. For example, an operator running a crane in the closed environment of a warehouse is likely to contend with payload oscillations caused by motion of the crane. These oscillations will make it difficult to manipulate the payload quickly and accurately. When the payload or surrounding obstacles are of a hazardous or fragile nature, the payload oscillations may present a significant safety risk as well. A different challenge is presented at the Hanford Site in Washington State where radiological packages are regularly stacked in tight matrix formations, requiring positioning accuracy greater than 3 cm. Because of the hazardous content of the payloads, operators often control the cranes remotely, making precise positioning difficult and time consuming. A similar problem is presented to operators moving cargo containers at shipping yards; operators must deal with motion-induced oscillations while accurately positioning payloads from distant or obstructed

vantage points. In addition, operators must also contend with external disturbances, such as wind.

The difficulties faced by crane operators can be grouped into three categories. These are 1) system oscillations induced by the motion of the crane, 2) system oscillations induced by external disturbances, and 3) accurate payload positioning. These aspects of crane systems are important because if they are managed properly, the ease-of-use, efficiency, and safety of crane systems can be significantly improved.

This thesis addresses motion and disturbance-induced payload oscillations, as well as payload positioning, in an effort to develop a single control scheme that manages these three areas of crane performance. To this end, individual control modules are designed to control each of the three aspects of the crane system. Later, they are combined to obtain a single unified controller, suitable for improving all three aspects of crane performance. The controllers developed in this thesis are tested experimentally on a 10-ton bridge crane in the Manufacturing Research Center (MARC) at Georgia Tech.

1.1 BRIDGE AND GANTRY CRANE SYSTEMS

Bridge cranes are load-lifting systems consisting of three main components: a trolley, a bridge, and a runway. The trolley is the load-lifting component and moves on (and parallel to) a beam or other member called the bridge. The bridge moves on (and parallel to) a stationary runway. The runway is usually comprised of two supporting members, such as beams, that are permanently affixed to a structure such as the walls of a warehouse. The bridge and the runway are oriented orthogonally.

The combination of the degrees of freedom made available along the bridge and the runway, along with the hoisting capability of the trolley, provide a large three-dimensional workspace reachable by the payload. A representation of a typical bridge crane is shown in Figure 1.

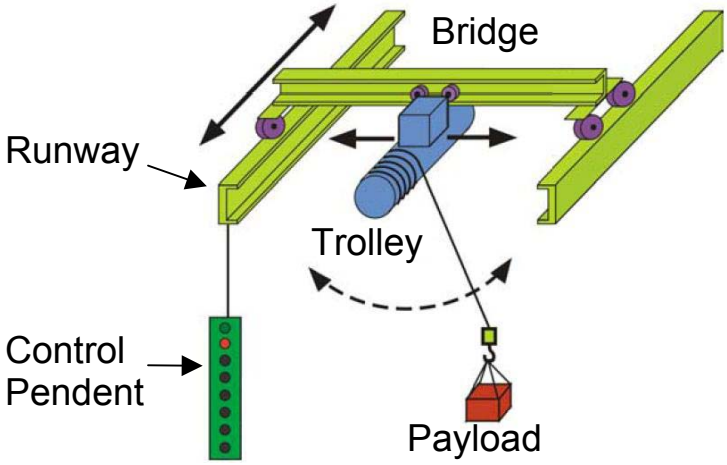

Figure 1: Illustration of a bridge crane.

Gantry cranes are also load-lifting systems consisting of three components: a trolley, a bridge, and a gantry. Like the trolley on a bridge crane, a gantry crane's trolley is the load-lifting component, moving on and parallel to the bridge. The bridge however, is affixed to a supporting structure called the gantry. The gantry extends downward from the bridge to the ground where it can be mobilized on wheels or a set of tracks. The motion of the gantry on the ground, the trolley on the bridge, and the hoisting of the payload provide the three degrees of freedom for the payload. A picture of a large gantry crane is shown in Figure 2.

Figure 2: Picture of a gantry crane at a shipping dock.

1.2 CRANE DYNAMICS

Developing controllers that improve crane performance begins with an understanding of the crane system dynamics. To this end, the dynamic equations of motion for the system are derived and a state space model developed.

Planer motion of the mechanical system can be modeled by a multi-body system consisting of two rigid bodies, as shown in Figure 3. The mass of the trolley and mass of the payload are labeled as m_t and m_p, respectively; acceleration due to gravity is represented as g; a viscous damping force, which acts on the payload, can be described by the damping coefficient b; and the length of the cable is labeled as L. For simplicity, the cable length is assumed to vary slowly with time, thus the time derivatives of this quantity are neglected. The trolley position, x, will be considered as the controlled variable. An obvious benefit to such a choice for the system input is that a model of crane motors and industrial drives is unnecessary at this juncture. Later these systems will be considered when determining appropriate reference signals for the crane. A similar formulation was used in [1].

With the crane modeled this way, the system then reduces to one degree of freedom with the cable angle, θ, used as the generalized coordinate.

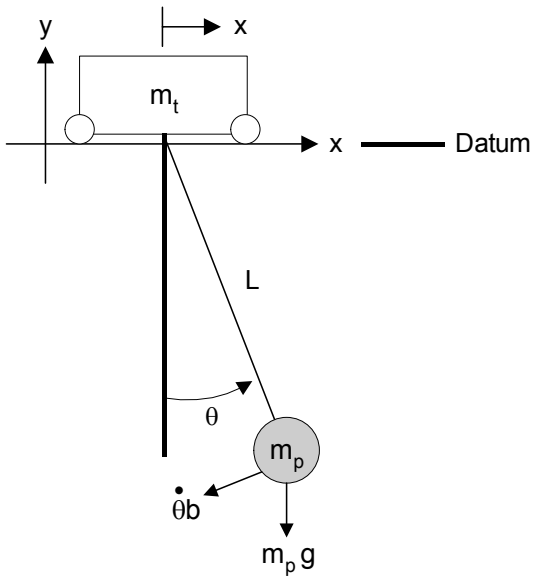

Figure 3: Multi-body model of the crane along one axis.

Using a Lagrange formulation to derive the system equations, we begin with the kinetic energy of the trolley and the payload:

$$T_t = \frac{1}{2} m_t \dot{x}^2 \text{, and } T_p = \frac{1}{2} m_t v_p{}^2 , \qquad (1) \text{ and } (2)$$

where $v_p{}^2$ is the squared velocity of the payload. $v_p{}^2$ may be computed from the position vector, $\boldsymbol{r}_p$, of the payload as follows:

$$v_p{}^2 = \dot{\boldsymbol{r}}_p \cdot \dot{\boldsymbol{r}}_p \text{, where } \dot{\boldsymbol{r}}_p = \frac{d\boldsymbol{r}_p}{dt} , \qquad (3) \text{ and } (4)$$

$$\boldsymbol{r}_p = \left(x + L\sin\theta\right)\hat{i} + \left(-L\cos\theta\right)\hat{j} . \qquad (5)$$

Substituting (3) through (5) into (2), and summing (2) with (1), we see that the total kinetic energy is:

$$T = \frac{1}{2} m_t \dot{x}^2 + \frac{1}{2} m_p \left[\left(\dot{x} + L\dot{\theta}\cos\theta\right)^2 + \left(L\dot{\theta}\sin\theta\right)^2\right]. \qquad (6)$$

With reference to the potential energy datum shown in Figure 3, we may write the potential energy, U, of the system as:

$$U = -m_p g L\cos\theta . \qquad (7)$$

The Lagrange equation for the generalized coordinate, θ, is:

$$\frac{d}{dt}\left(\frac{\partial T}{\partial \dot{\theta}}\right) - \frac{\partial T}{\partial \theta} + \frac{\partial U}{\partial \theta} = Q_\theta , \qquad (8)$$

where Q_θ is the generalized force acting on the system. The left hand elements of (8) are computed as:

$$\frac{d}{dt}\left(\frac{\partial T}{\partial \dot{\theta}}\right) = m_p\left(-L\dot{x}\dot{\theta}\sin\theta + L^2\ddot{\theta} + L\ddot{x}\cos\theta\right), \tag{9}$$

$$\frac{\partial T}{\partial \theta} = m_p\left(-L\dot{x}\dot{\theta}\sin\theta\right), \tag{10}$$

$$\frac{\partial U}{\partial \theta} = m_p gL\sin\theta\,. \tag{11}$$

The right hand element of (8) comes from a virtual work formulation of the non-conservative forces acting on the system.

$$\delta W = \boldsymbol{F}\cdot\delta\boldsymbol{r}_p = \left(Q_\theta\right)\delta\theta\,, \tag{12}$$

where $\boldsymbol{F}$ is the non-conservative force vector:

$$\boldsymbol{F} = \left(-b\dot{\theta}\cos\theta\right)\hat{i} + \left(-b\dot{\theta}\sin\theta\right)\hat{j}\,. \tag{13}$$

Substituting (13) into (12) and using the expression for $\boldsymbol{r}_p$ in (5), we see that:

$$\delta W = \left(-bL\dot{\theta}\right)\delta\theta\,. \tag{14}$$

Therefore,

$$Q_\theta = -bL\dot{\theta}\,. \tag{15}$$

Substituting (9) through (11), and (15) into the Lagrange equation, (8), the differential equation of motion for the system is:

$$\ddot{\theta} + \left(\frac{b}{Lm_p}\right)\dot{\theta} + \left(\frac{g}{L}\right)\sin\theta = \left(\frac{-\cos\theta}{L}\right)\ddot{x}. \tag{16}$$

The limited cable sway of our system allows us to use a small angle approximation, reducing (16) to:

$$\ddot{\theta} + \left(\frac{b}{Lm_p}\right)\dot{\theta} + \left(\frac{g}{L}\right)\theta = \left(\frac{-1}{L}\right)\ddot{x}. \tag{17}$$

Recognizing that (17) represents a second order damped oscillatory system, we may write:

$$\left(\frac{b}{Lm_p}\right) = 2\zeta\omega_n,\ \left(\frac{g}{L}\right) = \omega_n{}^2, \text{ and } \left(\frac{-1}{L}\right) = -\frac{\omega_n{}^2}{g}. \qquad (18),\ (19), \text{ and } (20)$$

We wish to obtain a final system representation relating the trolley velocity to the angle of the cable. For this reason we substitute $\dot{v}_t$ for $\ddot{x}$. Assuming zero initial conditions, and using the relations in (18) through (20), we obtain the following transfer function relating the cable angle to the velocity of the trolley:

$$\frac{\Theta(s)}{V_t(s)} = \frac{\left(-\omega_n{}^2/g\right)s}{s^2 + 2\zeta\omega_n s + \omega_n{}^2}. \tag{21}$$

A control canonical state space representation of the system is obtained directly from the coefficients of transfer function. By letting q_1 and q_2 be the states of the system, we have:

$$\dot{\boldsymbol{q}} = \begin{bmatrix} 0 & 1 \\ -\omega_n{}^2 & -2\zeta\omega_n \end{bmatrix}\boldsymbol{q} + \begin{bmatrix} 0 \\ 1 \end{bmatrix} v_t(t), \tag{22}$$

and

$$\theta(t) = \begin{bmatrix} 0 & \dfrac{-\omega_n^{\,2}}{g} \end{bmatrix} \boldsymbol{q} \,. \tag{23}$$

It is of interest to note that by the relationship between q_2 and θ established in (23), one may recognize that the state q_2 is equal to $-\theta L$. That is, $-q_2$ represents the relative horizontal displacement between the trolley and the payload. The state variable, q_1, has less physical meaning; $-q_1$ is a quantity whose derivative yields the relative displacement between the trolley and the payload.

1.3 CURRENT WORK

Most bridge and gantry cranes exhibit extremely light damping and are thus very oscillatory in response to motion of the overhead support unit (e.g. the bridge and/or the trolley) and external disturbances acting on the payload. Because bridge and gantry cranes play such a vital role in the world today, control of these systems has been the focus of a significant research effort over the past decades.

Fang et. al. proposed to control final trolley position and motion-induced oscillation through a proportional-derivative (PD) type control in which the coupling between the cable angle and the motion of the trolley is artificially increased [2]. Piazzi proposed a dynamic-inversion-based control for reducing transient and residual oscillation of the payload [3]. Kim implemented a pole-placement strategy on a real container crane to control motion and disturbance-induced oscillation, as well as final positioning [4]. In [5] Moustafa developed nonlinear control laws for payload trajectory tracking based on a Lyapunov stability analysis. An interesting approach to crane control was investigated by O'Connor. His control strategy is based on mechanical wave concepts and involves a learning of the unknown dynamics through an initial trolley motion, however this method was not expanded to accommodate disturbance rejection [6]. Finally, Fliess used a generalized state variable model suggested in [7], and then proposed a linearizing feedback control law. The position of the trolley and length of the payload cable were the controlled variables, and their respective reference trajectories were limited to a class of

fourth-order polynomials to insure minimal payload sway [1]. Disturbance rejection was not considered.

The control schemes developed in the literature may be broadly grouped into three categories: time-optimal control, command shaping, and feedback control. A forth, less common control scheme involves rule based control; Control rules are developed by observations of expert crane operators and implemented with fuzzy logic.

Time-optimal control is a common open-loop approach for obtaining swing free motion. One of the drawbacks to many time-optimal control schemes is their inability to be implemented in real-time owing to the necessity of precomputation of system trajectories. There is no known implementation of a time-optimal control scheme used with a commercial crane [8].

Command shaping is an implementable reference signal modification technique [9]. It is often used in conjunction with feedback to accommodate final positioning and disturbance rejection.

Feedback control is at the core of most strategies implemented for control of positioning, disturbance rejection, and motion-induced oscillations. The challenge in highly automated commercial crane applications has been the accurate sensing of payload and target positions. Gustafsson discusses these difficulties in detail for fully automatic commercial cranes in use at the Pasir Panjang terminal in Singapore [8].

1.4 THESIS OUTLINE AND CONTRIBUTIONS

The purpose of this thesis is to contribute to the body of work in the field by developing an easily implementable controller that controls the three areas of crane performance discussed previously. Ease of implementation is achieved by making use of a command shaping technique that is uniquely suited for low frequency, flexible systems. The control also makes use of a minimum number of sensors.

The underlying strategy of the controller is to allocate each area of crane performance to a simple control module. In this way, each module is tasked only with controlling motion-induced oscillation, external disturbances, or final positioning. Then, the three modules are combined into one unified control system.

The performance of the developed control is evaluated experimentally by implementing the control on an actual 10-ton bridge crane. For validation purposes, only planer motion of the crane is experimentally tested.

1.4.1 Thesis Overview

Chapter 2 will introduce the hardware, software, sensors, and communication capabilities of the 10-ton bridge crane being used as an experimental test bed for the developed control schemes. Chapter 3 will detail the development of the three dedicated control modules for motion-induced oscillation suppression, final positioning, and disturbance rejection. Chapter 3 will also consider the benefits and limitations of each controller. Chapter 4 will sequentially combine the individual control modules developed in Chapter 3 to obtain a single, unified control scheme capable of improving the multiple areas of crane performance. The interaction between the developed control and a human crane operator will also be discussed. Stability issues will be considered throughout the work. Finally, Chapter 5 will summarize the work presented in this thesis and discuss future objectives.

1.4.2 Contributions

The primary contributions of this thesis are:

1. A controller is designed, tested, and implemented on a 10-ton bridge crane that successfully controls motion and disturbance induced oscillations of the payload, as well as obtains precise payload positioning. A key feature of the control is its ease of implementation and minimum use of sensors.
2. A machine vision system is used to sense payload position. The vision system provides the added advantage of capturing coordinate information about targets. When the targets are located on non-stationary objects, such as a vehicle or shipping vessel, the developed controller has the ability to track these targets, enabling the precise hoisting of objects from moving platforms.
3. The developed control is particularly suited for use in different operational circumstances. Manual, partially automated, and fully automated operational

modes for the control are discussed. These variations of controller usage have direct benefit in various industrial applications.

4. Methods are presented for determining the oscillation inducing effects of nonlinear elements on input shaped signals. The nonlinear elements considered are found in many industrial control systems.

CHAPTER 2

EXPERIMENTAL SETUP

A 10-ton bridge crane has been used as an experimental test bed for the controllers developed in this thesis. The bridge crane resides in the Hibay of the Manufacturing Research Center at Georgia Tech, and is shown in Figure 4. The bridge of the crane spans the 10-meter width of the Hibay and runs the entire 50-meter length. The bridge travels along the runway at a height of 6.1 meters.

Figure 4: Bridge crane in the Manufacturing Research Center.

Ease of controller implementation is a key objective of this work. Therefore, knowledge of the crane's hardware, programming capabilities, communication capabilities, and operation was necessary to develop control strategies that can easily be integrated into the

existing crane infrastructure. This section describes how the system hardware and software were integrated over a data network to allow controlled operation of the crane.

2.1 HARDWARE OVERVIEW

The crane uses two 460-volt AC induction motors on the bridge and one on the trolley. Two Siemens Vector Masterdrives control the bridge and trolley motors. The drives are programmed to track a velocity reference signal sent as an analog voltage from a Siemens CPU 314C-2DP programmable logic controller (PLC). Under manual operation, the PLC generates these reference signals when an operator depresses pendent buttons, forward (positive step input), reverse (negative step input), or no button-push (no input). Hoisting of the load is controlled by simple on/off relays triggered by the corresponding pendent buttons. These signals are not routed through the PLC.

Advanced control is implemented on the crane by the addition of a portable, windows based computer (PC), a Banner LT3 Long-Range sensor, and a Siemens 723-2 machine vision system. These components are illustrated in Figure 5. Actual crane hardware is shown in Figure 6 through Figure 7.

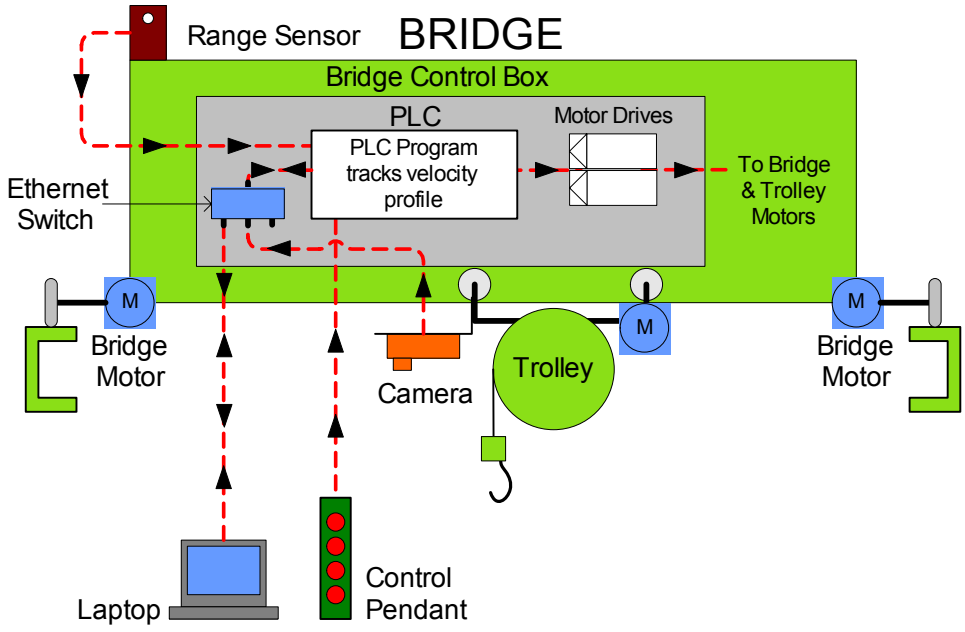

Figure 5: Crane hardware configuration.

The range sensor is located on the bridge of the crane and emits light pulses in the direction of bridge travel. A stationary retro reflecting surface reflects the emitted pulses back to the sensor where they are processed. The vision system is mounted in the center of the trolley, looking downward toward the payload, so that the payload and objects in and around a nine square meter area are captured in the camera's field of view.

The arrowheads in Figure 5 illustrate the direction of the data flow to and from the various components of the crane system. Depending on the implemented control strategy, data from the range sensor, vision system, or both are used by the PC as inputs to the control algorithm. The control algorithm produces a velocity reference signal that is routed to the PLC, and onto the motor drives.

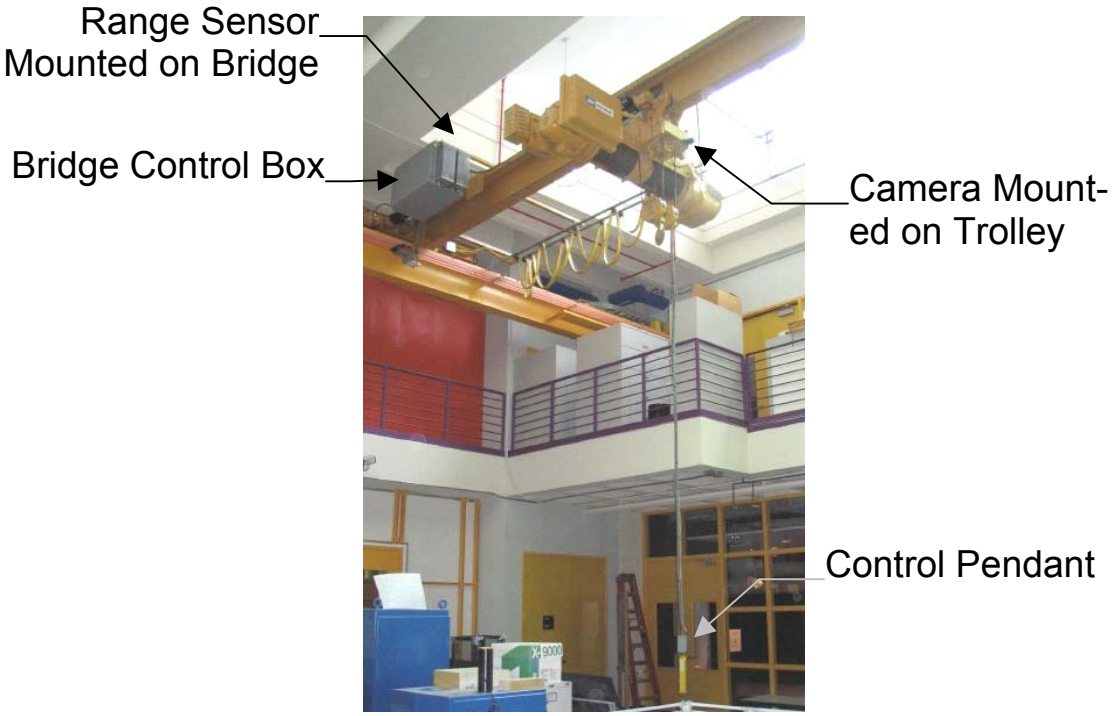

Figure 6: Bridge crane control components.

a) Machine vision camera.

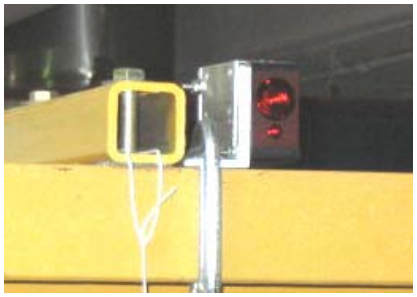

b) Laser range sensor.

Figure 7: Sensors used for the controller.

2.2 PROGRAMMING

Implementation of the various control modules developed in this thesis is accomplished through programming of the PC, PLC, and the vision system. The PLC program handles lower level functions such as error detection, timing of the data traffic across the communication network, and conversion of digital reference velocities from the PC to analog voltage signals suitable for the motor drives. The PC is programmed with the higher-level control schemes developed in this thesis. The main function of the PC is to receive sensor data, utilize the data in the control, and send a reference velocity to the PLC. A user-program within the vision system processes acquired images to obtain coordinate information about various objects.

2.2.1 PLC Programming

Programming of the PLC is accomplished using Simatic Step-7 statement list programming language. The PLC program utilizes a cyclical programming architecture illustrated in Figure 8. Cyclic architecture means that the operating system of the PLC runs in a program loop (the cycle) and calls the main programming block (OB1) once in every loop. The OB1 block is therefore executed cyclically. A timed interrupting block (OB35) may interrupt the cyclic operation of OB1 to execute code written within OB35. For instance, if a 20-millisecond (ms) timer is assigned as the interrupting period, then once each 20 ms, cyclic program processing of OB1 is interrupted and processing of OB35 begins. Once OB35 has been executed, the cyclic processing of OB1 is resumed at the point at which it was interrupted.

The main programming block, OB1, contains error checking code, such as detecting whether the bridge or trolley travel limit switches have been triggered, and insuring that the bridge and trolley motors are operating below their thermal limit. The timed interrupt block, OB35, is used to carry out time critical instructions: OB35 receives an analog signal from the range sensor, representing the position of the bridge; sends a digitized version of this signal to the PC; receives a reference velocity signal from the control pendent, the PC, or both; and forwards an analog voltage version of the reference velocity signal to the drives.

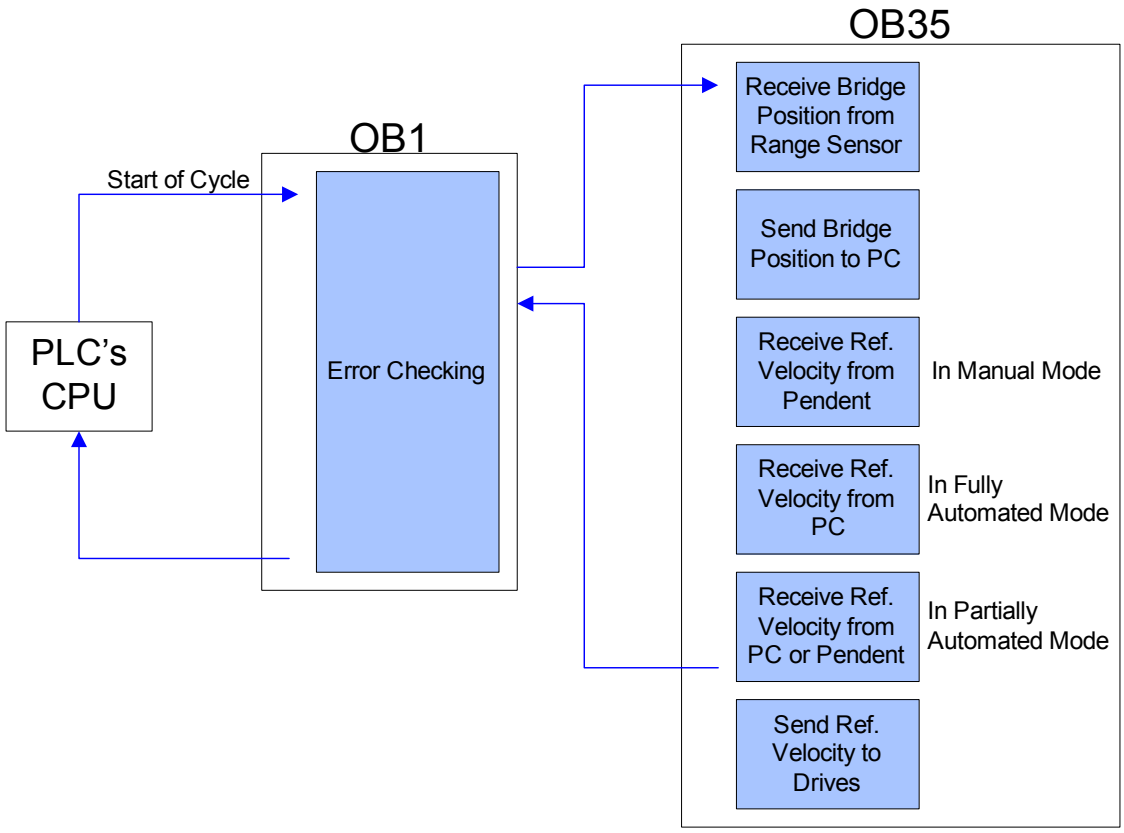

Figure 8: Cyclical architecture of the PLC control program.

The source of the reference velocity signal depends on the operating mode of the crane. The operational mode is selected by turning a mode selection knob located on the control pendent. Different sections of code contained within OB35 are executed depending on which operating mode is selected. This is also illustrated in Figure 8. There are three operational modes for the crane:

1) **Manual Mode**. Manual operation of the crane allows the user complete control over the motion of the bridge and trolley. Reference velocity signals are generated by the PLC that correspond to depressed buttons on the control pendent. These reference signals can be step inputs in velocity; however, if a command shaping algorithm is active, these signals will be modified, according to the command shaper implemented, prior to being forwarded to the motor drives.

2) **Fully Automated Mode**. In fully automated control mode, the motion of the bridge is controlled entirely by the controlling PC. The timed interrupt block, OB35, running on the PLC, receives reference velocity signals from the PC and forwards the analog version of these signals to the motor drives. The control will seek to drive the crane to a series of positions that correspond to an array of desired positions programmed into the PC. Once the crane has reached a desired position, it will remain stationary for a programmed period of time (perhaps to conduct hoisting operations) at which time the control will proceed to drive the crane to the next desired position.

3) **Partially Automated Mode**. Partially automated crane operation is essentially manual operation of the crane that has been enhanced with an automatic positioning feature. This mode allows the motion of the crane to be controlled by the operator's pendent button pushes while the operator is attempting to maneuver the crane towards some intended target point. Because of a distant or obstructed view, the operator may have difficulty in driving the crane precisely to the intended destination. Therefore, when the machine vision system has detected the target point within its field of view, the controlling PC will alert the operator that it is ready to assume control of the crane. The operator may either continue running the crane in manual mode or transfer operation to the PC, which will drive the crane to the intended destination.

   In this scenario, the programming block OB35 retrieves reference velocity signals from both the pendent, as well as the PC.

The circumstances under which the different operating modes are best suited, as well as how a human operator may interact with the control, are discussed in greater detail in Section 4.3.

2.2.2 PC Programming

For ease of implementation, a Windows based PC is used as the controlling node. Programming of the PC is accomplished with Microsoft Visual Basic. The software utilizes an event driven architecture. Event driven architecture means that certain blocks of code are executed when a certain event occurs. An event may constitute the initializing of the control code, receiving data from the vision system, or receiving data from the PLC. These three events trigger specific code in the program used for the control modules developed in this thesis. These events and the functions they trigger are illustrated in Figure 9.

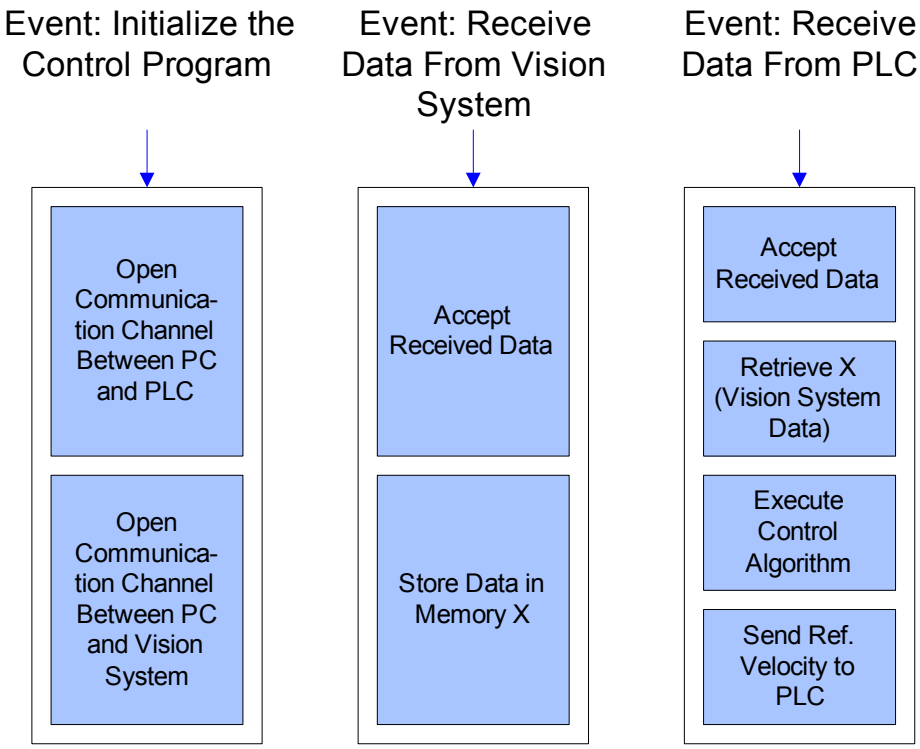

Figure 9: Event driven architecture of the PC control program.

The *Initialize the Control Program* event occurs only once when the control program is brought online. The purpose of the code processed when this event occurs is to establish a

communication channel between 1) the PC and the PLC, and 2) the PC and the vision system.

The *Receive Data From Vision System* event occurs repeatedly during operation. When this event is detected, the code within this event block instructs the PC to accept the data received from the vision system, and then to store the data in a memory location for use at a later time.

The *Receive Data From PLC* event also occurs repeatedly during operation of the control. When this event is detected, the code instructs the PC to accept the data received from the PLC; retrieve the vision system data previously stored by the other event block; use this data in the controlling algorithm to generate a reference velocity; and then immediately send this reference velocity to the PLC.

2.2.3 Vision System Programming

The Siemens 723-2 vision system is a stand-alone imaging sensor with on-board image acquisition, processing, digital I/O, and serial and Ethernet communications. The vision system is used to sense target and payload positions and relay this data to the PC. It accomplishes this by first acquiring a 1024 x 768 pixel image of the payload and surrounding area. Then, a user-program within the camera processes the image to obtain coordinate information about the payload and surrounding objects. Finally, the camera forwards this data to the PC over the established Ethernet connection.

The user-program operating within the vision system is created with a software tool provided by Siemens called Spectation. Ease of implementation of the overall control scheme is enhanced by the usability of the Spectation software to allow users to obtain various image data. Figure 10a depicts a sample image captured by the vision system, Figure 10b shows how this sample image was processed by the user-program to obtain the distance between two fiducial marks.

Image acquisition may be triggered internally on the camera at user defined periods or externally via a digital input signal to the camera. Depending on the amount of image processing required by the user-program, the minimum duration of one complete image processing cycle could range from 40 ms to over 200 ms.

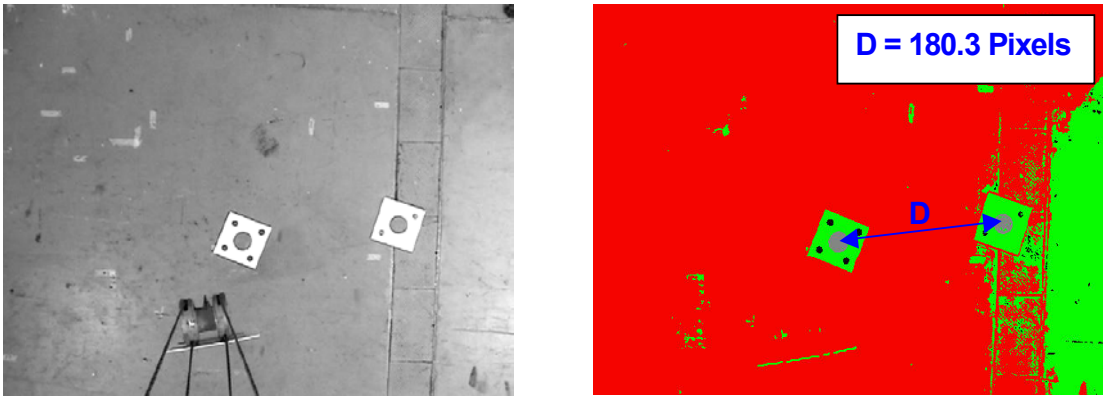

a) Sample vision system image. **b) Processed vision system image.**

Figure 10: Image captured with the machine vision system.

2.3 COMMUNICATION

Successful control of the crane is dependant on timely, predictable communication between the various components of the crane system. These components are the sensors that gather data needed for the control; the PC, which processes the sensor data to arrive at a desired reference velocity; and the PLC, which accepts data from the range sensor and PC, while sending data to the PC and motor drives. This data transfer network is illustrated in Figure 11.

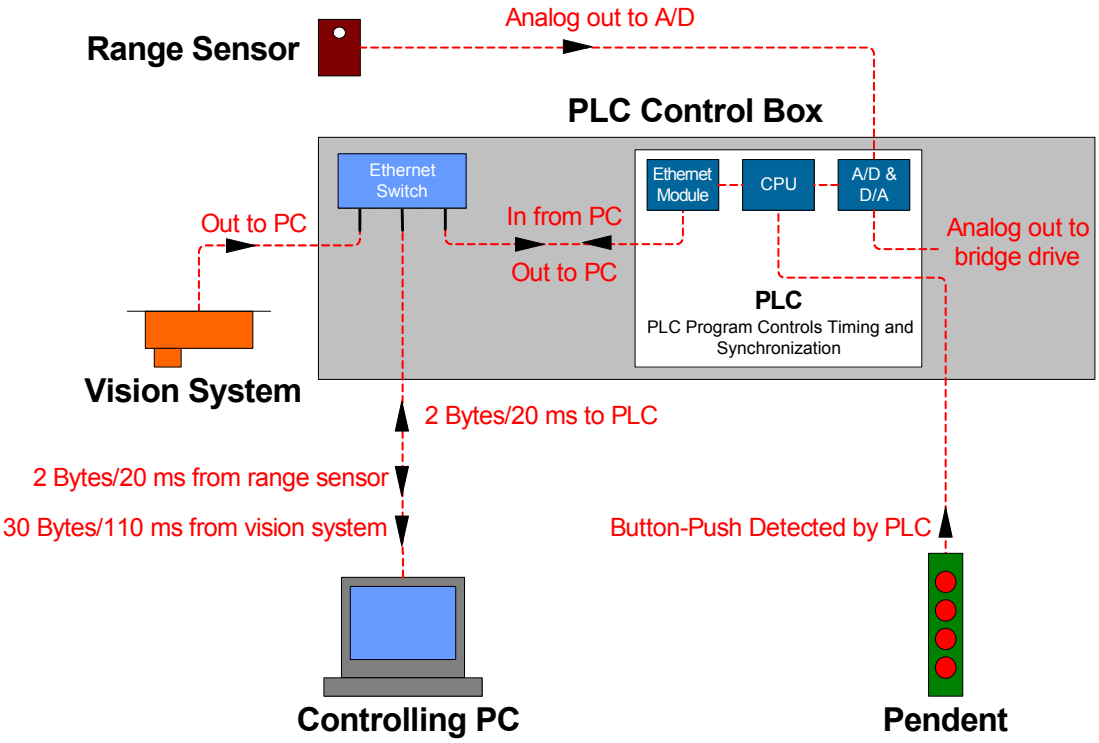

Figure 11: Crane system communication overview.

The PC, PLC, and vision system are connected via a dedicated industrial Ethernet switch to form a 3-node network. In this way, the PC, PLC, and vision system communicate directly with one another. The range sensor communicates with the PC by first sending an analog voltage signal to an analog-to-digital converter at the PLC. The PLC then forwards a digitized version of that signal to the PC over the Ethernet network.

The data packet exchange between the network nodes is facilitated with User Datagram Protocol (UDP). UDP offers a direct way to send and receive datagrams over an Ethernet network. The content and the timing of the datagrams being sent by the vision system, PLC, and PC are described below and also illustrated in Figure 11:

1) **Vision System**. Communication is established with the vision system by opening a standard windows socket to interface between the camera and the PC. A 30-byte data packet is sent to the PC after each image inspection; 12 bytes are used to describe x, y, and z coordinates of the crane hook, and another 8 bytes are used to describe the x and y coordinates of the target position. These positions are made relative to a stationary reference fiducial whose position is known. The time stamp of when the image was acquired is contained in 4 bytes. The remaining 6 bytes indicate the image number and reference fiducial identification number. The image acquisition and data transmittal cycle are triggered internally by the camera each 110 ms. The vision system receives no data.

2) **PLC**. Windows sockets on the PLC interface with the PC; they are created automatically in the PLC's Ethernet module. The PLC sends a 2-byte data packet to the PC each time the timed interrupt block, OB35, is processed in the PLC user-program (20 ms). These 2 bytes represent the position of the bridge as measured by the range sensor. Not only is this data packet used at the PC in the control algorithm, but it also serves as an external trigger for the PC to send reference velocity data to the PLC. In this way, data exchange between the two nodes is synchronized. The data sent to the PLC is accepted and used during processing of the OB35 block.

3) **PC**. Two windows sockets are created during the initialization of the control program. One socket interfaces with the vision system, the other with the PLC. Once every 20 ms, the PC receives a 2-byte data packet from the PLC. This data (along with the most recent data sent from the vision system) is processed internally in the control algorithm. A desired reference velocity, as determined by the control, is sent to the PLC by way of the corresponding socket.

CHAPTER 3

INDIVIDUAL CONTROL MODULES

A key objective of the work presented in this thesis is to develop a single control scheme that controls three aspects of crane performance, 1) motion-induced oscillation of the payload, 2) precision positioning of the payload, and 3) disturbance-induced oscillation of the payload. The underlying strategy of the controller is to address each area of crane performance with a simple control module, then, combine the control modules into a comprehensive control scheme. This chapter presents the development of each of the dedicated control modules.

3.1 MOTION-INDUCED OSCILLATION CONTROL MODULE

Consider again the transfer function of equation (21) for the crane system that relates the output angle, θ, to the velocity of the trolley, v_t:

$$\frac{\Theta(s)}{V_t(s)} = \frac{\left(-\omega_n^2 / g\right)s}{s^2 + 2\zeta\omega_n s + \omega_n^2}.$$

Recognizing that the velocity of the payload, v_p, is related to the velocity of the trolley by:

$$V_p(s) = s\frac{g}{\omega_n^2}\Theta(s) + V_t(s), \tag{24}$$

we may convert (21) to a transfer function that relates the output velocity of the payload, v_p, to the input velocity of the trolley, v_t:

$$\frac{V_p(s)}{V_t(s)} = \frac{2\zeta\omega_n s + \omega_n^2}{s^2 + 2\zeta\omega_n s + \omega_n^2}. \tag{25}$$

From (25) we may then obtain the velocity response of the payload to a step input in velocity. For a lightly damped system this response is shown in Figure 12. It should be

noted that the simulated step in velocity of the trolley cannot be achieved on a physical system, as it would require an infinite amount of acceleration. This issue will be discussed in section 3.1.3.1.

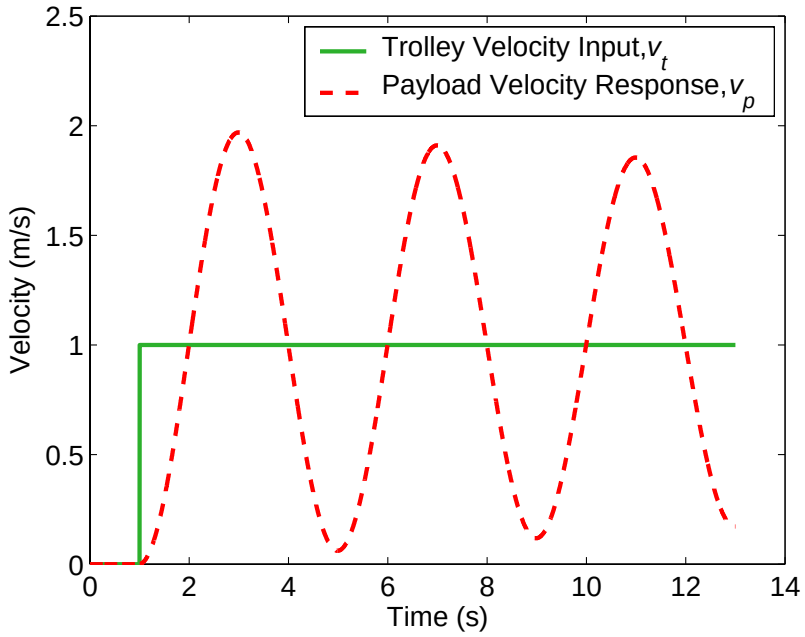

Figure 12: Lightly damped second-order response to a step input.

A variety of techniques have been developed for controlling the dynamic response of flexible systems, like the one shown above, including command shaping and closed-loop feedback control.

A feedback controller's inherent strength lays in the fact that it can detect errors and respond accordingly. Such a controller is well suited to precisely position the final location of a crane's bridge or trolley. If, however, the feedback controller must minimize cable sway, the control task becomes much more problematic. Accurate sensing of the payload must be implemented, which is often costly or difficult. When sensing of the payload is available, the feedback utilized to control the cable sway responds only if cable sway exists. In this way, the control is inherently *reactive*.

Another technique used for negating a system's flexible modes is command shaping. Command shaping does not require the feedback mechanisms of closed-loop controllers. Instead, the control scheme reduces oscillations in an *anticipatory* manner as opposed to the *reactive* manner of feedback. Vibration suppression is accomplished with a *reference*

signal that anticipates the error before it occurs, rather than with a *correcting* signal that attempts to restore the system back to a desired state. In the context of crane control, this means that sensing of the payload sway is not necessary. As a result, command shaping is easier to implement than feedback control. For these reasons, command shaping is a fundamental strategy employed in the development of a control module to reduce motion-induced oscillations.

3.1.1 Command Shaping for Oscillation Reduction

In general, command shaping is the process by which a reference command for a system is modified. The type of modification to the reference command depends on the desired effects the modification will have on the system's response. If the system exhibits flexible dynamics, then it is often desirable to modify the reference command so that the flexible modes will be minimally excited.

Conventional modifications used for this type of oscillation reduction involve signal filtering. This modification reduces the undesired dynamics by creating lowpass or notch filters so that undesired system modes are minimally excited. Typical frequency filters include the Hamming, Butterworth, Chebyshev, Parks-McClellan, and Elliptical filters.

Traditional filtering techniques have been only marginally effective at reducing residual oscillation in mechanical systems [10], in addition, traditional filtering has the drawback of greatly increasing a system's settling time [10], an undesirable consequence if the purpose of reducing the system oscillations is to make the system move faster.

3.1.2 Input Shaping

Another form of command shaping that is effective at improving the transient and steady state response of mechanical systems, while minimally increasing settling time, is input shaping. In broad terms, input shaping involves modifying a reference command in such a way that resonant modes of a system combine destructively, resulting in low residual oscillation. To demonstrate destructive interference, consider the system response of a lightly damped second-order system, such as the crane, to a series of two impulses, as shown in Figure 13. Figure 13a shows the system response to the impulses if they were each applied alone. Figure 13b shows the combined system response. These figures

demonstrate that when an impulse of appropriate magnitude is applied half-a-period after the first impulse, the responses of the system combine destructively, resulting in zero oscillation.

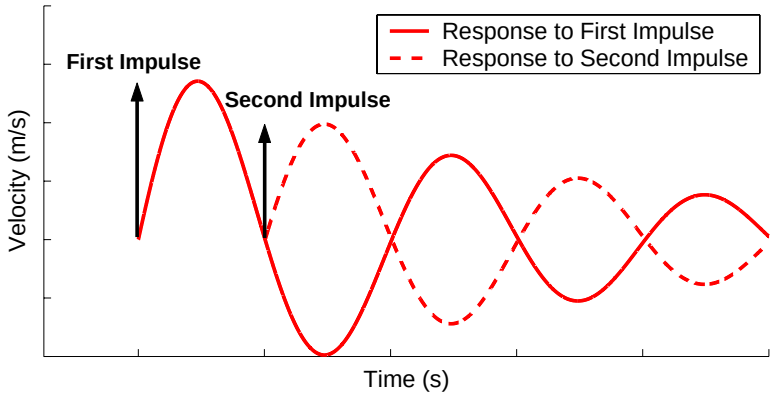

a) System response to each impulse.

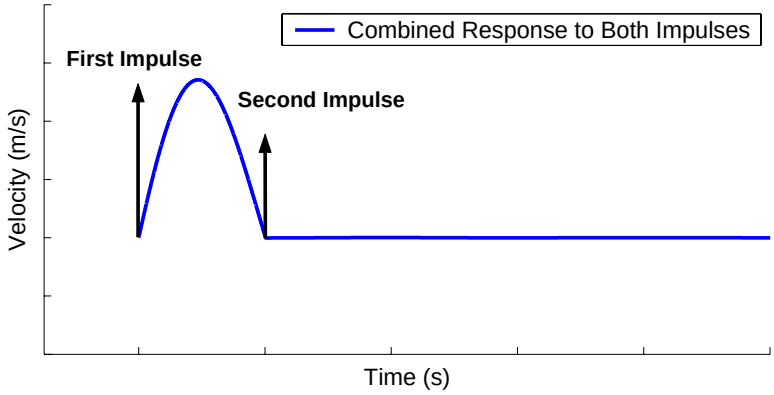

b) System response to both impulses.

Figure 13: Destructive interference of system oscillations caused by a sequence of impulses.

The input shaping process is an extension of the concept illustrated in Figure 13 that allows any arbitrary reference command to result in zero residual oscillation rather than just a sequence of impulses. This extension is made by convolving the sequence of impulses, known as an input shaper, with an arbitrary reference signal to produce a shaped command that is then used to drive a system. This process is illustrated in Figure 14.

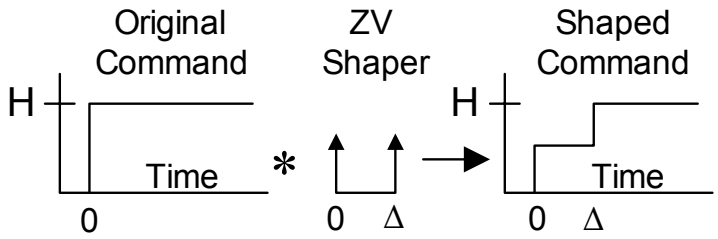

Figure 14: The input shaping process.

Once the sequence of impulses is convolved with the original command, the shaped command has the same oscillation reducing properties as the original set of impulses. This concept is illustrated in Figure 15 where the two-impulse sequence of Figure 13 has been convolved with a step input. The result is a staircase command that also eliminates residual oscillation. The response of this system to the shaped command contrasts sharply with the response to the unshaped command that was shown in Figure 12.

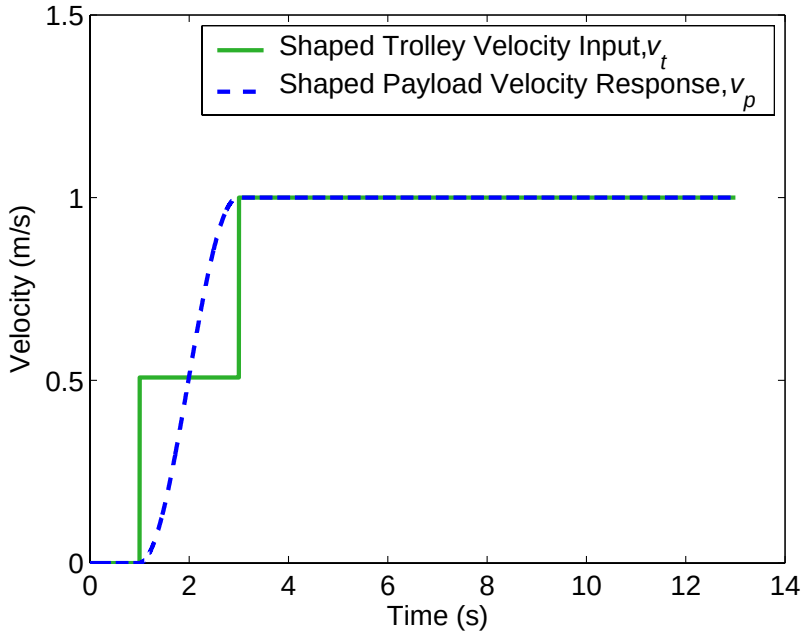

Figure 15: Lightly damped second-order response to a shaped step input.

The amplitudes and time locations of the impulses that will limit the unwanted dynamic response are determined by solving a set of constraint equations. The constraint equations are usually categorized as residual oscillation constraints, robustness constraints, impulse constraints, and time optimality.

3.1.2.1 Input Shaper Constraint Equations

To constrain the residual oscillation, we need an expression for the residual oscillation amplitude as a function of the impulse sequence[1]. If we assume the system can be modeled as a second-order harmonic oscillator, or a superposition of second-order systems, then we start with the response from a single impulse:

$$y_0(t) = \left[\frac{A_0 \omega}{\sqrt{1-\zeta^2}} e^{-\zeta\omega(t-t_0)} \right] \sin\left(\omega\sqrt{1-\zeta^2}\,(t-t_0)\right), \tag{26}$$

where A_0 is the amplitude of the impulse, t_0 is the time the impulse is applied, ω is the natural frequency, and ζ is the damping ratio. The response from a sequence of impulses is just a superposition of the responses given in (26). Using the simplification:

$$\omega_d = \omega\sqrt{1-\zeta^2}\,, \tag{27}$$

the response to a sequence of impulses after the time of the last impulse is:

$$y_\Sigma(t) = \sum_{i=1}^{n} \left[\frac{A_i \omega}{\sqrt{1-\zeta^2}} e^{-\zeta\omega(t-t_i)} \right] \sin\left(\omega_d (t-t_i)\right), \tag{28}$$

where A_i and t_i indicate the amplitude and time of the i^{th} impulse and n is the total number of impulses. Given (28), an expression for the *amplitude* of oscillation can be formed by using the trigonometric identity:

$$\sum_{i=1}^{n} B_i \sin\left(\omega t + \phi_i\right) = A_\Sigma \sin(\omega t + \psi)\,, \tag{29}$$

where,

---

[1] The following development parallels that given in [11].

$$A_{\Sigma} = \sqrt{\left(\sum_{i=1}^{n} B_i \cos(\phi_i)\right)^2 + \left(\sum_{i=1}^{n} B_i \sin(\phi_i)\right)^2} \quad . \tag{30}$$

The expression for the phase shift, ψ, is unimportant for our purposes here and ϕ_i is the argument of the sine term in (28). From the expression in (28):

$$B_i = \frac{A_i \omega}{\sqrt{1-\zeta^2}} e^{-\zeta\omega(t-t_i)}. \tag{31}$$

To obtain the residual oscillation amplitude, we evaluate (30) at the time of the last impulse, $t = t_n$. Substituting (31) into (30) and bringing the constant portion of the coefficients out of the square root term yields:

$$A_{\Sigma} = \frac{\omega}{\sqrt{1-\zeta^2}} e^{-\zeta\omega t_n} \sqrt{[C(\omega,\zeta)]^2 + [S(\omega,\zeta)]^2}, \tag{32}$$

where,

$$C(\omega,\zeta) = \sum_{i=1}^{n} A_i e^{\zeta\omega t_i} \cos(\omega_d t_i), \tag{33}$$

and

$$S(\omega,\zeta) = \sum_{i=1}^{n} A_i e^{\zeta\omega t_i} \sin(\omega_d t_i). \tag{34}$$

To express the amplitude of residual oscillation in a non-dimensional manner, we can divide (32) by the amplitude of residual oscillation from a single impulse of unity magnitude, A_1, to get the percentage oscillation equation:

$$V(\omega,\zeta) = \frac{A_{\Sigma}}{A_{\uparrow}} = e^{-\zeta\omega t_n}\sqrt{[C(\omega,\zeta)]^2 + [S(\omega,\zeta)]^2}\,. \tag{35}$$

If $V(\omega,\zeta)$ is set equal to zero at the modeling parameters, (ω_m, ζ_m), and a requirement is enforced that the magnitude of the impulses must be positive, then the shaper that satisfies the equation is called the Zero Vibration (ZV) shaper [9]. If a different constraint that the magnitude of the shaper's impulses, A_i, must equal 1 or -1 is considered in the formulation, then the resulting shaper that satisfies the constraint equations is called a Unity Magnitude, Zero Vibration (UM-ZV) shaper [12]. Because of the restriction on the amplitudes of the impulses, this shaper may be used on systems with simple on-off actuators, such as thruster jets on satellite systems, and the on-off relay-type actuators of many cranes not fitted with variable velocity compatible hardware. These two input shapers will be used throughout this thesis. For a lightly damped system, the shapers and their respective convolutions with step inputs are shown in Figure 16a and Figure 16b.

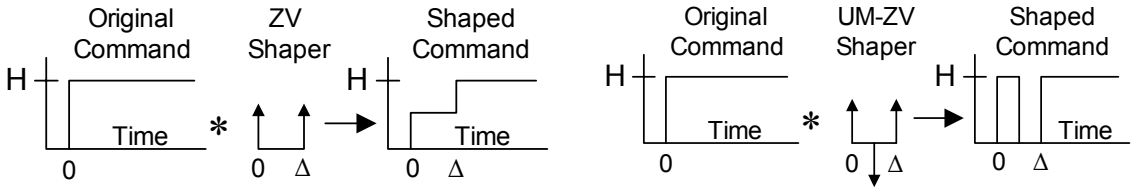

a) Convolution with ZV shaper. **b) Convolution with UM-ZV shaper.**

Figure 16: Step inputs convolved with two different zero-oscillation shapers.

It is important to note from Figure 16 that after the convolution with the input shaper, the rise time of the original command is increased by time Δ, the duration of the shaper. For this reason it is often desirable to design shapers with minimal duration.

3.1.3 Control Module Design

Utilizing the formulation from the proceeding section, a control module to cancel the motion-induced oscillation of the payload was designed that utilizes an input shaper. To design the input shapers used in the control, the system's damped natural frequency and damping ratio are needed.

At a nominal hook height approximately 2.3 meters above the ground the damped natural frequency of oscillation for the MARC crane was measured to be 1.62 radians/second. These oscillations were recorded on a video; the motion of the hook in Cartesian space was later extracted from the video to provide a graph of the hook motion. Once the oscillation amplitudes were measured from the graph, a logarithmic decrement calculation estimated the damping ratio for the crane, $\zeta = 0.012$. This is consistent with previously tested bridge cranes [13].

Singer and Seering solved equations (33) and (34) from section 3.1.2.1 for the amplitudes of a two-impulse ZV shaper in terms of the damping ratio and the damped natural frequency [9]. Singhose et al. numerically solved for the time locations of the three-impulse UM-ZV shaper, also in terms of the damping ratio and damped natural frequency [14]. These results are summarized in Table 1.

Table 1: Impulse magnitudes and time locations for the ZV and UM-ZV shapers as a function of ζ and ω_d.

SHAPER	A_i	t_i	M_0	M_1	M_2	M_3
UM-ZV	+1	t_1	0	0	0	0
	-1	t_2	0.16724	0.27242	0.20345	0
	+1	t_3	0.33323	0.00533	0.17914	0.20125
	$t_i = (M_0 + M_1\zeta + M_2\zeta^2 + M_3\zeta^3)T, \quad T = 2\pi/\omega_d$					
ZV	A_i		t_i			
	$\frac{1}{1+K}$		0			
	$\frac{K}{1+K}$		T/2			
	$K = \exp\left(-\frac{\zeta\pi}{\sqrt{1-\zeta^2}}\right), \quad T = 2\pi/\omega_d$					

As previously mentioned, the UM-ZV shaper may be used with systems utilizing simple on-off, relay-type actuators, because the impulse amplitudes of this shaper are 1 or –1.

Another advantage of this shaper can be seen from Table 1; its duration is approximately 33% less than that of the ZV shaper. This may provide a benefit in time critical applications.

Using the results of Table 1, the magnitudes and time locations of a ZV and UM-ZV shaper were calculated to cancel the oscillation at the nominal hook height. These shapers are shown in Table 2.

Table 2: Impulse magnitudes and time locations for the ZV and UM-ZV shapers for the crane system at the nominal cable length.

SHAPER	A_i	t_i (s)
UM-ZV	+1	0
	-1	0.661
	+1	1.293
ZV	A_i	t_i (s)
	0.509	0
	0.491	1.939

These input shapers are implemented in the control module by convolving them with a reference signal, V_r, and passing the shaped reference signal, V_s, onto the system for which the shapers were designed. A block diagram of this process is shown in Figure 17.

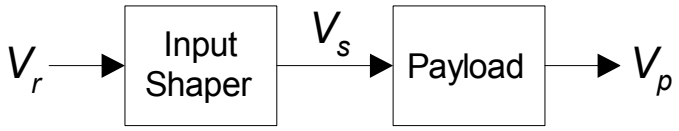

Figure 17: Block diagram of input shaping control.

The plant is comprised of the transfer function from equation (25) and the experimentally determined damping ratio and damped natural frequency. The input shaper block may be comprised of any of the shapers designed above. A simulation of the plant response to a ZV shaped step input, and a UM-ZV shaped step input are shown in Figure 18b and Figure 18c. For comparison, the unshaped response is shown in Figure 18a.

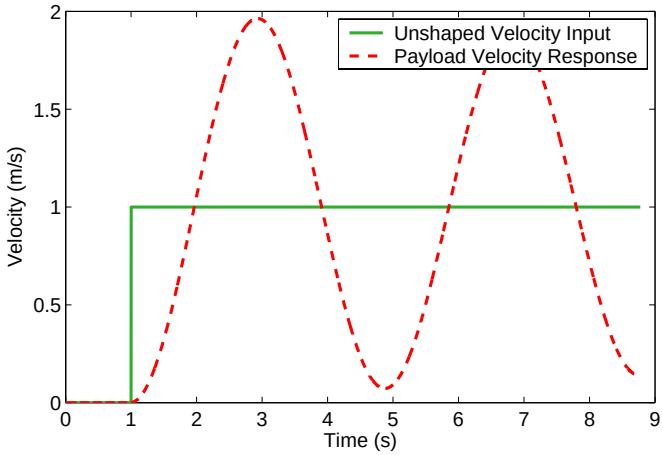

a) Unshaped response.

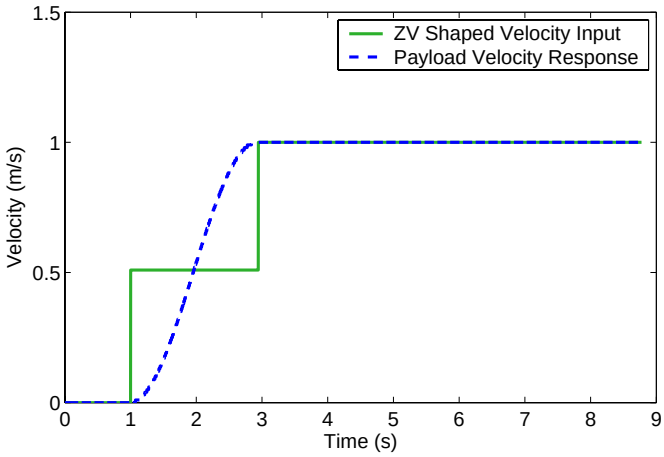

b) ZV shaped response.

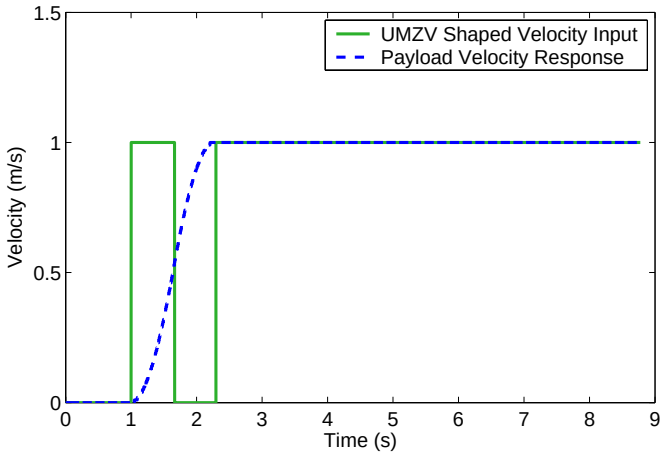

c) UM-ZV shaped response.

Figure 18: Simulated system response to a step command and shaped step commands.

3.1.3.1 Incorporation of the Drive & Motors into System

Inherent to the control scheme shown in Figure 17 and simulated in Figure 18 is the assumption that the overhead support unit (e.g. the bridge or the trolley) is precisely following the shaped velocity commands. If this were the case, the drive and motors would have to be capable of providing infinite acceleration to the support unit, which of course is not possible. Instead, the velocity response of the drive and motors to the shaped velocity commands must be considered, as this response is what is passed on to the payload. In light of this, we may construct the revised block diagram of the control scheme, shown in Figure 19.

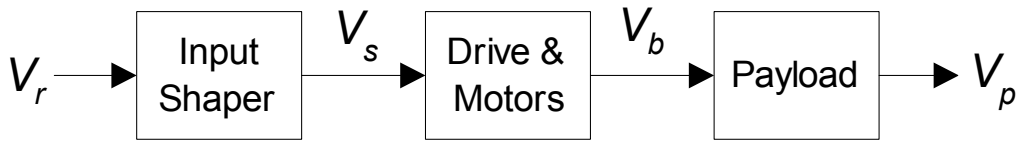

Figure 19: Block diagram of input shaping control with drive and motors.

To obtain an accurate model of the drive and motors, the response of these components to several baseline commands was recorded and analyzed. Specifically, the baseline commands were 1) a step input corresponding to 100% of maximum velocity, 2) a step input corresponding to 50% of maximum velocity, and 3) a step in velocity from 100% to –100% of maximum velocity. These commands, along with the crane's velocity responses are shown in Figure 20a through Figure 20c.

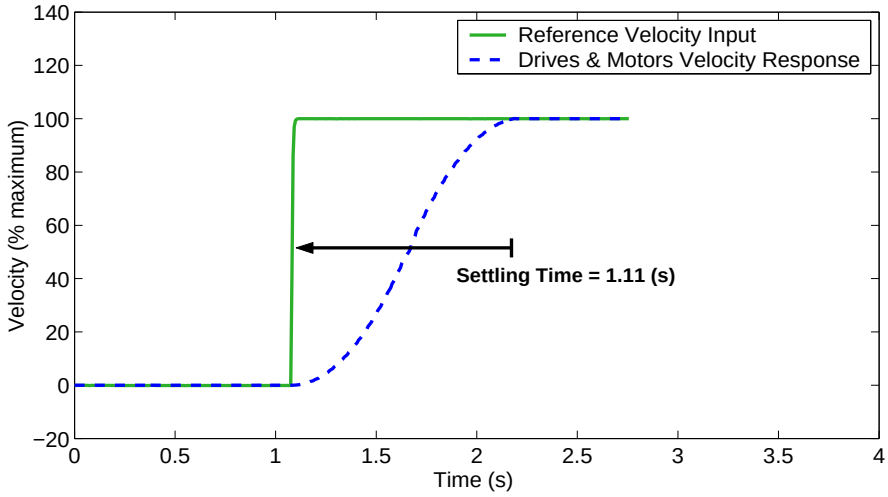

a) Response to a step input of 100%.

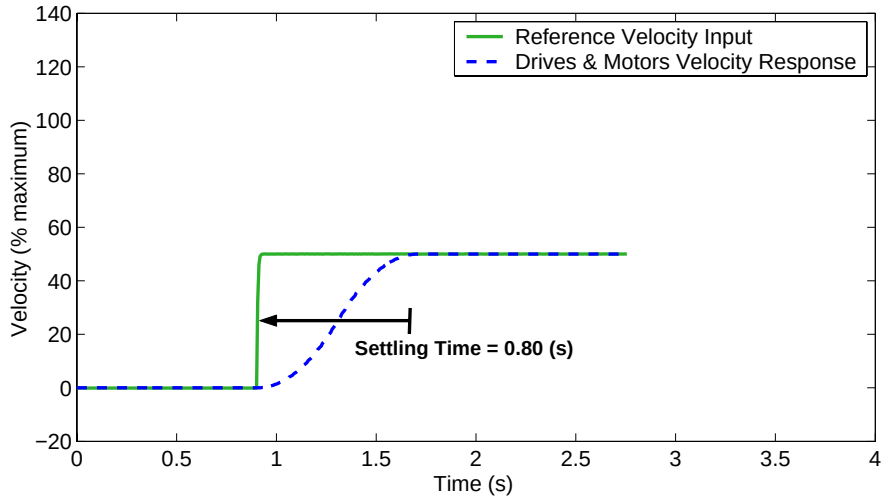

b) Response to a step input of 50%.

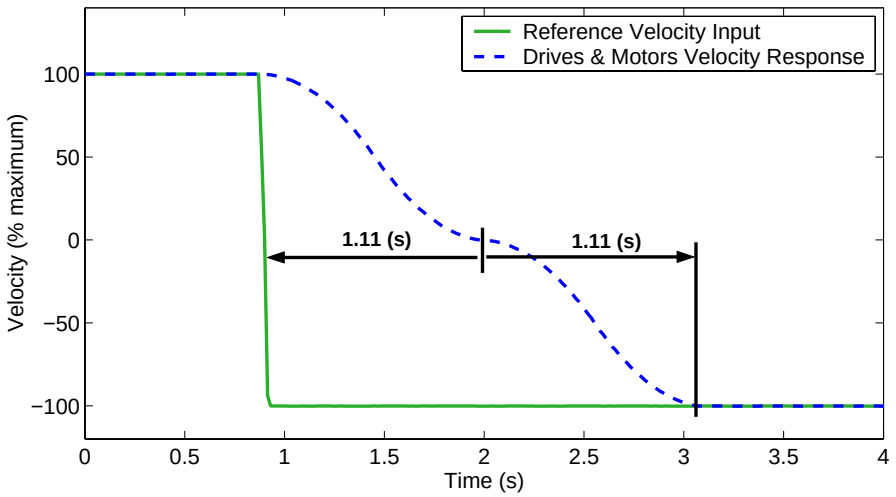

c) Response to a step from 100% to –100%.

Figure 20: Experimental drive and motor response to step inputs.

In all three plots one will notice the zero slopes at the beginning and end of each response and minimal overshoot of the target velocity. These characteristics suggest that the drive and motors have a response similar to a second-order heavily damped system. However, the discrepancy in the settling times between Figure 20a and Figure 20b suggest that the system is also acceleration limited. Finally, Figure 20c shows that when the bridge is commanded to transition from a positive velocity (forward) to a negative velocity (reverse) the system responds in a way that appears to be a combination of two separate responses: 1) the response to a step from 100% to 0%, followed by 2) the response to a step from 0% to –100%. In response to the first issued command, the crane would follow a velocity profile like that shown in the first part of Figure 20c. If the second step command from 0% to –100% is issued after the crane reaches zero velocity, the crane would follow a velocity profile like that shown in the second part of Figure 20c.

As a first step to developing a model of the drives and motors, a simple two-component block diagram was developed that provides simulated data similar to the experimental results. This model is shown in Figure 21.

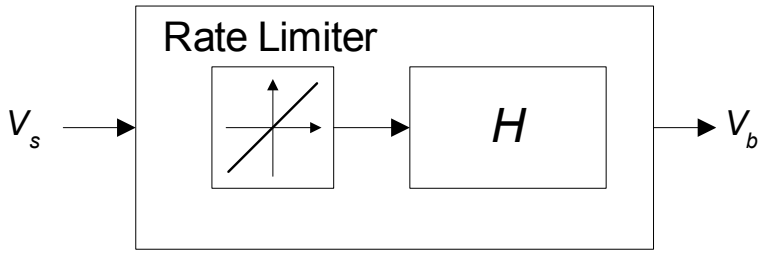

Figure 21: Model of the bridge drive and motors.

The rate limiter in the model limits the slew rate of the signal entering the block. *H* is a second-order heavily damped plant, having complex poles in the imaginary plane. A curve fit was performed in Matlab to obtain the damping ratio and damped natural frequency for the second-order plant, and the slew rate parameter for the rate limiter; these values are 0.86, $6.98\frac{rad}{s}$, and $\frac{160\%}{s}$, respectively. The model provides a reasonable approximation to the actual response of the drive and motors when the commanded velocity profile does not transition from a positive velocity to negative velocity, or vice-versa.

As discussed previously, the response of the drive and motors to a transitional input signal is composed of two responses: 1) the response of the system to the positive (or negative) portion of the input signal followed by 2) the response of the system to the negative (or positive) portion of the input signal. To incorporate this characteristic of the actual system into the model of the system, a third element may be added to block diagram of Figure 21. The revised block diagram is shown in Figure 22.

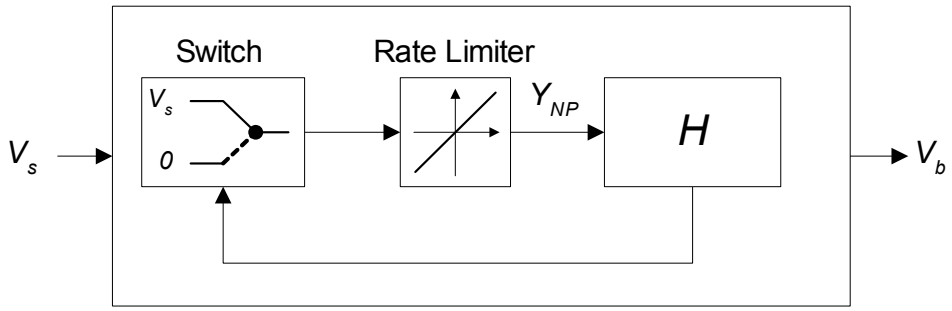

Figure 22: Revised model of the bridge drive and motors.

As illustrated in this figure, the switching element either passes the original reference signal, V_s, or a signal of *0* to the rate-limiting block. The output of the switch is dependant on the signals V_s and V_b according to the following formula:

$$SwitchOutput = \begin{cases} V_s, Sign(V_s) = Sign(V_b) \\ V_s, \quad |V_b| \le 0.9\% \\ 0, \quad Otherwise \end{cases} \tag{36}$$

The response of the revised model follows closely with the actual system response as seen in Figure 23a through Figure 23c. In these figures, the simulated response is overlaid with the actual system response.

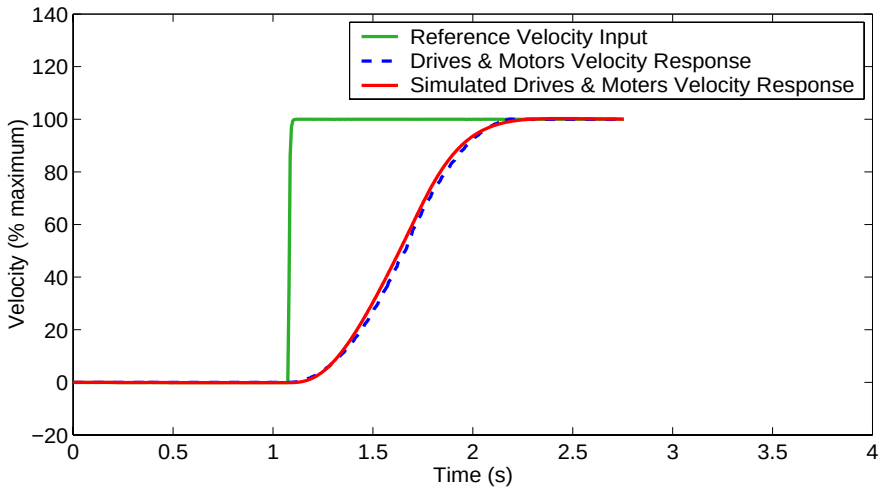

a) Actual and simulated response to a step input of 100%.

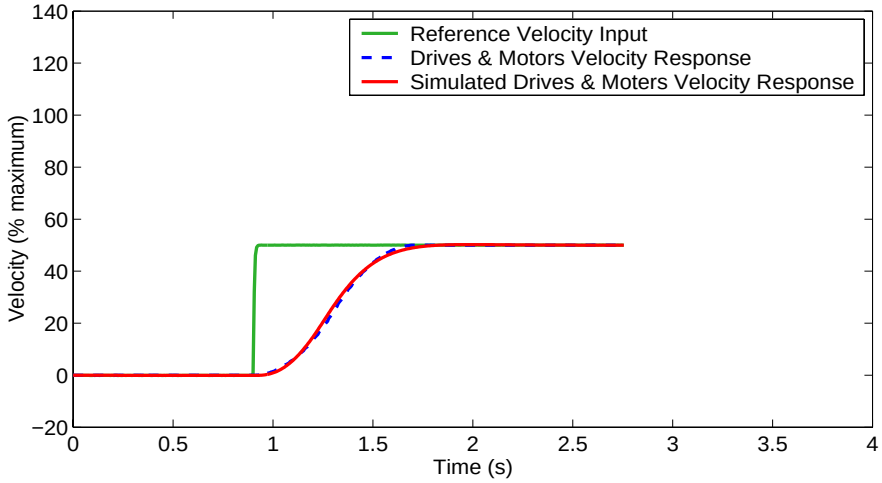

b) Actual and simulated response to a step input of 50%.

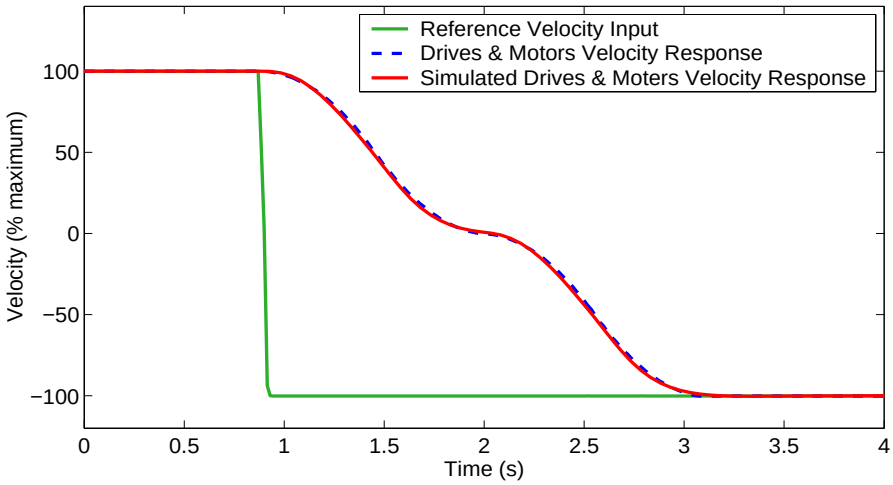

c) Actual and simulated response to a step from 100% to –100%.

Figure 23: Comparison of actual and simulated responses to step inputs.

3.1.3.2 Influence of the Drive & Motors Model on Input Shaping

A key issue to be addressed is the influence that the drive and motors will have on the effectiveness of the input shaper to eliminate oscillations from the payload. If the drive and motors can be represented as a linear transfer function, then there is no detrimental effect on the oscillation suppression of the input shaper; this is due to the commutability of the input shaper and a linear plant. However, the model contains a nonlinear rate limiter, as well as a nonlinear switch; therefore the possibility of representation by a transfer function is precluded. Instead, the effects of the nonlinear elements may be understood conceptually.

Consider the block diagram of a system shown in Figure 24 where an arbitrary reference signal, X, is modified by an input shaper to produce a shaped command, X_s. Assume that the reference signal obtains some steady state value by time, T. Also assume that the input shaper is designed to cancel the oscillations of a linear plant, G. If X_s is used as an input to a nonlinear plant, such as the drive and motors model, then the response of the nonlinear plant may be represented as Y_{NP}.

The same nonlinear plant response, Y_{NP}, can be obtained by modifying some baseline command, W, by an input shaper (not necessarily consisting of an impulse sequence appropriate for eliminating the oscillations in G), reducing the system to that of Figure 25, an equivalent system that contains no nonlinear elements. If it can be shown that the input shaper of the equivalent system consists of an impulse sequence suitable for eliminating oscillations in G, and that the baseline command, W, obtains some steady state value, then the nonlinear elements of the original system will have no detrimental effects on the oscillation suppression properties of the shaped signal, X_s. This is because the original system behaves as if the signal Y_{NP} was created by shaping a command, W, by an input shaper designed for G.

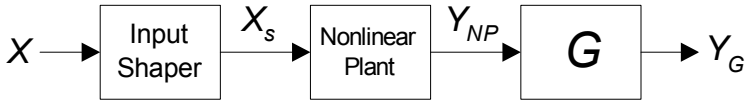

Figure 24: Generalized input shaping control with nonlinear plant.

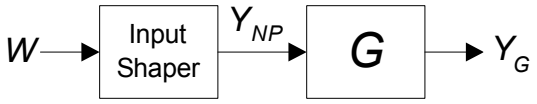

Figure 25: Equivalent input shaping control without nonlinear plant.

The process of resolving an arbitrary signal, such as Y_{NP}, into a base command, such as W, and an input shaper is called deconvolving. The input shaper resulting from the deconvolution process may or may not consist of an impulse sequence appropriate for eliminating the oscillations of G. If it does not, then the shaped command, Y_{NP}, will also be unable to cancel the oscillations of G. This occurrence indicates that the nonlinear elements of the original system diminish the oscillation reduction properties of the correctly designed input shaper.

Therefore, to determine how the nonlinear elements of a system affect the oscillation suppression properties of an input shaper, one may examine the components resulting from the deconvolution process. Specifically, we may evaluate whether or not the response of a nonlinear plant to a shaped input that obtains some steady state value can be deconvolved into 1) a baseline command that obtains a steady state value, and 2) an input shaper appropriate for the linear plant.

To this end, Section 3.1.3.3 first considers the simple model in Figure 21 that contains only the rate limiter. Later, in Section 3.1.3.4, the switching element of the modified model (Figure 22) is also considered.

3.1.3.3 Effects of a Rate Limiter on Input Shaping

To determine whether the response of the drive and motors model shown in Figure 21 can be deconvolved into an acceptable baseline command and input shaper, first note that the model is comprised of a linear and nonlinear element. Without loss of generality, we may consider only the nonlinear rate limiter because the second-order plant, H, may be combined with the linear payload plant, G, to form a new linear plant, $\hat{G}$. Then, the problem is reduced to that of Figure 26. We wish to find a range of slew rates, S, of the

rate limiter such that the output, Y_{NP}, may be resolved into an acceptable reference signal, W, and an input shaper appropriate for reducing oscillations in $\hat{G}$ [2].

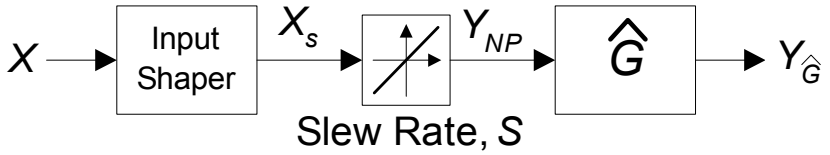

Figure 26: Generalized input shaping control with nonlinear rate limiter.

We may show that the desired resolution of Y_{NP} is possible after examining the response of the rate limiter to a shaped step input. In Figure 27, a step input has been shaped by a ZV shaper designed to cancel oscillations in $\hat{G}$. The response of the rate limiter to the shaped input, X_s, has been overlaid for a range of R_{ZV} values. R_{ZV} is non-dimensional ratio that relates how rapidly a reference signal may be altered by the rate limiter to how rapidly a ZV input shaper alters a reference signal. Specifically, for an undamped system, R_{ZV} is related to the slew rate, S, by:

$$S = \frac{50\%}{\Delta_{ZV}} R_{ZV} . \tag{37}$$

The symbol Δ_{ZV} represents the duration of the ZV input shaper. Note that the x-axis has been normalized to this duration.

[2] For the crane system, the oscillatory poles in the payload plant are highly dominant when compared with the oscillatory poles of H from the drive and motors model. Therefore, the input shaper used to cancel oscillations in $\hat{G}$, is the same as the one used to cancel the oscillations in G.

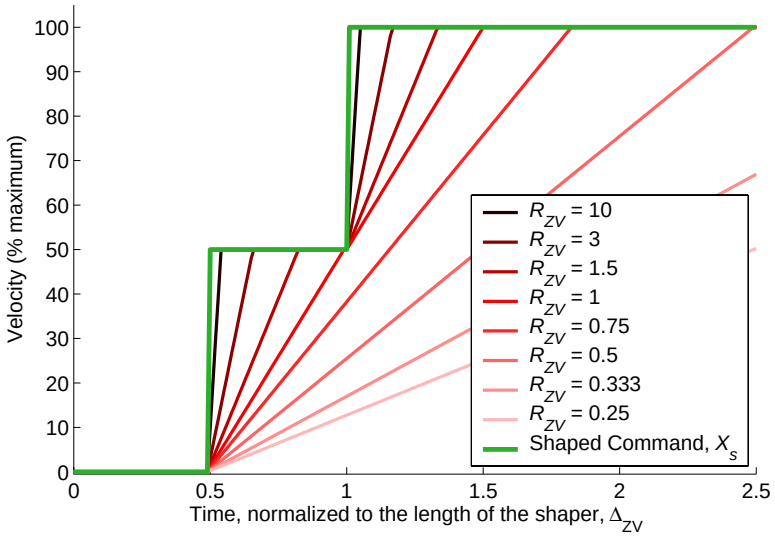

Figure 27: Response of a rate limiter for different slew rates, *S*.

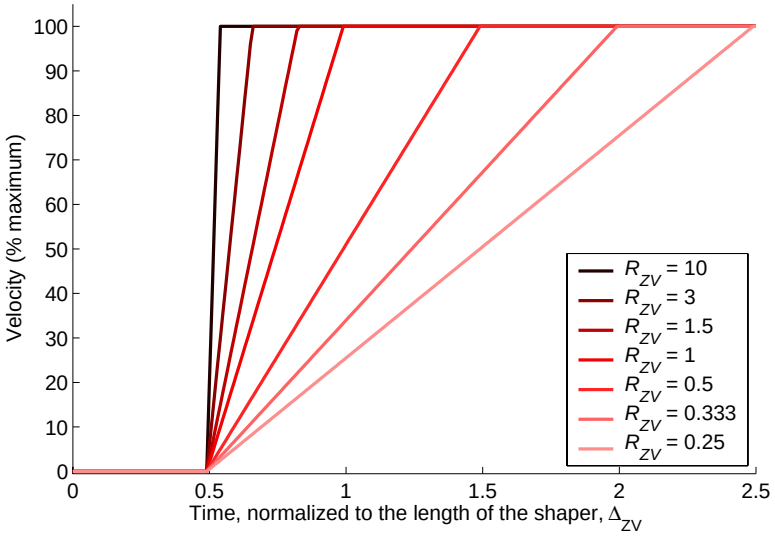

Figure 28: Deconvolved reference signal for different slew rates, *S*.

By close inspection of the rate limiter response curves in Figure 27, one may ascertain the shape of several reference commands, shown in Figure 28. When modified by the ZV input shaper designed for $\hat{G}$, these reference commands precisely reproduce the corresponding response curves of Figure 27. Specifically, for every response curve with a slew rate corresponding to an R_{ZV} value between ∞ and 1, a related step-like reference command, W, may be generated that has the same steady state value as the original step command. Graphically, this means that any response curve of Figure 27 that intercepts

the shaped command, X_s, at the 50% height can be deconvolved into a reference command, W, and the original input shaper. Response curves not intercepting the shaped command at the 50% height can be deconvolved in this manner only if they have a slew rate that corresponds to an R_{ZV} value of $1/n$, where n is any positive integer.

Using the principles outlined above, we can determine a critical range of slew rates. When the slew rate of the rate limiter is within this critical range, a ZV shaped signal that obtains some steady state value can induce a response from the rate limiter that can be deconvolved into the following components: 1) a reference signal that obtains a steady state value, and 2) the original ZV input shaper. This resolution means that the ZV shaper works perfectly with the original system, even though the system contains a nonlinear rate limiter. A similar formulation may be derived for a UM-ZV input shaper designed for an undamped system. These principles are summarized in Table 3.

Table 3: Acceptable slew rates for a nonlinear rate limiter in an input shaping control.

<table>
<tr><td>SHAPER</td><td colspan="3"> 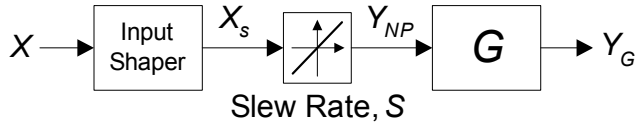
</td></tr>
<tr><td rowspan="2">ZV</td><td>Acceptable R_{ZV} Values</td><td>$1 \le R_{ZV} < \infty$, or $R_{ZV} = \frac{1}{n}$</td><td>$n = 1, 2, 3, \ldots$</td></tr>
<tr><td colspan="3">$R_{ZV} = \frac{\Delta_{ZV}}{50\%} S$</td></tr>
<tr><td rowspan="2">UM-ZV</td><td>Acceptable R_{UMZV} Values</td><td>$1 \le R_{UMZV} < \infty$,
or $R_{UMZV} = \frac{1}{n}$</td><td>$n = 6i + 1$;
$i = 0, 1, 2, \ldots$</td></tr>
<tr><td colspan="3">$R_{UMZV} = \frac{\Delta_{UMZV}}{200\%} S$</td></tr>
</table>

Table 3 defines one class of nonlinear elements that will have no negative effect on the oscillation reduction properties of an input shaper. For the nonlinear rate limiter of the drive and motors model to be in this class, the "*R*-value" of the limiter must be within the acceptable "*R*-values" as defined above; the R_{ZV} and R_{UMZV} values for the crane's rate limiter are dependent on the slew rate, *S*, of the crane, and the duration of the input shapers, Δ. Because the input shapers are designed to cancel the oscillations of the payload, the durations of these shapers are dependant on the cable length of the crane as defined by the following equations:

$$\Delta_{ZV} = \frac{\pi}{\sqrt{\frac{g}{L}\left(1-\zeta^2\right)}} \tag{38}$$

$$\Delta_{UMZV} = \frac{2\pi}{3\sqrt{\frac{g}{L}\left(1-\zeta^2\right)}} \tag{39}$$

In Figure 29 the R_{ZV} and R_{UMZV} values for the crane are plotted as the cable length of the crane varies. The table shows that a ZV input shaper, designed for the crane at a given cable length between 1 and 6 meters will always perform well because the value of R_{ZV} is well above 1. However, a UM-ZV shaper, designed for the crane at a given length between 1 and 6 meters will perform well only at cable lengths greater than 3.5 meters because the value of R_{UMZV} is less than 1 at other cable lengths.

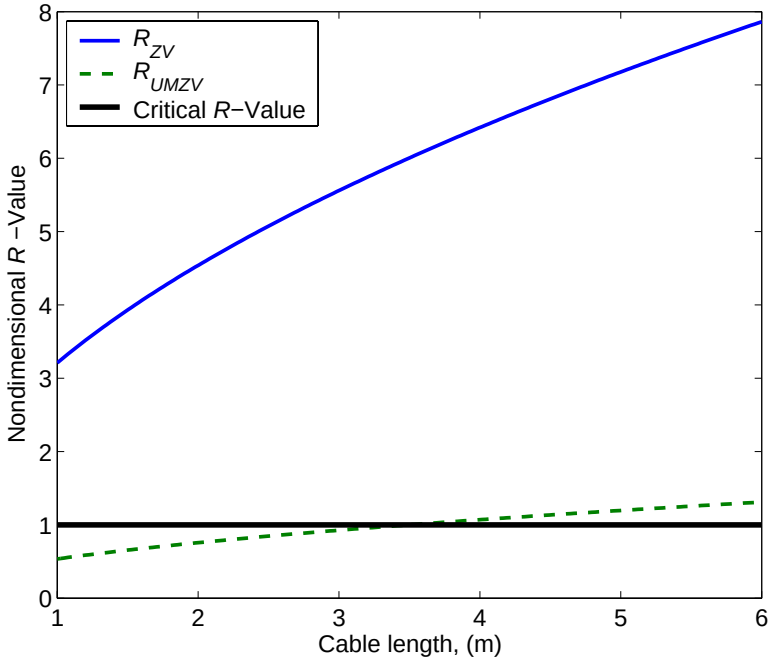

Figure 29: R_{ZV} and R_{UMZV} values for the MARC crane at varying cable lengths.

Given the limitation in the slew rate for the drive and motors, one may conclude that the ZV shaper designed for a given cable length will always successfully control the motion-induced oscillations of the payload at the given length. A UM-ZV shaper, on the other hand, will not perform well if designed and implemented at cable lengths less than 3.5 meters.

3.1.3.4 Effects of a Switching Element on Input Shaping

Now we may turn out attention to the revised model of the drive and motors that was shown in Figure 22. In Figure 30, this model has been incorporated into the input shaping control scheme. A reference signal, V_r, is shaped by an input shaper designed for the payload plant. Next, the shaped signal, V_s, interacts with the drive and motors, causing a velocity, V_b, in the overhead support unit of the crane. Finally, the payload plant reacts with velocity V_p.

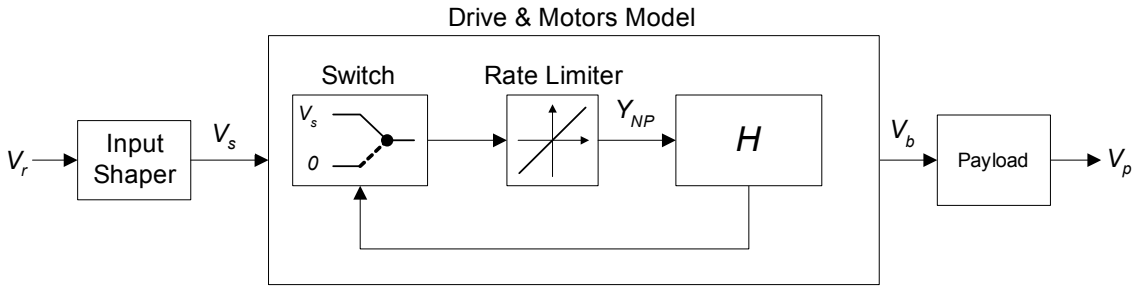

Figure 30: Input shaping control system with drive and motors model.

The switch element allows the model to respond in a way similar to the actual system when transitional velocity commands are issued to the crane. Transitional velocity commands are those which change the direction of travel of the crane (positive velocity to negative velocity or vice versa). When these types of commands are issued, the switch temporarily outputs a signal of *0*, otherwise the switch outputs the shaped signal, V_s.

During periods of time when the switch outputs V_s, the drive and motors model performs identically to the simplified model of Figure 21, behaving as if the switching element were not present. The effects, therefore, of the switching element during these times on the oscillation reducing properties of the input shaped signal are null; any oscillation inducing influences must be due to an insufficient *R*-value of the slew rate limiter.

The switch outputs a signal of *0* only when transitional velocity commands are issued to the crane. This signal will continue to be issued until the actual velocity of the crane is sufficiently close to *0* itself. Only at this time will the switch revert to passing the shaped signal, V_s. Consequently, the command that is sent to the rate limiter is altered from the original shaped command, V_s. The degree to which it is altered depends on how quickly the crane is capable of changing its positive (or negative) velocity to a velocity of *0*. For the model of the drive and motors, this performance characteristic is related to ω_H, the natural frequency of the linear plant, *H*, (not to be confused with ω_n, the natural frequency of the linear payload plant). If the crane quickly changes its velocity to *0*, then the switch will alter the original command for a relatively short duration. On the other hand, if the crane takes a great deal of time changing its velocity to *0*, then the switch will alter the original command for a relatively lengthy duration. The following illustrative example shows how the switch alters a shaped command for different crane speeds.

Figure 31 shows a transitional velocity command from 100% velocity to –50% velocity (dashed green line) that has been shaped by a ZV input shaper to produce the shaped command, V_s (solid green line). For a system that can quickly change its velocity, the altered velocity command (dark blue line) is nearly identical to the shaped command. This system is capable of changing velocity quickly because H, the second-order plant in the drive and motors model, has a high natural frequency (ω_H = 40 radians per second). As the natural frequency of H is reduced, the degree to which the switch alters the original command is amplified. This is seen by the lines corresponding to the decreasing values of ω_H. These commands are passed through the rate limiter, becoming further modified, as seen in Figure 32, before finally entering the linear plant, H.

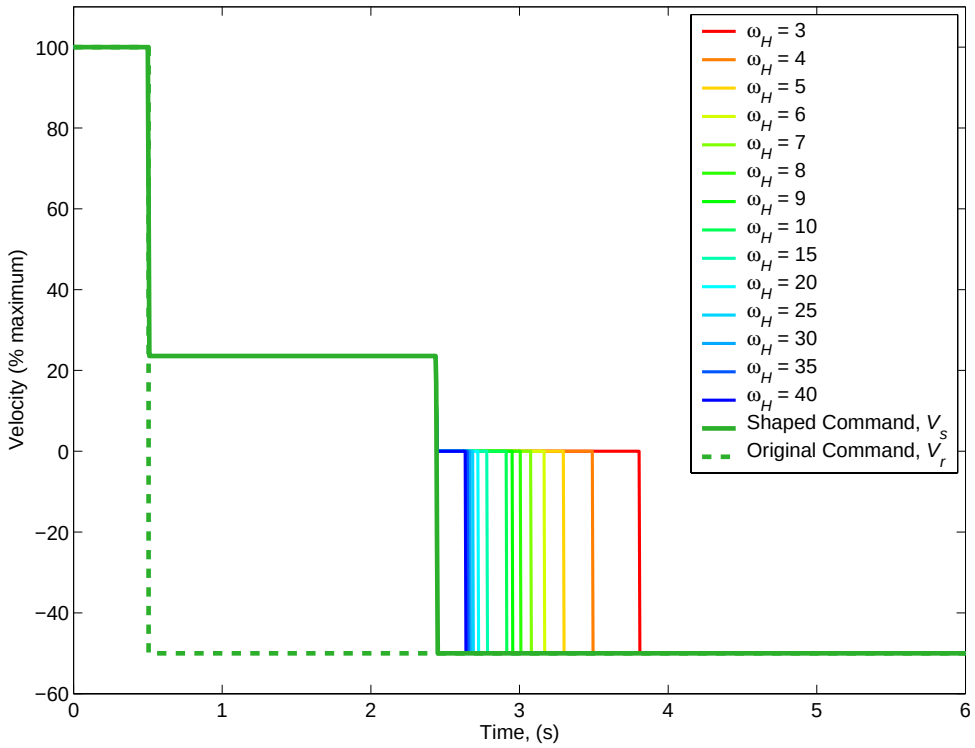

Figure 31: Shaped command altered by the switch element.

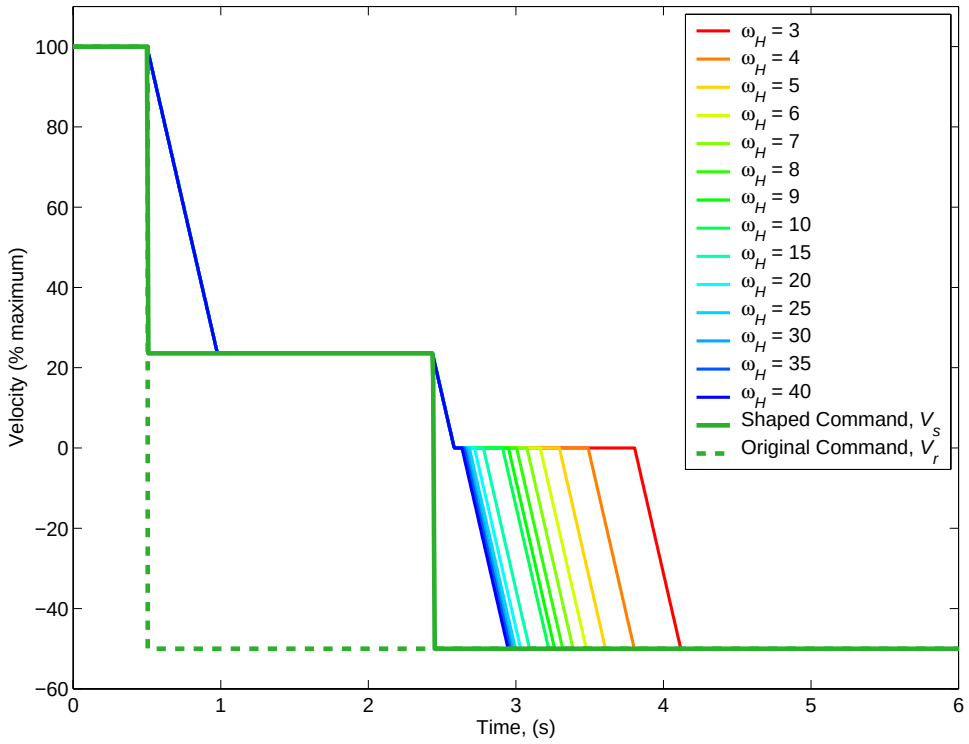

Figure 32: Shaped command altered by the switch and rate limit elements.

The effects that the switching element has on the oscillation reducing properties of input shaped signals may be determined by inspecting the altered velocity signals in Figure 32. The first important feature of these curves to note is that the *R*-values of the rate limiter, causing the sloped sections of the curves, are all greater than 1. This fact may be determined by observation; the curves of Figure 31 contain three downward steps, as do the curves of Figure 32. For this reason, we know that the rate limiter has no detrimental effects on the oscillation reducing properties of the incoming signals. We may, therefore, consider directly the signals of Figure 31, neglecting the effects of the rate limiter.

These signals interact with the system in a way shown in Figure 33, where Y_{NP} represents the velocity signals in Figure 31, and G is a linear plant composed of the payload plant and H from the drive and motors model.

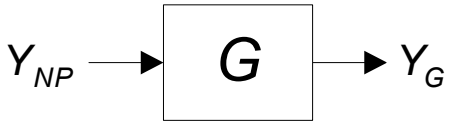

Figure 33: Altered velocity signals interacting with a linear plant.

This type of system was discussed in Section 3.1.3.2. It was shown that the system could be deconvolved into a baseline command, W, and an input shaper (not necessarily appropriate for eliminating oscillations in G). The deconvolved system was shown in Figure 25; it is also shown below for reference. As discussed previously, a nonlinear element of a system has no detrimental effects on input shaped signals if Y_{NP} can be deconvolved into an appropriate input shaper, and baseline command. If this resolution is not possible, one may conclude that the switch has a detrimental effect on the oscillation reducing capabilities of the input shaped signal. Therefore, we wish to deconvolve the signals of Figure 31 and analyze the resulting components.

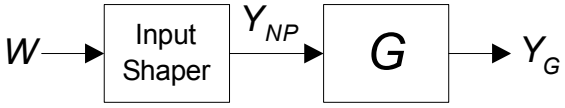

From Figure 25: Equivalent input shaping control without nonlinear plant.

The signals of Figure 31 can be deconvolved into a step command from 100% velocity to –50% velocity and a three-impulse input shaper. This baseline command is identical to the original unshaped command that was used to generate the shaped signal, V_s, and therefore has the same steady state value as the original command. It is shown with the dashed green line in both Figure 31 and Figure 32.

Next, we may determine if the three-impulse input shaper, shown in Figure 34, is appropriate for eliminating oscillations in G. This is accomplished by considering the magnitudes and time locations of the shaper's impulses. The first impulse has a magnitude of 1/2, the second, a magnitude of 1/6, and the third, a magnitude of 1/3. The time locations for the first and second impulse remain constant for every velocity curve shown, $t_1 = 0.0$ seconds and $t_2 = 1.94$ seconds; the time of the third impulse varies as ω_H varies; when $\omega_H = 40$ radians per second, $t_3 = 2.13$ seconds, when $\omega_H = 3$ radians per second, $t_3 = 3.31$ seconds.

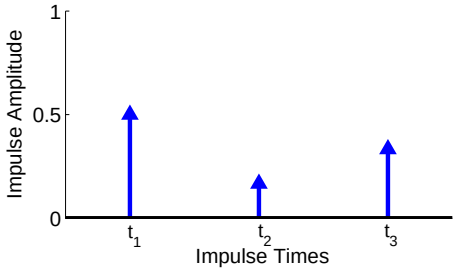

Figure 34: Three-impulse input shaper.

In [15], Singhose et. al. showed how input shapers can be visually represented through the use of vector diagrams. Vector diagrams are graphs in polar coordinates (r–θ space). A vector diagram is created by setting r_i equal to the i^{th} amplitude, A_i, of an impulse sequence, and setting θ_i equal to $t_i * \omega$, where t_i is the time of the i^{th} impulse and ω is the frequency of the system for which the input shaper is being used.

When a vector diagram is created in this manner, it becomes a useful tool for analyzing the oscillation reducing properties of an input shaper. The vector diagram of the three-impulse input shaper resulting from the deconvolution is shown in Figure 35. Here the time of the third impulse is seen to vary as ω_H varies.

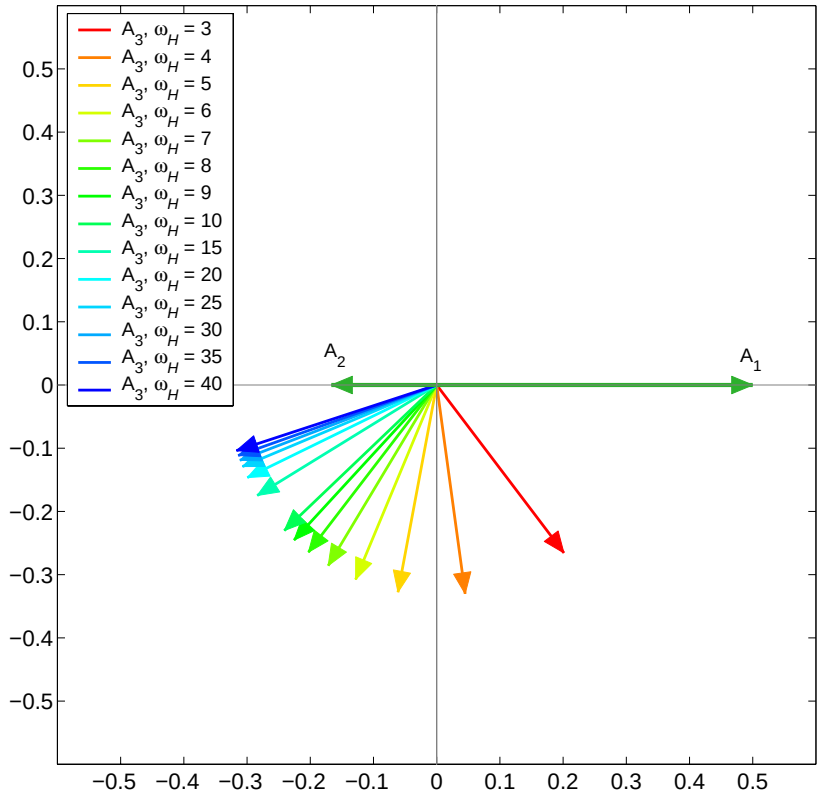

Figure 35: Vector diagram of a three-impulse shaper with different time locations of the third impulse.

To determine the amplitude of oscillations that an input shaper will induce, we may look at the resultant vector. The resultant is the vector sum of the individual impulse vectors [15]; the magnitude of the resultant vector has special significance. It is proportional to the amplitude of the residual oscillation in a system. Hence, for lightly damped systems, a correctly designed input shaper will have a resultant vector with a magnitude nearly equal

to zero. In the case of the three-impulse input shaper, the time location of the third impulse varies, thereby causing the vector sum of the three impulses to vary as well. This can be seen in Figure 36, where the resultant vector is plotted for each of the different natural frequencies of H. When the system responds very quickly ($\omega_H = 40$ radians per second), the resultant vector has a relatively small magnitude, as seen by the blue line. As the natural frequency of H is decreased, a corresponding increase in the magnitude of the resultant vector is seen. However, for each case, the resultant vector has a non-zero magnitude.

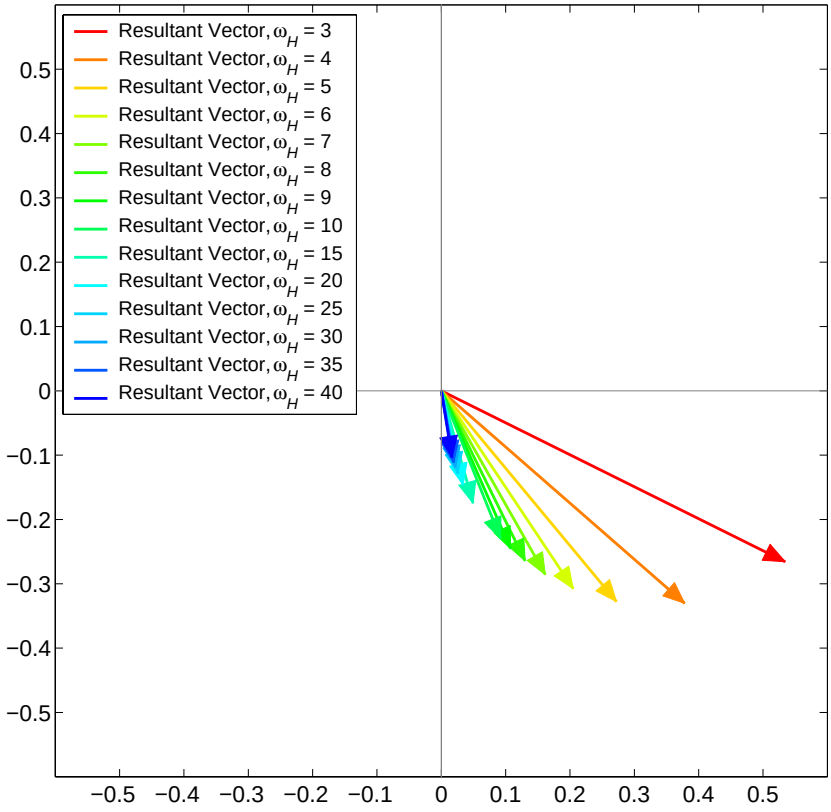

Figure 36: Resultant vectors for the three-impulse shaper with different time locations of the third impulse.

Let us briefly summarize the progression of thought thus far:

1) In Figure 30, a baseline command, V_r, is shaped by an input shaper designed to cancel oscillation in the payload plant. The shaped signal is intercepted by the nonlinear drive and motors model, comprised of a switching element, a rate limiter, and a heavily damped second-order plant, H. The drive and motors model modify the shaped signals, V_s, before they are passed on to the payload plant.

2) The nonlinear elements of the drive and motors model may affect the ability of the input shaper to reduce oscillations in the payload.

3) Section 3.1.3.2 suggests that studying the effects of the nonlinear elements on shaped signals can be accomplished by deconvolving Y_{NP}, the response of the nonlinear elements, into a baseline command and some input shaper (not necessarily the same input shaper used to generate V_s).

4) If Y_{NP} can be deconvolved into a baseline command that obtains some steady state value, and an input shaper that can cancel oscillations in the payload plant, then the nonlinear elements of the drive and motors will have no detrimental effect on the oscillation reducing properties of the original input shaper.

5) Considering only the influence of the rate limiter on the input shaper, Section 3.1.3.3 showed that for sufficiently high *R*-values, the response of a rate limiter can be deconvolved into the appropriate components, precluding the rate limiter from negatively altering shaped signals.

6) Section 3.1.3.4 considers the influence of both the rate limiter and switch on input shaping. The switch modifies a shaped signal only when transitional velocity commands are issued to the crane. The degree to which the switch modifies these commands is dependant on the natural frequency of *H*, the second-order plant in the drive and motors model.

7) The rate limiter further alters the signals coming from the switching element; however, these alterations have no negative effect on the input shaped signals because of a sufficiently high *R*-value. Therefore, the effects of the switching element on shaped signals may be understood by considering the switch's response (Figure 31) to a transitional velocity command instead of the rate limiter's response (Figure 32) to a transitional velocity command.

8) The response of the switch to a transitional velocity command can be deconvolved into a step command and several different three-impulse shapers. The step command has the same steady state value as the original baseline command. Then, what's needed to show the effect of the switching element on

the original input shaper is to determine whether or not the three-impulse shapers can eliminate oscillations in the payload.

9) In [15], Singhose et. al. showed that an analysis of a three-impulse shaper may be accomplished by considering its vector diagram representation. The magnitude of the resultant vector is proportional to the magnitude of residual oscillation the shaper will induce into the system. Therefore, for a lightly damped system, a properly designed input shaper will have a resultant vector with a magnitude nearly equal to zero.

10) The resultant vector diagram for the three-impulse shapers (Figure 36) shows that the magnitude of the resultant vectors vary with the natural frequency of *H*. In every case, the resultant vector has a non-zero magnitude; therefore the corresponding three-impulse shaper is not suitable for entirely eliminating oscillations in the payload. Further, as the natural frequency of *H* is decreased, the magnitude of the corresponding resultant vector increases.

The preceding progression provides a foundation for showing that the nonlinear elements of the drive and motors model respond to transitional velocity commands in a way that is equivalent to the response of a step command shaped by a three-impulse input shaper. This equivalent response induces residual oscillations in the payload plant that are proportional to the magnitude of the non-zero resultant vectors. Therefore, we may conclude that the switching element, when subjected to a shaped transitional velocity command, inhibits the shaped command from entirely eliminating the oscillations of the payload. The switching element will permit larger oscillations in the payload when *H* has a low natural frequency.

These results were demonstrated through simulation. For varying natural frequencies of *H*, the system shown in Figure 30 was subjected to a step command, V_r, from 100% velocity to –50% velocity. For each trial, the amplitude of the residual oscillation was recorded. These results are shown in Figure 37. As predicted, increased amplitude of the residual oscillation accompanied a decrease in the natural frequency of *H*.

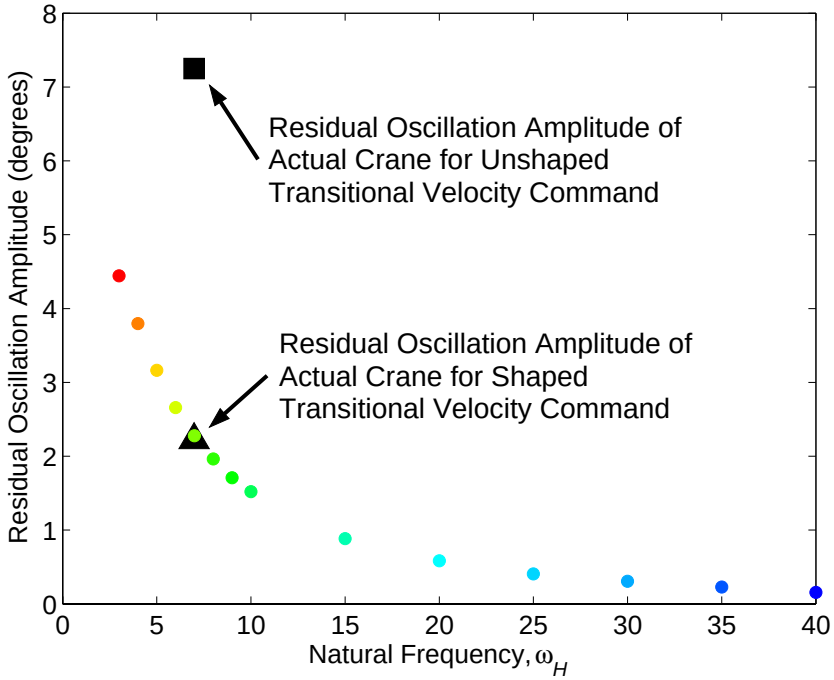

Figure 37: Natural frequency of *H* affecting the residual oscillation of the payload.

The natural frequency of *H* that most closely reproduces the actual response of the crane was calculated to be approximately 7 radians per second. The simulated results from Figure 37 predict that at this frequency, the payload of the physical system will exhibit a small degree of oscillation when shaped transitional velocity commands are issued to the crane. Experimentally, this prediction proved accurate. The residual oscillation amplitude of the actual crane caused by a shaped step from 100% velocity to –50% velocity is shown by the black triangle. Notice that the measured value is coincident with the predicted value. For reference, the residual oscillation amplitude of the actual crane caused by an unshaped step from 100% velocity to –50% velocity is shown by the black square.

These results indicate that the drive and motors nonlinearities degrade the input shaping process when transitional velocity commands are issued to the crane. However, even with the degradation, input shaping is superior to using unshaped transitional commands.

3.1.4 Experimental Results

The performance of the controller developed in the preceding section was rigorously tested on the 10-ton bridge crane. The areas of performance evaluated were 1) the oscillation suppression of the controller at different cable lengths, and 2) how the control affected operational efficiency and safety.

3.1.4.1 Vibration Suppression at Different Cable Lengths

The control shown in Figure 38 was implemented on the crane. One objective in experimentally testing the control was to verify the effects that the nonlinear elements of the crane system have on the oscillation suppression capabilities of the ZV and UM-ZV input shapers.

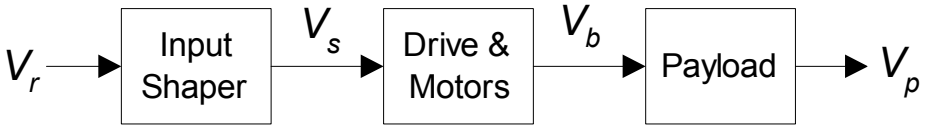

Figure 38: Implemented input shaping control.

Experiments were conducted by varying the length of the cable between 5.75 meters and 2.25 meters. The duration of the shaper being used (and the magnitudes of the impulses in the case of the ZV shaper) were adjusted for optimal oscillation suppression at each discrete cable length. In this way, any residual oscillation of the hook may be mostly attributed to an insufficient slew rate of the rate limiter and/or unmodeled dynamics.

Motion was induced into the bridge by sending a step command, V_r, to the control, representing maximum velocity. At the same time, coordinate information about the hook was captured by the vision system. Later, the captured data was analyzed to determine the amount of residual oscillation exhibited by the payload for each trial.

The results of the experiment are shown in Figure 39. The horizontal axis represents the cable lengths at which the various trials were conducted. The vertical axis represents the peak-to-peak magnitude of oscillations of the hook after the motion of the bridge was initiated. Shown with the blue triangles is the residual oscillation while using the ZV shaper. As predicted, oscillations are effectively reduced throughout the entire range of

cable lengths. The results for the UM-ZV shaper are shown with the green circles. This shaper performed well at cable lengths greater then 3.5 meters; however, at cable lengths less than 3.5 meters, performance degraded slightly. This result harmonizes with that obtained theoretically by considering the R_{UMZV} value. For comparison, the magnitudes of payload oscillations caused by unshaped motion are shown with red stars.

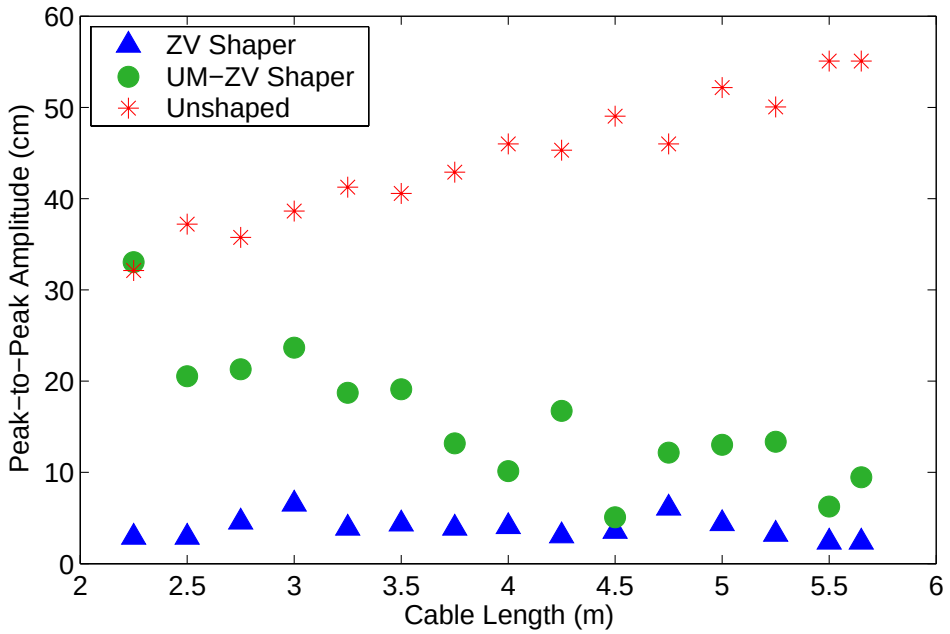

Figure 39: Residual payload oscillation for ZV, UM-ZV, and unshaped bridge motion.

These results clearly demonstrate that even with the nonlinear motor and drive dynamics, input shaping provides significant oscillation reducing benefits.

3.1.4.2 Controller Effects on Operator Efficiency and Safety

It has been shown that input shaping is a simple and effective way of reducing motion-induced oscillation in a bridge crane. However, because input shaping alters intended commands, the control has the potential to confuse or annoy the operator, and may lead to poorer overall performance. To gage the effects that the shaped control has on the overall performance of the system, a study of operator behavior in a simulated work environment was conducted [16]. Two aspects of the research considered the controller's

effects on the efficiency and safety of the system. This section presents several key results and figures from this study.

A simulated work environment was comprised of two obstacle courses, shown schematically in Figure 40a and Figure 40b. Experienced and novice crane operators were asked to drive the crane through the obstacle courses both with and without input shaping. The objective for the operators was to move the hook from a starting region, shown by the green square, to an ending target region, shown by the red circle. Two possible routes existed for the operators to choose between, a long and open path, and a shorter, more restrictive path. While the crane was in motion, a downward looking video recorder captured the hook's motion. Coordinate information about the hook motion was later extracted from the video using a tracking algorithm in Matlab.

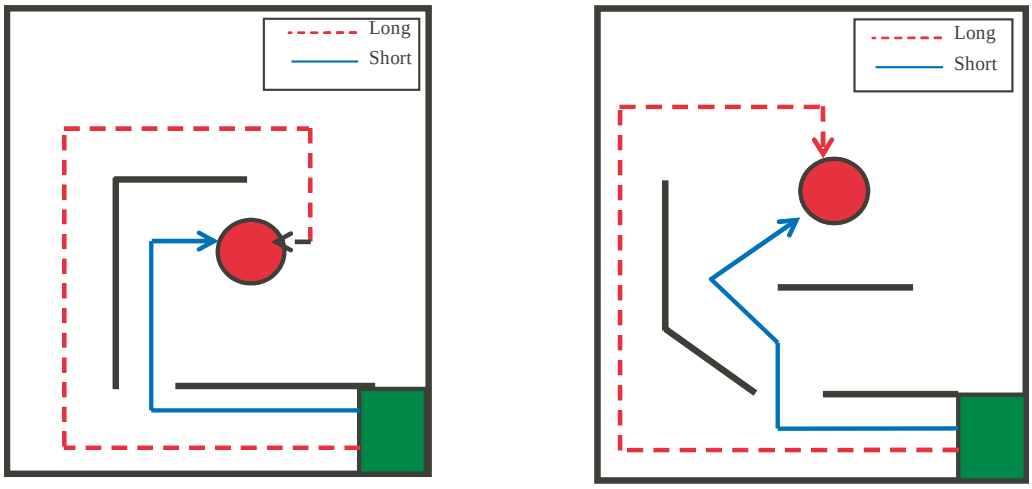

a) Obstacle course 1. **b) Obstacle course 2.**

Figure 40: Obstacle courses used for input shaping experiments.

Figure 41 depicts a typical shaped and unshaped response of the crane during a trial. During unshaped motion, the trajectory shows that the hook oscillates when the crane is commanded to move and after it is commanded to stop, in addition, the payload is seen to collide twice with surrounding obstacles. In contrast, the shaped trajectory shows that the motion-induced oscillations were eliminated and no collisions were made.

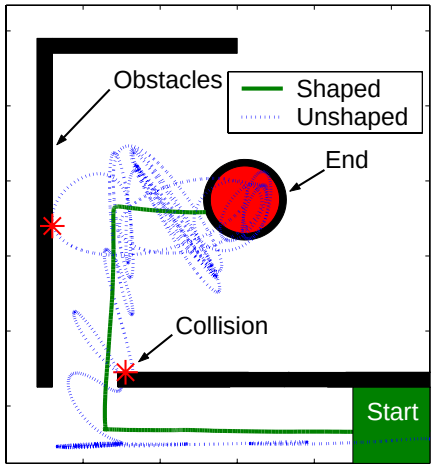

Figure 41: Obstacle course showing shaped and unshaped hook motions.

To gage the effects that the shaped command had on the operational efficiency of the crane, the run times of each operator were recorded with and without the input shaping control module. The run time was defined as the time duration from the start of the crane motion until the hook remained within the ending target region. These times for the two courses are shown in Figure 42a and Figure 42b. The blue bars represent the run time for the unshaped motion while the yellow bars represent the run time for shaped motion. For course 1 and course 2, the average run time for shaped motion was 31 seconds and 51 seconds, respectively, while the average run time for unshaped motion was 88 seconds and 135 seconds, respectively. These figures clearly indicate the efficiency advantage of the input shaped control.

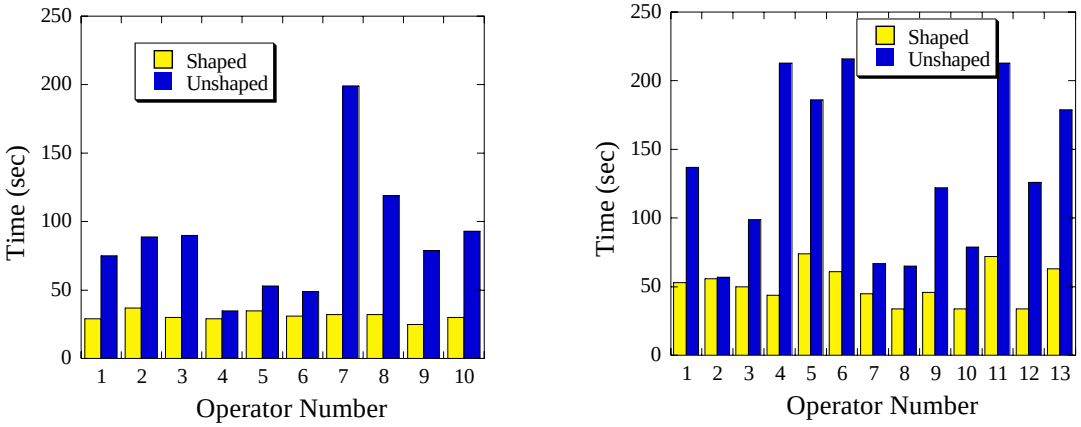

a) Course 1. **b) Course 2.**

Figure 42: Run times for the obstacle courses.

Because a crane operator must be extremely careful in avoiding collisions between the payload and surrounding obstacles, understanding the effects that shaped control has on this area is critical. To measure these effects, a third obstacle course was constructed; it is shown in Figure 43. The crane operators were again asked to navigate from a starting region to an ending region. Each operator drove the crane through the course ten times, five times using input shaping and five times without using input shaping. The number of collisions that the operators had while navigating the obstacle courses was recorded. Figure 44 shows the average number of collisions that the operators had over the five trials. This figure shows that the shaped control significantly decreased the number of collisions, thereby improving operational safety of the crane.

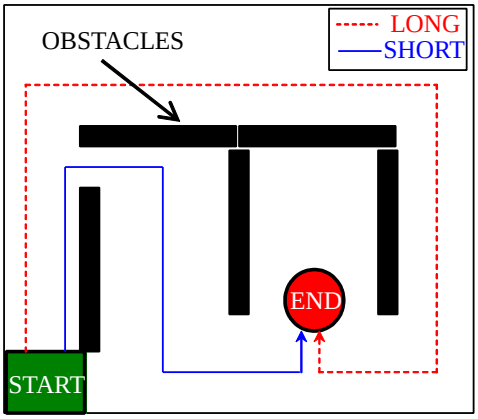

Figure 43: Obstacle course 3.

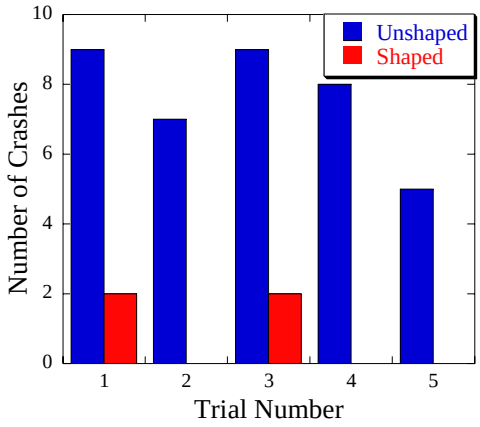

Figure 44: Average number of collisions for each trial.

3.1.5 Robust Input Shapers

It should be noted that for the experiments conducted in this and the preceding section, the input shapers used in the control were designed specifically for the cable length at which the crane was operating. On systems that do not have a feedback mechanism for detecting cable length, by which an implemented input shaper may be adjusted in real time, one must consider the robustness of the input shaper. Specifically, we may consider the robustness of an input shaper to adequately reduce oscillation at cable lengths for which the shaper is not designed.

One method of quantifying the robustness of an input shaper is to compare the amplitude of residual oscillation as a function of the modeling error. Figure 45 displays this comparison for several standard input shapers, including the ZV and UM-ZV shapers used in the previous experiments. The horizontal axis is the ratio of the actual frequency of the system to the frequency for which the input shaper was designed. The vertical axis represents the percentage of residual oscillation after a movement. This percentage is the amplitude of oscillation when input shaping is used divided by the amplitude of oscillation when shaping is not used. The robustness of a shaper is determined by observing how much of the robustness curve is beneath some acceptable oscillation threshold, usually 5%. By observation of the graph, one will notice that the ZV and UM-ZV shapers are the most sensitive shapers to modeling error.

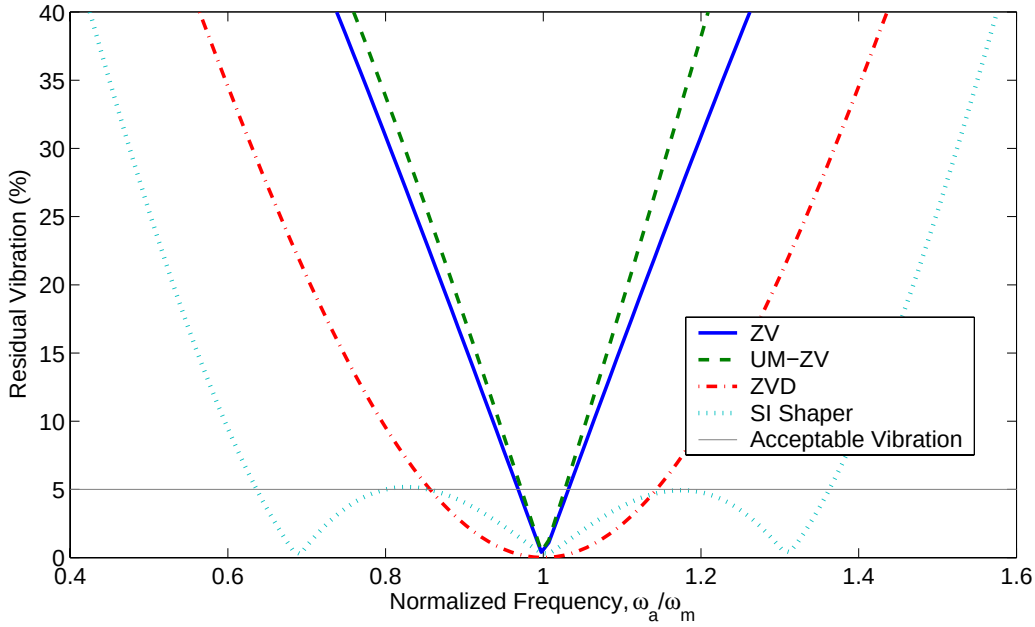

Figure 45: Robustness curves for some standard input shapers.

Input shapers have been developed that increased robustness to modeling errors [17] [9] [18] [19] [20]. Singer developed the earliest form of robust input shaping by setting the derivative with respect to frequency of the residual oscillation equation in (35) equal to zero, and solving for an appropriate shaper [17] [9] . The resulting input shaper was called the Zero Vibration and Derivative (ZVD) shaper. Later, Singhose el al. developed methods for shaper design that allows for an arbitrary amount of robustness at a given acceptable oscillation threshold [20]. A form of these specified insensitivity (SI) shapers was implemented on a bridge crane at the Savanna River Technology Center. The experimental results showed that the SI shapers greatly reduced residual oscillation over a large range of cable lengths [13]. The robustness curves for the ZVD and an example SI input shaper are shown in Figure 45.

On a control lacking sensory feedback of the cable length, the ZV and UM-ZV shapers cannot be modified in real time to provide optimal oscillation suppression at varying cable lengths. Instead, using robust input shapers in the place of the ZV or UM-ZV shapers will allow the control to successfully reduce oscillations over a wide range of cable lengths.

3.1.6 Module Summary

A control has been developed to reduce motion-induced oscillation of the payload. The oscillation suppression capabilities of the control have been shown to be effective on linear plants. The control has also been shown to be effective on systems with a special class of nonlinear plants. Further, significant improvements in the areas of safety and efficiency have been demonstrated in a real world environment through the use of the control.

Another benefit of the control is the ease of implementation. When robust shapers are used, no sensors of any kind are required. Also, the input shapers used as the controlling element were easily programmed into operation on the existing infrastructure of the crane.

Because the control contains no mechanism for reducing non-motion-induced oscillation, it is most effective on systems where the payload is not subject to wind or other disturbing forces. Also, there is no mechanism in the control for precision positioning of the payload, though the reduction of cable sway will certainly ease this task for an operator.

3.2 FINAL POSITIONING CONTROL MODULE

To develop a control scheme that enables precision positioning of the payload, we may first begin by again considering the state space representation of the crane system from (22):

$$\dot{\boldsymbol{q}} = A\boldsymbol{q} + bv_t(t),$$

where

$$A = \begin{bmatrix} 0 & 1 \\ -\omega_n{}^2 & -2\zeta\omega_n \end{bmatrix}, \text{ and } \; b = \begin{bmatrix} 0 \\ 1 \end{bmatrix}.$$

As discussed in Section 1.2 the state, q_2, represents the relative horizontal displacement between the overhead support point and the payload. The state, q_1, has a less physical

meaning; $-q_1$ is a quantity whose derivative yields the relative displacement between the overhead support point and the payload.

Computing the eigenvalues of A, we have:

$$\lambda = -\zeta\omega_n \pm \omega_d i \,. \tag{40}$$

Because the real part of the eigenvalues of A are negative, then the states $\boldsymbol{q}$ are asymptotically stable in the sense of Lyapunov. Therefore, q_1 and q_2 always approach zero. By this formal treatment of the system's state equations, an obvious fact is emphasized; the payload will always come to rest directly beneath the overhead support point. Therefore, precise positioning of the overhead support point is equivalent to precise positioning of the payload. This fact enables the development of the control to proceed with an easily implementable support-unit-position based control rather than with a more difficult payload-position based control.

3.2.1 Control Module Design

A simple proportional-derivative (PD) control has been designed to control the position of the hook in the direction of bridge travel. A block diagram of the controller is shown in Figure 46. A desired bridge position is issued to the control as a position reference signal, P_r. A laser range sensor provides sensory feedback of the bridge position, P_b. These two signals are compared to generate to an error signal, P_E, which is sent to the PD block. In response to the error signal, the PD block generates a signal representing a desired bridge velocity. To prevent this signal from over-driving the bridge beyond a maximum safe velocity, a saturation block has been inserted after the PD control block. The reference velocity, V_r, truncated by the saturation block, is sent to bridge drive and motors, where the bridge responds with a velocity, V_b. Finally, the payload responds to the bridge velocity in an open-loop manner, with velocity, V_p.

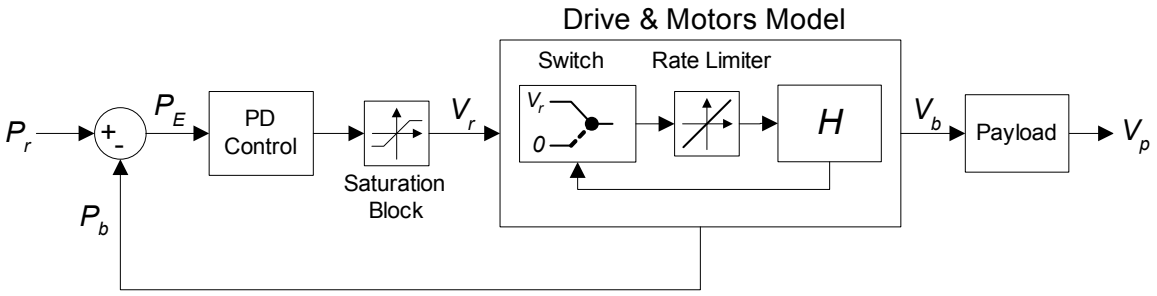

Figure 46: Block diagram of the positioning control module.

3.2.2 Stability Analysis

The stability of the control shown in Figure 46 may be determined by first considering the outputs, V_b and V_p, of the drive and motors plant, and the payload plant. The system is considered to be BIBO stable if for any bounded inputs into the system, the outputs, V_b and V_p are also bounded. Secondly, because of the presents of hard nonlinearities (e.g. the saturation block, switching element, and rate limiter) one must also be concerned about the existence of limit cycles.

3.2.2.1 BIBO Stability

Utilizing the method outlined in [21], one may determine the BIBO stability of the system by considering the eigenvalues of H, and the payload plant. For the drive and motors the eigenvalues are:

$$-0.6 \pm 3.56i \,. \tag{41}$$

The eigenvalues for the payload were previously determined in (40) as:

$$\lambda = -\zeta\omega_n \pm \omega_d i \,.$$

Then, for any bounded input into each of these plants, the outputs V_b and V_p will also be bounded because both plants have eigenvalues with negative real parts. The boundedness of V_b is immediately apparent because of the saturated boundedness of V_r. And, because V_b is bounded, V_p is also bounded.

3.2.2.2 Existence of Limit Cycles

Predicting the presents of limits cycles in systems with "hard" nonlinearities like saturation or rate limiting elements has been performed for many years through the use of methods based on the sinusoidal input describing function. The describing function method is an approximating technique that allows one to predict a range of controller gains for which a system will likely not exhibit limit cycles. Because of the approximate nature of the technique, three kinds of inaccuracies are possible [22]:

1) The amplitude and frequency of the predicted limit cycle are not accurate.
2) A predicted limit cycle does not actually exist.
3) An existing limit cycle is not predicted.

Historically, the describing function method has been used on systems with exactly one nonlinear element. Recently, new studies have been conducted to better understand limit cycles that may exist due to multiple nonlinear elements [23]. For a system with simultaneous rate limiting and saturation blocks in the loop, Amato et. al. showed that the response of the nonlinear elements to a sustained sinusoidal input may be divided into twelve distinct classes, each of which has it's own unique describing function [24]. Ten of the twelve describing functions are dependant on both the amplitude of the limit cycle, as well as the frequency. Therefore, to conduct a describing function analysis of the system in Figure 46, one would have the nontrivial task of conducting twelve separate analysis, ten of which are made more difficult because of the dependence on the limit cycle frequency. The addition of the switching element compounds the difficulty.

In light of the fact that a successful describing function analysis of the system would yield approximate results at best, in addition to the fact that such an analysis would prove to be tedious and lengthy, a more straight forward approach to obtaining a range of acceptable controller gains is through simulations and experimental verification.

The bridge response to a commanded change in position of two meters was repeatedly simulated as the proportional gain, K_p, was varied between 0.2 and 8. During the simulations, the derivative gain, K_d, was held constant at 0.25. To determine whether the selected gains sustain a limit cycle, the settling time of the bridge response, as well as

the maximum overshoot of the bridge response was recorded for each trial. These results are shown in Figure 47a and Figure 47b, respectively.

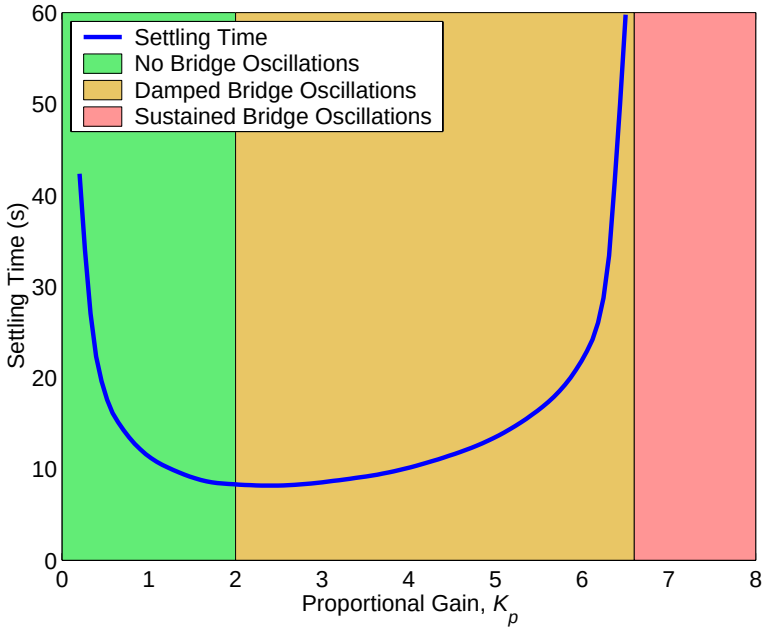

a) Simulated settling time for the positioning control module.

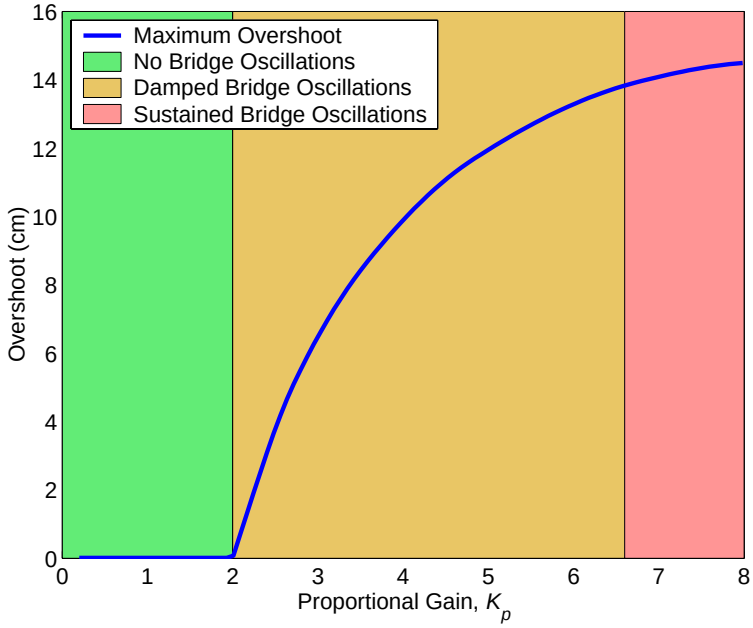

b) Simulated bridge overshoot for the positioning control module.

Figure 47: Simulated maximum overshoot and settling time for the bridge.

Characteristic of a sustained limit cycle is an infinite settling time and a nonzero overshoot. The simulated crane response exhibited both of these features when the proportional gain, K_p, was increased above 6.6. This range of proportional gains is shown in the red regions of Figure 47. The orange regions show the range of proportional gains for which the bridge responded with finite settling times and non-zero overshoots. The green regions show the values of the proportional gain where the bridge responded with no oscillations.

A family of the curves shown in Figure 47 was generated by varying the value of the derivative gain, K_d. These are shown in Figure 48. The solid, dashed and dash-dotted lines on the figures correspond to derivative gains of 0.25, 0.50, and 0.75, respectively. These figures predict that as the derivative gain is increased, the range of proportional gains for which a limit cycle will not be sustained is also increased.

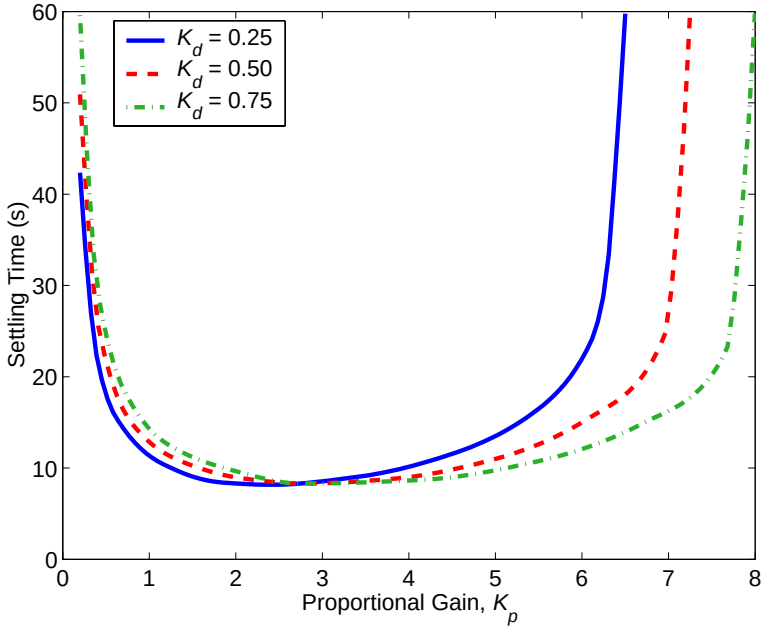

a) Simulated settling time for the positioning control module.

Figure 48: Simulated maximum overshoot and settling time for the bridge for different derivative gains.

(Continued on next page)

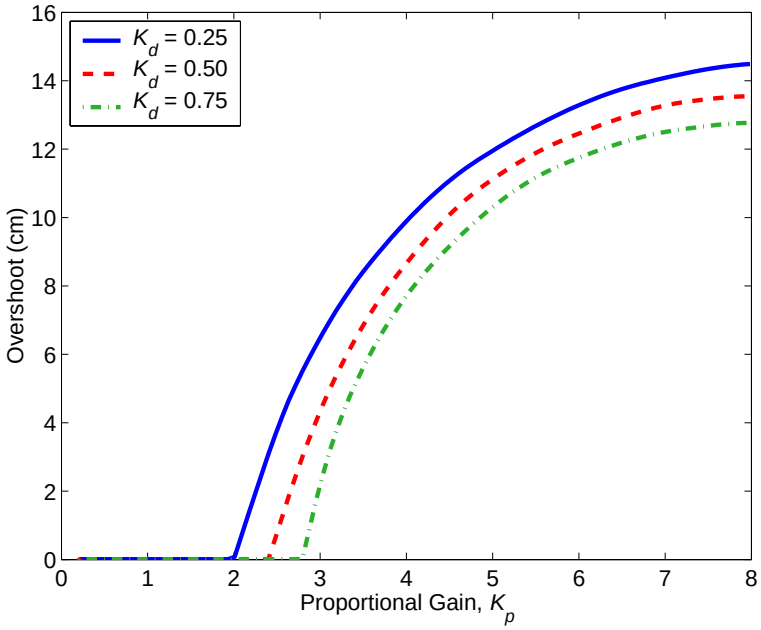

b) Simulated bridge overshoot for the positioning control module.

Figure 48: Simulated maximum overshoot and settling time for the bridge for different derivative gains.

3.2.3 Experimental Results

The acceptable range of controller gains predicted through the simulations was verified experimentally on the 10-ton bridge crane. The 2-meter commanded move was issued to the crane while coordinate information about the bridge was collected. The data was later analyzed to determine the settling time for each combination of proportional and derivative gains tested. These results are shown in Figure 49. The circles, triangles, and squares correspond to a derivative gain of 0.25, 0.50, and 0.75, respectively. For reference, the simulated settling times have been overlaid with the continuous lines. This figure reveals a close correlation between the predicted and actual settling times and verifies the non-existence of limit cycles for certain gain combinations.

Gain combinations that prevented limit cycles in the tested 2-meter crane movements will also prevent limit cycles for any arbitrary move distance. This is because limit cycles are only induced around the equilibrium vicinity of the commanded final bridge position, and not in the transient positions of the crane.

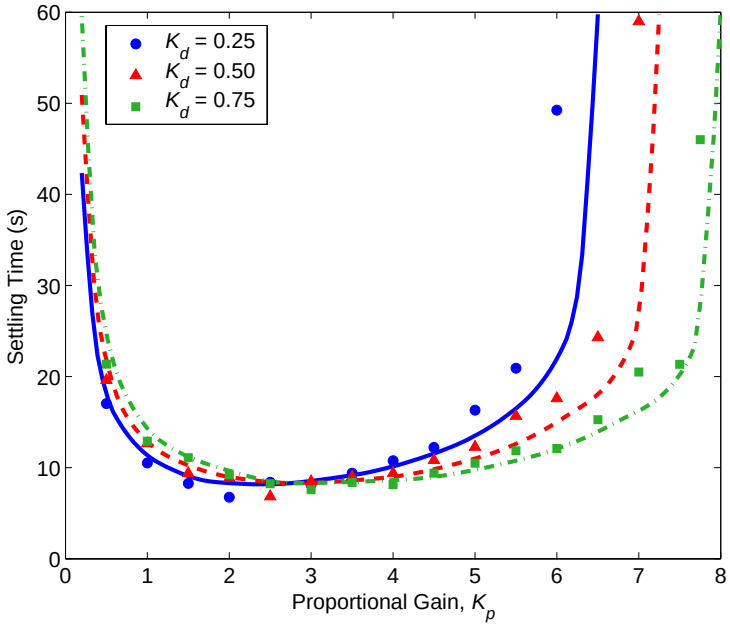

Figure 49: Experimental settling times for the positioning control module overlaid with the simulated settling times.

The positioning performance of the control module was verified by allowing the control to drive the crane to 25 arbitrary reference positions within the workspace of the crane. For each of the 25 trials, the crane's initial position was changed. After each trial, the error between the final and commanded position was recorded.

The response of the crane to a typical position command is shown in Figure 50. For this experiment, the crane started at the 0-meter location and was then commanded to move to the 2-meter location. The dashed curve of Figure 50 shows the simulated response of the bridge. The experimental response is overlaid with the solid curve. The derivative gain, K_d, used in the control was set to 0.25. The proportional gain, K_p, was selected by using the graphs from Figure 47a and b. Specifically, the gain was selected that had the minimum settling time within green region of the graphs. In this way, it was expected that the bridge would have a fast response while exhibiting no oscillations.

Figure 50 demonstrates that the bridge performed as predicted, exhibiting no oscillations and having a response very nearly equal to the simulated response. Furthermore, the final position of the bridge was within 5 millimeters (mm) of the commanded position.

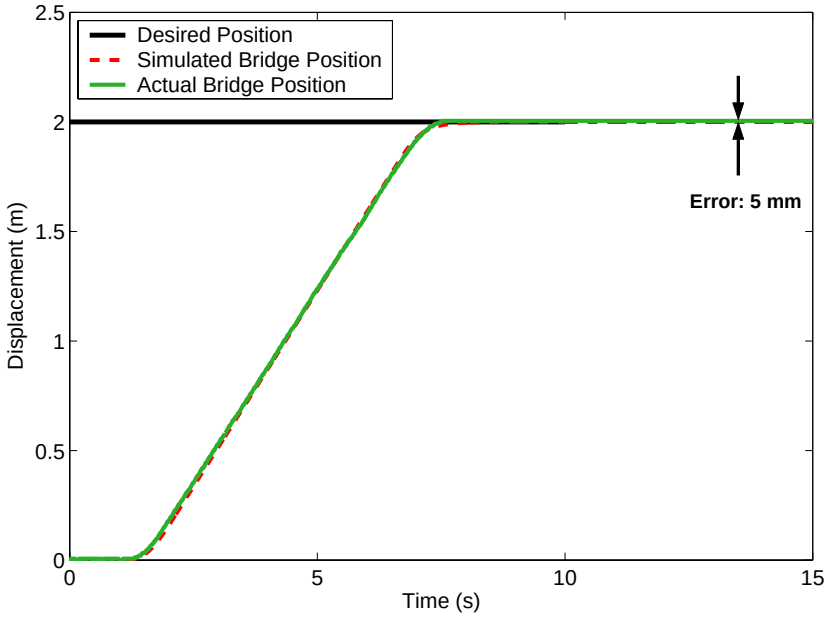

Figure 50: Actual and simulated bridge response to a reference command of 2 meters.

The positioning error result for each of the 25 trials is shown in Figure 51. In each case, the steady state error was less than 11mm.

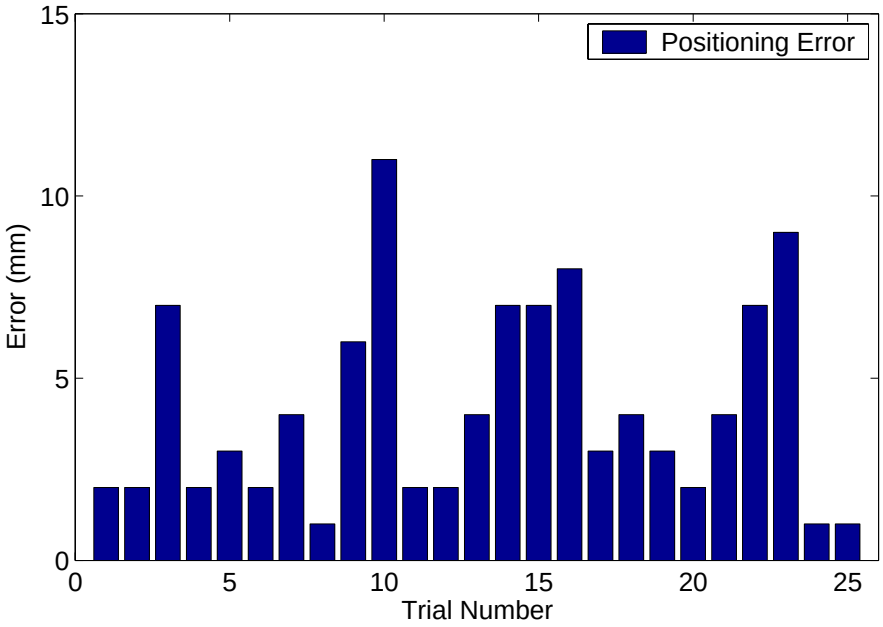

Figure 51: Positioning error for random moves throughout the crane workspace.

3.2.3.1 Controller Effects on Payload Oscillations.

The PD bridge control module has no mechanism, such as an input shaper, to control the oscillations of the payload. For this reason it can be assumed that, in general, the payload will have considerable residual sway. This is evident in Figure 52 where the position of the hook is overlaid with the previous experimental results.

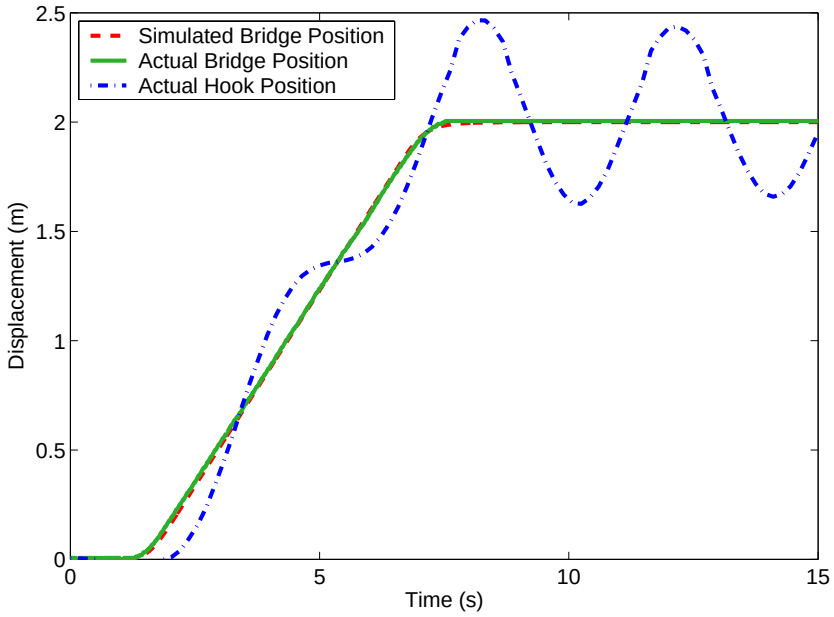

Figure 52: Actual and simulated bridge response to a reference command of 2 meters with the position of the hook shown.

3.2.4 Module Summary

A PD control module has been developed to precisely position the bridge. The positioning capabilities of the control have been shown to be effective throughout the workspace of the crane.

Because of the presents of "hard" nonlinearities in the controller and the controlled plant, one must address the potential existence of limit cycles. Simulations have predicted a range of controller gains that will not induce sustained limit cycles into the system. Further, these simulations also aid in the selection of appropriate controller gains. Experimental tests verified the theoretical predictions. The control module contains no mechanism for reducing payload oscillations. Therefore it would likely not improve the safety or efficiency of crane operation if implemented on its own.

The control was easily implemented on the crane by the addition of a single sensor to measure the position of the bridge. The PD control was programmed using Visual Basic running on a Windows based computer; communication between the crane and the computer was established by an industrial Ethernet connection.

3.3 DISTURBANCE-INDUCED OSCILLATION CONTROL MODULE

A control module was designed to eliminate the cable sway caused by external disturbances acting on the payload, such as wind. This type of disturbance alters the cable angle of the payload, θ_p. For this reason, the disturbance may be modeled as inducing a disruptive angle, θ_d, summed with the undisturbed angle, θ_p, to produce the actual cable angle of the system, θ_a. A disturbance of this sort is schematically illustrated in Figure 53.

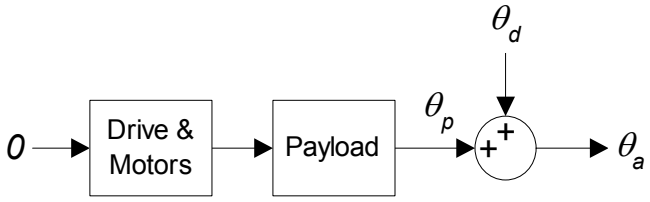

Figure 53: External disturbance affecting the output angle of the payload.

3.3.1 Control Module Design

A first step toward eliminating the oscillations resulting from disturbances was to implement a PD controller based on the sensed payload angle, θ_a. The control generates a correcting velocity signal that causes the overhead support unit to absorb the energy of the disruptive oscillations. A block diagram of this control strategy is shown in Figure 54, where the corrective velocity signal is V_c. To maintain the velocity limit, a saturation block truncates excessive reference velocities prior to being sent to the drives and motors.

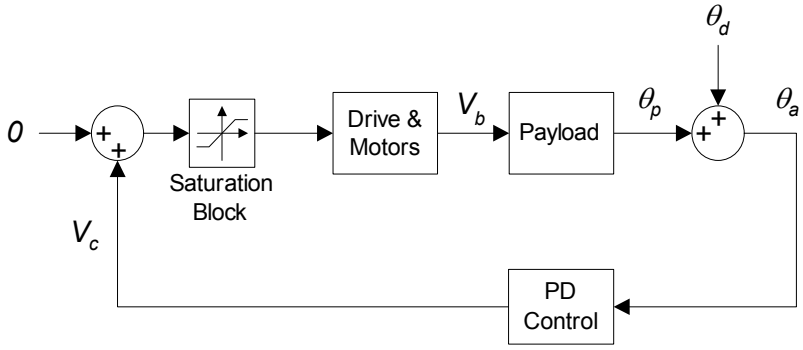

Figure 54: Disturbance rejection control module.

3.3.2 Stability Analysis

The stability of the control shown in Figure 54 may be determined in a similar way to that of the positioning control of the preceding section. First, the BIBO stability of the payload plant and the drive and motors plant is considered. Secondly, given the saturation block preceding the drive and motors model and the dual nonlinear elements within the drive and motors model, one must also be concerned about the existence of limit cycles.

3.3.2.1 BIBO Stability

From the analysis of Section 3.2.2.1, the BIBO stability of H, the second-order plant in the drive and motors model, as well as the payload plant was established. Then, for any bounded input into each of these plants, the outputs will also be bounded. Due to the presents of the saturation block in the disturbance control, the drive and motors will always have a bounded input, and because the output of the drive and motors is bounded, the angle, θ_p, will always be bounded. If the assumption is made that only non-infinite disturbances will act on the system, then one is assured that the output of the system, θ_a, is always bounded. Therefore, one may conclude that the system of Figure 54 is BIBO stable.

3.3.2.2 Existence of Limit Cycles

A similar approach was used to predict the presents of limit cycles in the disturbance control module as was used in Section 3.2.2.2 for the positioning control module; a range of controller gains for which the system will not sustain limit cycles was predicted through simulations and experimentally verified.

The control module was simulated using Simulink. A disturbance was modeled that caused the cable angle to be initially displaced from the vertical by approximately 7 degrees. The action of the feedback control attempted to restore this displacement back to zero. The response of the system to the disruption was repeatedly simulated for different values of proportional gain, K_p, and derivative gain, K_d. To determine whether the selected gains sustain a limit cycle, the settling time of the simulated bridge response was recorded. These results are shown in Figure 55. Specifically, the settling times of the bridge for a derivative gain of 1, 2, and 3 are shown with the solid, dashed, and dash-

dotted lines, respectively, as the proportional gain is varied from 0 to 16. The figure predicts that as the proportional gain is increased from zero to some nominal value, the settling time reaches a minimum. As the proportional gain is further increased beyond the nominal value, the settling time increases without bound, a characteristic of a sustained limit cycle. Therefore, for a given derivative gain, a proportional gain may be selected for which limit cycles will not be sustained and the settling time for the bridge will be minimized.

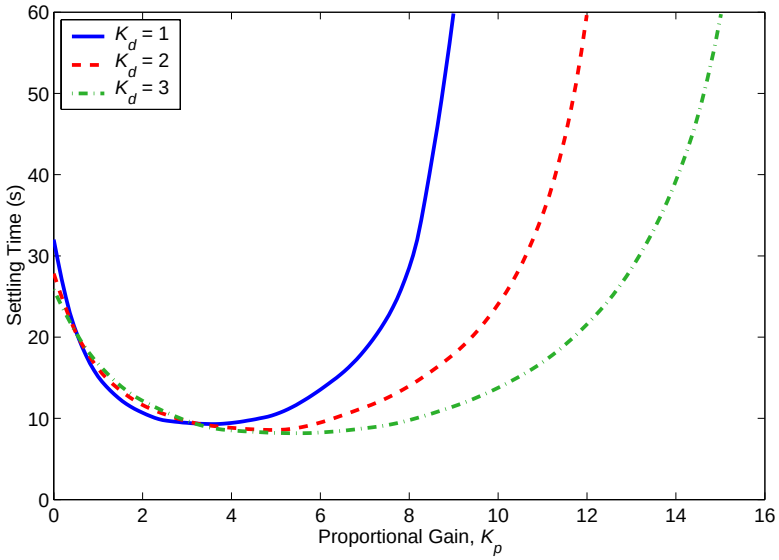

Figure 55: Simulated settling times for the disturbance rejection control module.

3.3.3 Experimental Results for the Disturbance Rejection Control Module

The disturbance rejection properties of the control module were tested experimentally on the actual bridge crane for several combinations of proportional and derivative gains. For each permutation of gains tested, an external disturbance was allowed to act on the payload that caused the cable to be displaced from the vertical by approximately 7 degrees. While the control attempted to eliminate the oscillations resulting from the applied disturbance, coordinate information about the bridge and the payload were recorded and later analyzed to the determine how quickly the control action eliminated the disturbance. A result typical of the experiments is shown in Figure 56, where the derivative and proportional gains were both set to 3. The bridge position, shown with the solid line, is overlaid with the payload position, shown with the dashed line. The feedback control was turned on at time $t = 7$ seconds. The oscillations of the payload

were damped out by time $t = 18$ seconds. This 11-second settling time coincides with the prediction shown in Figure 55. Note that although the control eliminated the external disturbance, it did not return the bridge to its starting position.

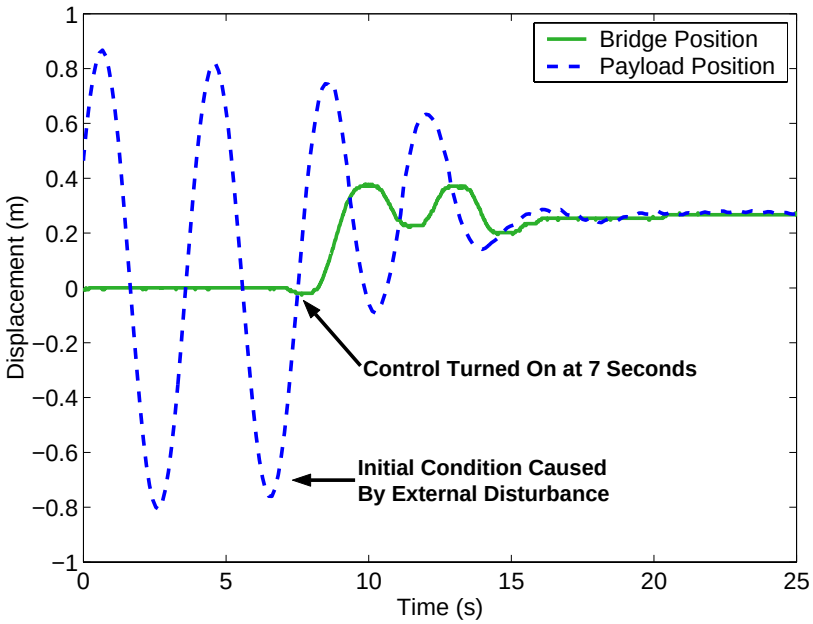

Figure 56: Cancellation of disturbance induced oscillations.

The settling times of the bridge for the different combinations of proportional and derivative gains tested are shown in Figure 57. The circles, triangles, and squares correspond to derivative gains of 1.0, 2.0, and 3.0, respectively. For reference, the simulated settling times are shown with continuous lines. This figure reveals a close correlation between the predicted and actual settling times and verifies the non-existence of limit cycles for a large range of gain combinations.

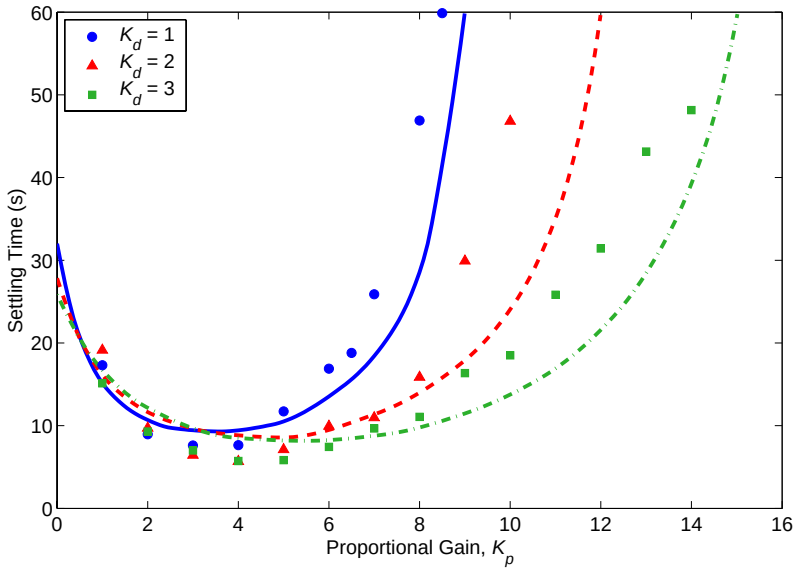

Figure 57: Experimental settling times for the disturbance rejection control module overlaid with the simulated settling times.

3.3.4 Effects of an Input Shaped Velocity Input

The control module shown in Figure 54, with the zero velocity input at the left hand side, acts as a regulator, continually driving the crane to absorb the disruptive oscillations caused by external disturbances. That is, in its current state, the control commands the crane to remain stationary until an angular displacement of the payload is detected. Only at this time does the crane move under the guidance of the control. A more practical application of a disturbance rejection controller would be to allow the crane to follow some desired velocity profile, while also rejecting disturbance related oscillations. In this way, the crane may be used for constructive purposes other than simply rejecting disturbances. In order to accomplish this, the zero velocity input at the left hand side of the control must be replaced by some desired velocity.

If a non-zero velocity input were present at the left hand side of the control, then the control would seek to eliminate motion-induced oscillations, as well as any disturbance-induced oscillations. A natural question arising from this circumstance is what effects would the feedback control have on an input-shaped velocity profile. Would the benefit of input shaping to eliminate the motion-induced oscillations be preserved?

To address how the control system reacts to a shaped input, we may consider the open-loop block diagram of Figure 58a and the block diagram of the disturbance

rejection control module shown in Figure 58b. For each, V_s is a shaped step input, optimally designed to eliminate oscillations in each respective system. For the disturbance control module, V_s also has maximum and minimum values that are within the thresholds of the saturation block. An important difference between the two control schemes is the signal directly entering the drive and motors plant. For the open-loop case, this signal is V_s, the shaped step command itself; for the disturbance rejection controller, this signal is X, the shaped step command that has been modified by V_c, and truncated by the saturation block.

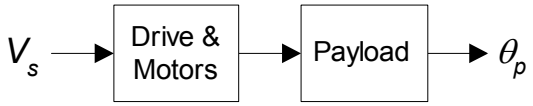

a) Open loop block diagram.

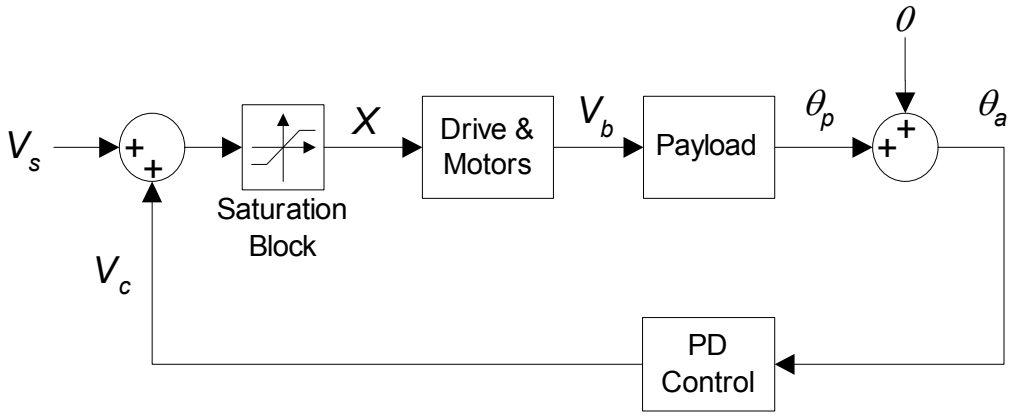

b) Disturbance rejection control module with non-zero input.

Figure 58: Comparison of open-loop and disturbance rejection block diagrams.

The solid and dashed lines of Figure 59a show the shaped input, V_s, and simulated angular response, θ_p, for the open-loop system. The vertical axis on the left hand side of the plot corresponds with the shaped input; the vertical axis on the right hand side of the plot corresponds with the angular response. As expected, the system responds by exhibiting one-half period of oscillation, at which point the input shaped signal eliminates the remaining oscillations. The displacement of the response at the beginning of the move is needed in order to cause the velocity of the payload to coincide with that of the overhead support unit. In contrast, oscillations caused by external disturbances tend to amplify the difference between the payload velocity and overhead support unit velocity.

In this sense, angular displacements caused by shaped motion are desired and advantageous, whereas angular displacements caused by disturbances are undesired and disruptive.

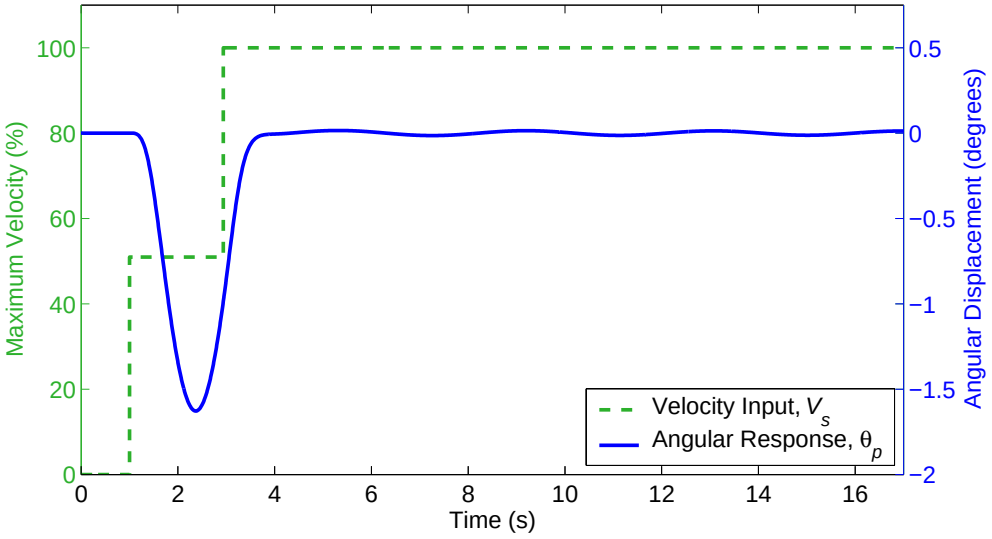

a) Simulated input and response for the open-loop system.

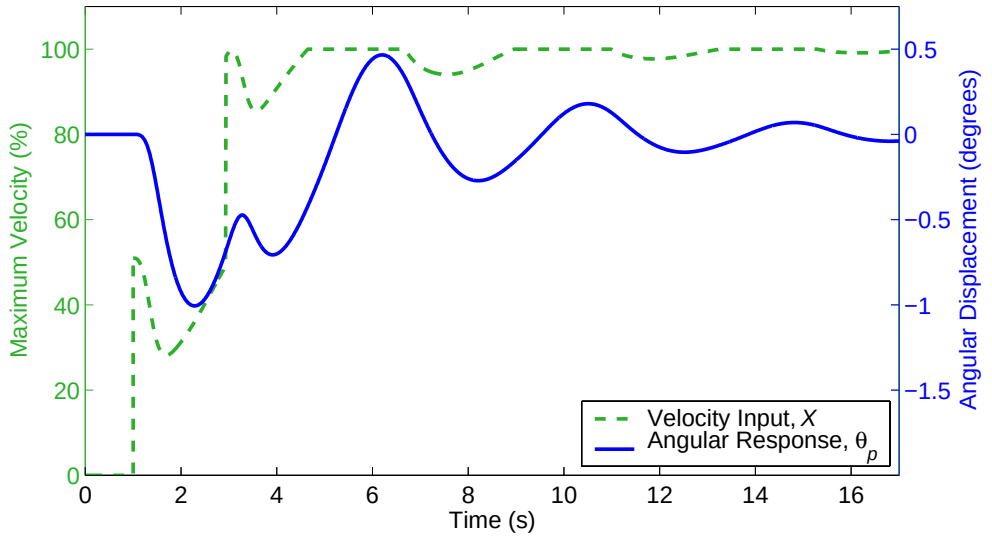

b) Simulated input and response for the disturbance rejection system.

Figure 59: Comparison of open-loop control to disturbance rejection control in response to shaped inputs.

The disturbance rejection control cannot distinguish between the desired angular displacements caused by shaped motion and the disruptive displacements caused by disturbances. For this reason, the control attempts to eliminate the desired deflections just

at it would the disruptive ones. As a result, the signal, X, directly entering the drives and motors is notably altered from the shaped input, V_s, thereby also altering the response, θ_p, of the payload. These adverse effects are shown in Figure 59b. Again, the dashed line represents the input into the drives and motors. The simulated angular response to this signal is shown with the solid line. One may notice that the disturbance rejection control *does* achieve the objective of restoring the angular displacement of the payload to zero, however it is less effective than simply allowing the shaped input to run its course. Further, the velocity input, X, is more agitated than the simply shaped input, V_s, inducing greater actuator effort.

Given that input shaped reference velocities are adversely altered by the control module, it would be advantageous if the control could distinguish between the desired payload displacements caused by shaped commands and the disruptive oscillations caused by external disturbances. In this way, the control may react only to restore disturbance-induced oscillations and not those induced by shaped motion.

3.3.5 Model-Augmented PD Control of Cable Angle.

A modification to the disturbance rejection control module provides a feature by which the control may distinguish between motion-induced oscillations and disturbance-induced oscillations. Figure 60 shows a block diagram of the modified control scheme. The control scheme includes the addition of a *model* of the drive and motors, and a *model* of the payload dynamics. These elements are shown with the blue blocks and text at the top of the figure. For emphasis, these blocks are contrasted with the *actual* drive and motors and the *actual* payload plant; these elements are shown with the green blocks and text at the center of the figure.

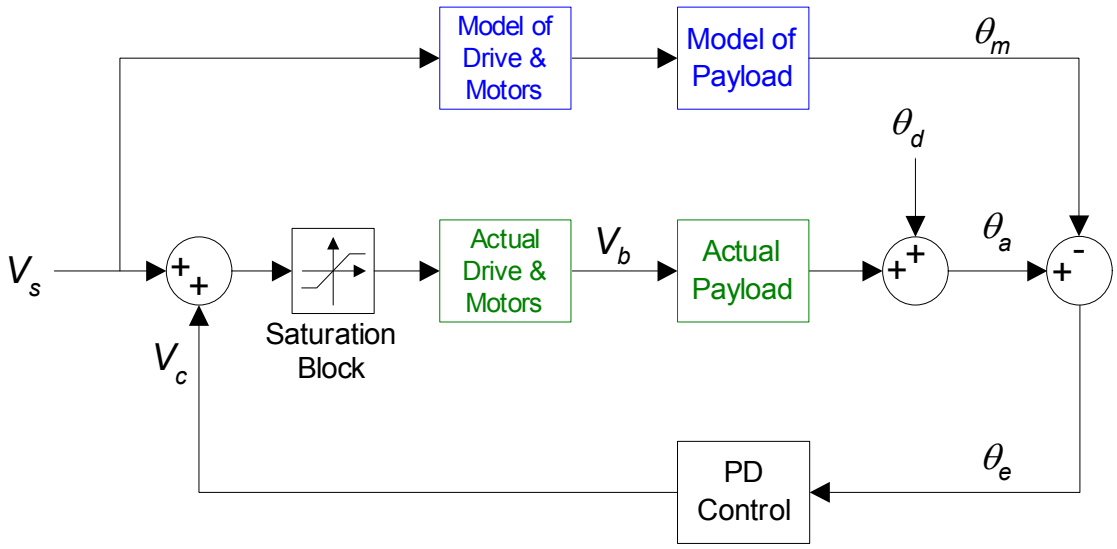

Figure 60: Model-augmented disturbance rejection control module.

Assume that a shaped reference velocity, V_s, has maximum and minimum values that are within the thresholds of the saturation block. Then, in the absence of any disruptive angle, θ_d, the response of the model, θ_m, and the response of the actual system, θ_a, to the reference velocity, will be nearly equal. Any differences will arise exclusively from inaccuracies in modeling parameters and sensing errors of the actual cable angle. As a result, no corrective velocity signal will be generated from their difference, θ_e. If, however, a disturbance is present, then the comparison of θ_m to θ_a will allow the feedback control to generate a correcting signal. A correcting signal could also be generated in the absence of a disturbance if there are gross inaccuracies in modeling parameters or sensing errors of the actual cable angle. Any corrective velocity signal generated is added to the shaped reference velocity signal, and subsequently sent to the actual crane system. By the principle of superposition, the combined commands allow the crane to accomplish two objectives: reject disturbance-induced oscillations, and track the reference velocity.

It should be noted that the principle of superposition, in the strictest sense, does not hold for the system in Figure 60 because this system contains a series of hard nonlinearities. Namely, these elements are the saturation block preceding the actual drive and motors, and the nonlinearities within the actual drive and motors. The reason that the system behaves as if holding to the principle of superposition is because of the nature of the combined velocity signals. By V_s being within the upper and lower thresholds of the

saturation block, and because V_c is oscillatory in nature, the combined signal remains within the linear regions of the nonlinear elements for significant portions of time. During these periods, the system is linear, allowing the combined signal to contribute to the objectives of disturbance rejection and velocity tracking.

3.3.6 Experimental Results for the Model-Augmented Disturbance Rejection Control Module.

The model-augmented disturbance rejection control module was implemented and tested on the actual bridge crane. To evaluate how well the control distinguished between motion-induced and disturbance-induced oscillations, a step command from 0% velocity to 100% velocity was shaped by a ZV input shaper and used as a reference command. The control, seeking to eliminate the disturbance-induced oscillations, generated a corrective velocity signal in response to the *difference* between the actual cable angle, θ_a, and the cable angle generated from the model of the system, θ_m. The corrective velocity signal was added to the shaped reference velocity to produce the signal, X.

Figure 61a shows the velocity and angular displacement signals. The vertical axis on the left hand side of the plot corresponds to the velocity signals sent to the drive and motors; the vertical axis on the right hand side of the plot corresponds to the angular response of the crane. For comparative purposes, an identical experiment was conducted using the unmodified disturbance rejection controller; these results are plotted in Figure 61b.

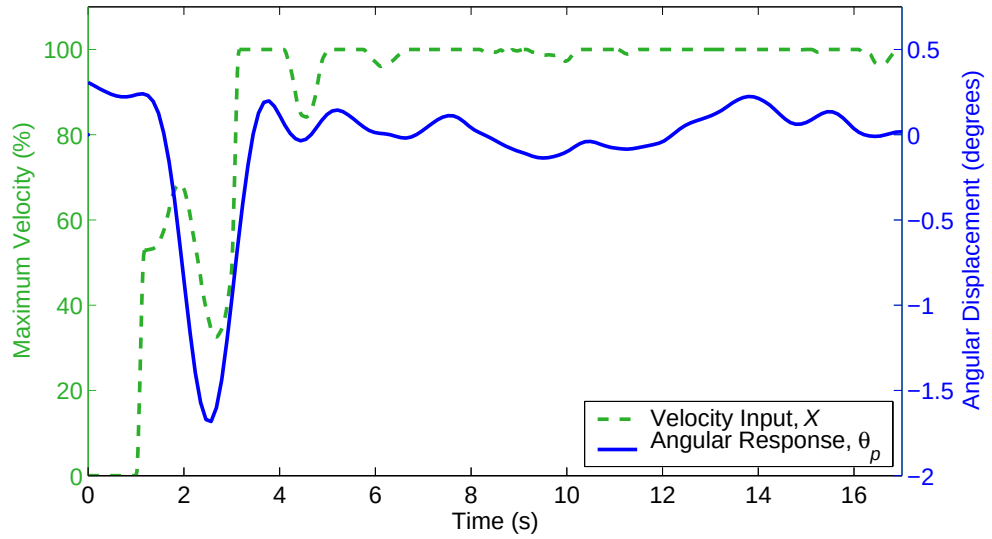

a) Performance of the model-augmented disturbance rejection control module.

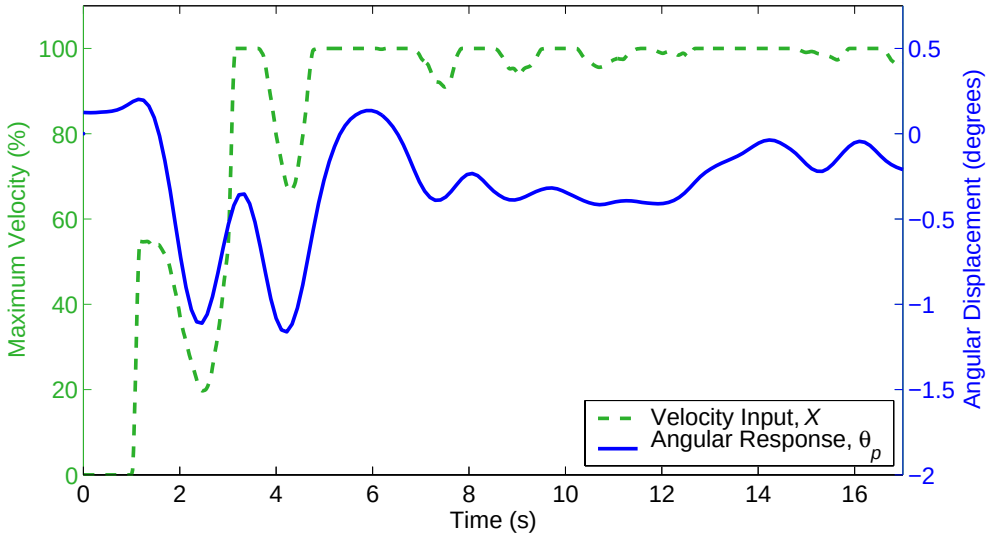

b) Performance of the unmodified disturbance rejection control module.

Figure 61: Comparison of the experimental performance of the model-augmented and unmodified disturbance rejection control modules.

As expected, the angular response of the crane under the guidance of the modified controller (solid line of Figure 61a) is comprised of one-half period of oscillation followed by relatively little movement. In contrast, the angular response of the crane under the guidance of the unmodified controller (solid line of Figure 61b) is more oscillatory, taking approximately four seconds longer to settle around zero degrees.

The contrast between the angular response from the two figures indicates that the model-augmented control module is effective a distinguishing between motion-induced oscillations and disturbance-induced oscillations. However, observation of the captured velocity profiles does show that the modified control still attempts to cancel some portion of the motion-induced oscillations. This phenomenon is most heavily attributed to imprecise measurements of the cable angle coupled with time delays in the system.

3.3.7 Module Summary

A control scheme has been developed that enables the controlled system to track a shaped reference velocity, while also rejecting disturbances. A key feature of the control is its ability to distinguish between motion and disturbance-induced oscillations of a payload. This distinction enables the control to generate corrective velocity signals only in response to disruptive payload displacements instead of desired payload displacements caused by shaped motion of the crane.

Limit cycles that may be induced into the system because of "hard" nonlinearities in the controller and the controlled plant are addressed by simulations that predict safe controller gains. The predictions are experimentally verified.

The control module is suitable for tracking shaped velocity profiles and eliminating external disturbances. Therefore, it would not be useful for payload positioning if implemented on its own.

The control was implemented on the crane by the addition of a machine vision system to provide measurements of the hook position. The PD control was programmed in the same manner as the positioning module of Section 3.2. Communication between the vision system and the computer was established by an industrial Ethernet connection.

CHAPTER 4

COMBINING THE CONTROL MODULES

The three control modules developed in Chapter 3 are shown in Figure 62a through c. Using the input shaping control module, any arbitrary reference velocity, V_r, can be shaped by an input shaper designed to cancel oscillations in the payload plant. The resulting shaped signal, V_s, will eliminate the motion-induced oscillations of the payload. In Section 3.1.3.2, the effects of the drive and motors on the shaped signal were considered; it was shown that the drive and motors will inhibit the oscillation reducing capabilities of ZV-shaped signals only when transitional velocity commands are issued, and then only to a small degree. Section 3.1.4.1 showed that using a ZV input shaper is more effective at reducing oscillations over the entire range of cable lengths than a UM-ZV shaper, although the UM-ZV shaper yields a faster rise time.

In Section 3.2, a bridge positioning control scheme was developed. It was shown that because the payload always comes to rest beneath the overhead support point, that an easily implementable bridge-position based control could be implemented, rather than a more difficult payload-position based control. The error between the desired bridge position and the actual bridge position is used to generate a reference velocity, V_r. As the crane tracks this velocity, it will be driven toward the desired set point.

Finally, in Section 3.3, a disturbance rejection control scheme was developed. The key elements of the control are the plant models that respond to the shaped velocity signal. The purpose of these models is to provide a means by which payload oscillations caused by external disturbances may be distinguished from payload oscillations caused by motion of the overhead support unit. This distinction allows the feedback control to generate a corrective velocity signal based only on the disturbance-induced payload oscillations. Given that the corrective velocity signal, V_c, is oscillatory in nature, and that the shaped velocity signal, V_s, is restricted to be within the minimum and maximum thresholds of the saturation block, we may be assured that the dual objectives of disturbance rejection and velocity tracking will be accomplished.

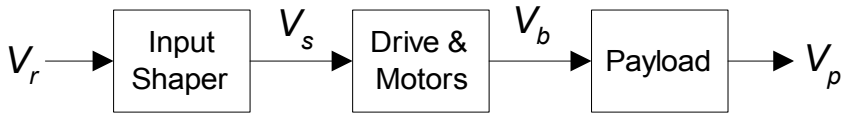

a) Input shaping control module.

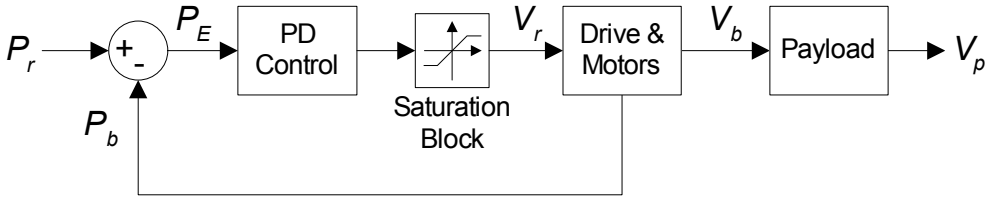

b) Position control module.

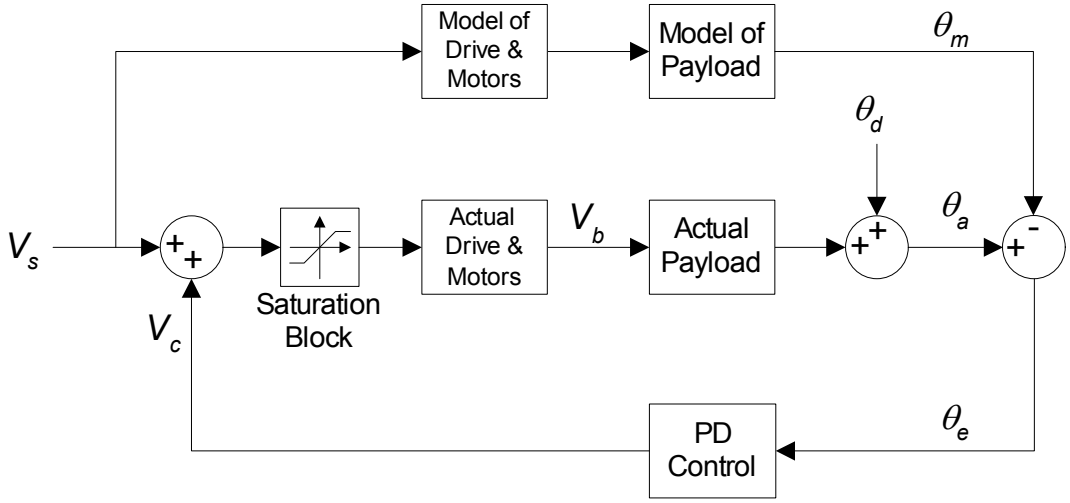

c) Disturbance rejection control module.

Figure 62: Individual control modules.

This chapter presents an architecture in which the three individual control modules are joined to form one complete control scheme. In doing so, the combined controller will possess the collective attributes of the individual controllers, namely, suppression of motion-induced oscillations, precision positioning capabilities, and the capacity to reject disturbance-induced oscillations.

As a first step in describing how the three modules may be combined, Section 4.1 first combines the input shaping module with the positioning module. Later, Section 4.2 adds the disturbance rejection control module. Both theoretical and experimental data are provided throughout the sections to demonstrate the effectiveness of the combined control strategy.

4.1 COMBINING INPUT SHAPING AND POSITIONING CONTROL MODULES

The positioning control of Figure 62b generates a reference velocity, V_r, which drives the bridge toward a desired set point. This signal, though enabling the crane to achieve a desired final position, also induces oscillations in the payload. A more desirable control scheme would allow precise positioning of the crane, while also eliminating these motion-induced oscillations. To this end, the input shaping control module of Figure 62a has been incorporated with the positioning control module of Figure 62b. The combined control scheme is shown in Figure 63.

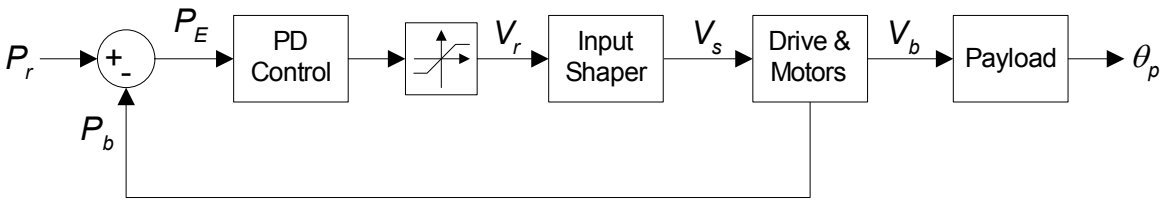

Figure 63: Combined input shaping and positioning controller.

In this combined scheme, the PD control still generates a signal, V_r, which drives the crane toward a desired position; however, this signal is now used as the input to the input shaping control module, to produce a shaped signal, V_s. In this way, the shaped signal serves the dual purpose of driving the crane toward a desired position, while also preventing motion-induced oscillations in the payload.

With the insertion of the input shaper into the forward path of the positioning control loop, the question of system stability arises. This is because the input shaper effectively delays a portion of the signal by a time equal to the duration of the shaper.

4.1.1 Stability of Shaper-in-the-Loop Systems

In Sections 3.1 and 3.2, two analysis tools were used to determine the stability of the positioning control module and disturbance rejection control module, namely, the BIBO stability analysis, and a simulation/experimentation technique that determined the existence of limit cycles. These tools may again be used to investigate the stability of the shaper-in-the-loop system. Here, the details of the analysis are forgone and the results are briefly stated.

From the BIBO stability analyses of the positioning control module conducted in Section 3.2.2.1, we may ascertain that the addition of the input shaper within the positioning controller does not affect the BIBO stability of the combined control. This is because the shaped signal, V_s, maintains the same boundedness as the unshaped signal, V_r. Also, using the same method presented in Section 3.2.2.2, a range of controller gains, K_p and K_d, may be found for which the combined system does not sustain limit cycles.

In addition to the BIBO stability and limit cycle existence analyses, a third analysis tool is available that gives one a deeper understanding of shaper-in-the-loop systems; we may consider the combined input shaper and positioning control from the perspective of the Laplace domain.

We may begin the analysis by constructing a simplified block diagram of the combined control from Figure 63. The control is simplified by neglecting the three hard nonlinearities, namely, the saturation block, and the nonlinear switch and rate limiter within the drive and motors block. These eliminations yield the entirely linear closed-loop system shown in Figure 64.

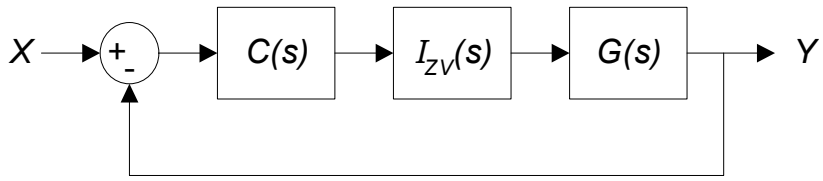

Figure 64: Simplified shaper-in-the-loop system.

Here, *C(s)*, $I_{ZV}(s)$, and *G(s)* are the Laplace representations of the PD control block, a ZV input shaper, and the drive and motors block, respectively.

For *C(s)*, we have

$$C(s) = K_o\left(K_p + K_d s\right), \tag{42}$$

where K_p and K_d are the proportional and derivative gains, respectively, and K_o is an open-loop scaling factor.

For G(s), we have

$$G(s) = \frac{{\omega_H}^2}{s(s^2 + 2\zeta\omega_H s + {\omega_H}^2)}, \tag{43}$$

where ω_H and ζ are the natural frequency and damping ratio associated with the heavily damped system within the drive and motors model.

Recognizing that a ZV input shaper is constituted by an impulse of magnitude A_1, followed by an impulse of magnitude A_2, delayed by time t_2, we may represent the shaper in the Laplace domain as

$$I_{ZV}(s) = A_1 + A_2 e^{-st_2}. \tag{44}$$

With the Laplace representation of each element at our disposal, we may proceed by considering the closed-loop characteristics of the system. In Figure 65, a root-locus plot of the system is shown.

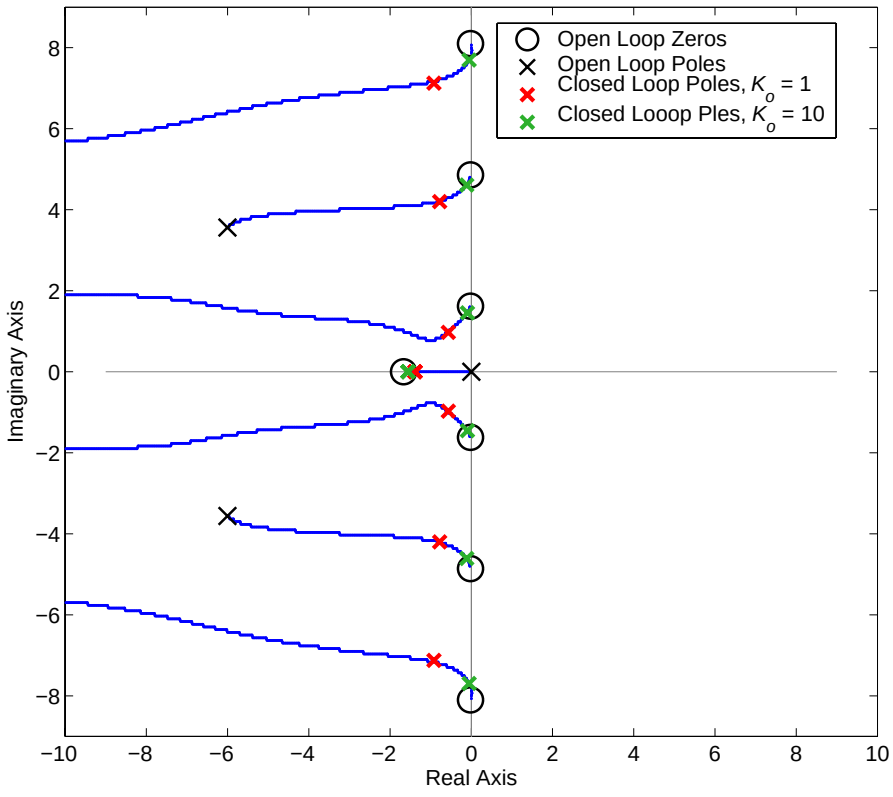

Figure 65: Root locus plot of linearized system.

The open-loop poles, shown with the black X's, are contributed by the transfer function, *G(s)*. The input shaper contributes an infinite column of open-loop zeros along the imaginary axis, shown with the black circles. And finally, *C(s)* contributes a single open-loop zero with negative real part, also shown with a black circle. The closed-loop poles of the system correspond to a proportional and derivative gain 0.8 and 0.5, respectively; these poles are represented by the red X's when the scaling gain was set to 1.0 and by the green X's when the scaling gain was set to 10.0.

The significant feature of this root-locus plot is that the poles of the closed-loop system remain strictly in the negative left-hand plane for the range of scaling gains shown. For the input shaper to cause instability in the shaper-in-the-loop system, these closed-loop poles would have to be in the positive right-hand plane. Therefore, we may be assured, at least for the linearized system of Figure 64, of stability.

The Laplace domain analysis does not provide confirmation of the stability of the nonlinear system in Figure 63, it does, however, serve to provide insight into the dynamics of shaper-in-the-loop systems in general. It also gives one an understanding of how the system in Figure 63 performs when operating in its linear region[3].

4.1.2 Experimental Results

The positioning and oscillation reducing properties of the control were verified experimentally on the 10-ton bridge crane. An experiment was conducted in a manner identical to that of the positioning experiment in Section 3.2.3. The crane was driven to 25 arbitrary reference positions, while coordinate information about the bridge and payload were gathered. Both the residual oscillation amplitude of the payload and the final positioning error were recorded for each of the 25 trials. A derivative and proportional gain of 0.6 and 0.8, respectively, were used during the trials.

The response of the crane to a typical position command is shown in Figure 66a. For this experiment, the crane started at the 0-meter location and was then commanded to move to the 2-meter location. The solid green curve represents the actual position of the

[3] An initial investigation toward a fundamental understanding of how input shapers affect closed-loop stability was conducted in [25].

bridge throughout the experiment; the dashed blue curve represents the position of the payload. For contrast, a similar plot is shown Figure 66b. This plot represents the position of the bridge and payload under the guidance of the positioning control module alone.

The contrast between these two figures demonstrates the effectiveness of the combined input shaping and positioning controller at precision positioning and minimizing motion-induced payload oscillations.

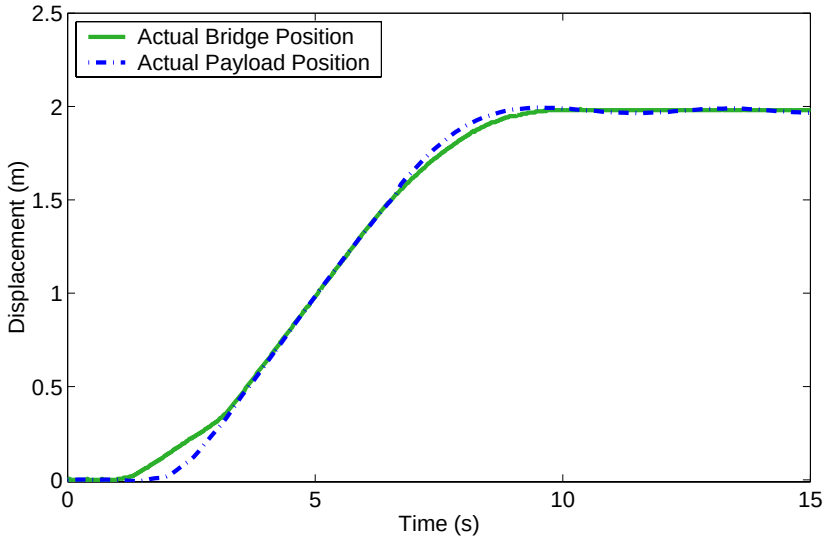

a) Actual crane response using combined input shaper and positioning control.

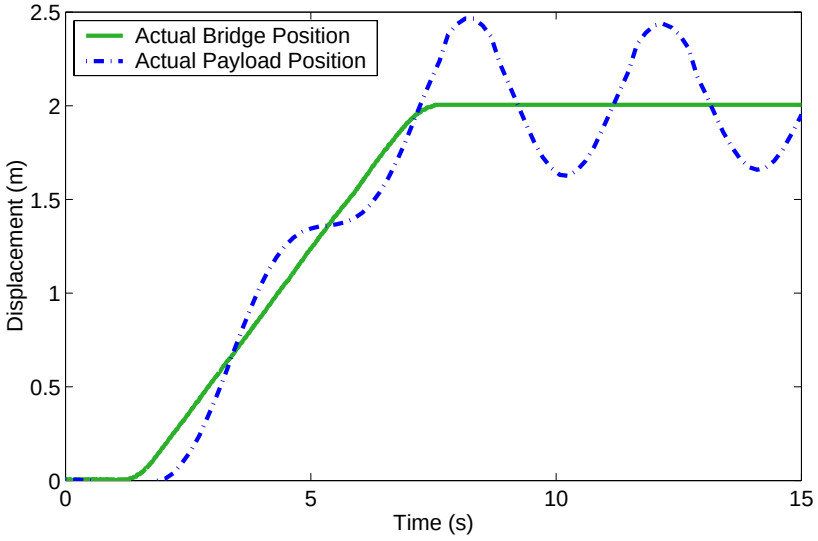

b) Actual crane response using positioning control only.

Figure 66: Performance comparison between the positioning module only and the combined positioning and input shaping controller.

The positioning error result for each of the 25 trials (Figure 67) is shown along with the residual oscillation amplitude of the payload for each of the 25 trials (Figure 68). The vertical axis in Figure 67 represents the final positioning error between the desired bridge position and the actual bridge position. The vertical axis of Figure 68 represents the residual peak-to-peak oscillation amplitude of the payload. Notice that this axis has been normalized to the residual peak-to-peak oscillation amplitude for unshaped crane motion.

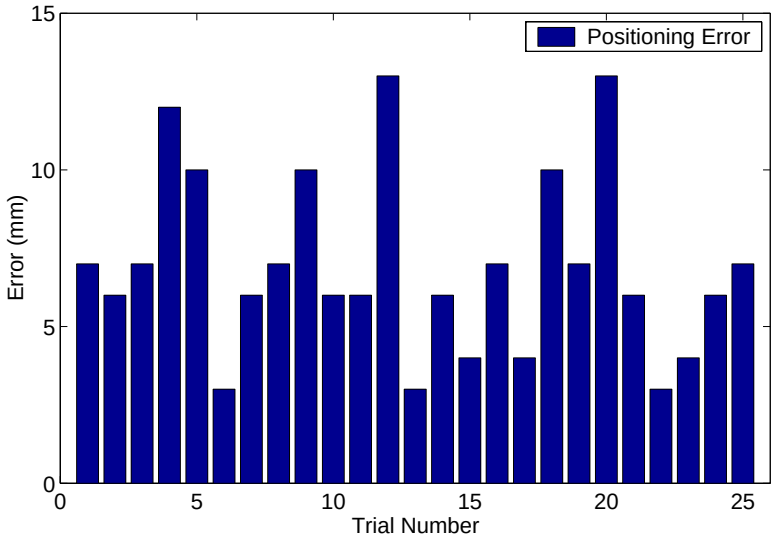

Figure 67: Final positioning error of the crane under the guidance of the input shaping and positioning controller.

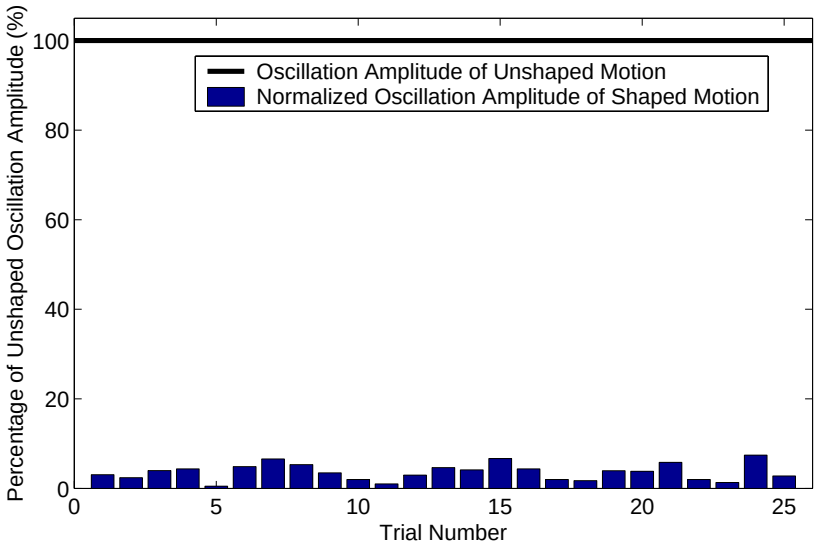

Figure 68: Residual payload oscillation amplitude of the crane under the guidance of the input shaping and positioning controller.

These figures demonstrate that with the implemented control, the crane may be positioned within 13 mm of a commanded position while keeping the oscillations to approximately 5% of the oscillation amplitude normally excited with unshaped motion. The final positioning error may be further reduced beyond what was accomplished here by increasing the proportional controller gain.

4.2 Combining Input Shaping, Positioning, and Disturbance Rejection Control Modules

The disturbance rejection controller from Figure 62c was designed to serve the dual purpose of reference velocity tracking and disturbance rejection. One condition is stipulated on the reference velocity: the minimum and maximum values of the signal must be within the saturation thresholds of the saturation block. This condition assures that the control will operate within its linear region at least some of the time.

A suitable reference velocity for the disturbance rejection controller would be the shaped reference velocity from the combined input shaping and positioning controller. By design, this signal is already bounded between the upper and lower saturation thresholds of the saturation block. Furthermore, it has been shaped to cancel oscillations in the payload plant. To use this signal as the input to the disturbance controller, the disturbance controller may be combined with the input shaping and positioning controller in the manner shown in Figure 69.

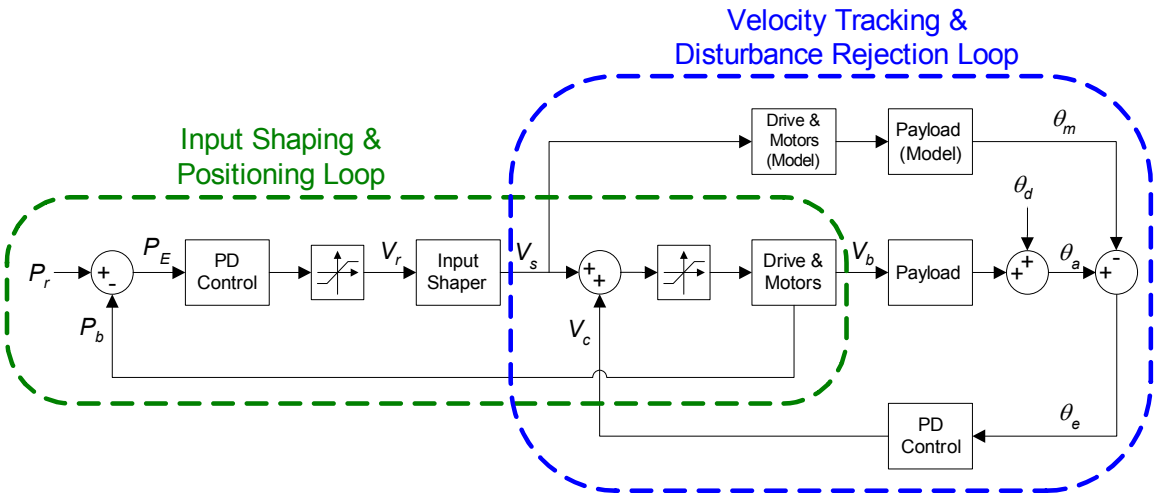

Figure 69: Combined input shaping, positioning, and disturbance rejection controller.

The input shaping and positioning control (shown within the green dashed line) serves to generate a shaped reference velocity that is used as an input to the disturbance rejection control (shown within the blue dashed line). The disturbance rejection control receives the shaped signal, V_s, and tracks it, while also rejecting disturbances. Because V_s continually drives the crane toward a desired set point, the disturbance rejection control will achieve the dual objectives of positioning and disturbance rejection. Furthermore, because V_s is an input-shaped command, motion-induced oscillations of the payload will be reduced. In this way, the combined input shaping, positioning, and disturbance rejection controller (IPDC) eliminates motion-induced oscillations, disturbance-induced oscillations, and enables precise positioning of the payload.

4.2.1 Experimental Results

The IPDC was implemented and tested on the 10-ton bridge crane in the MARC. To evaluate the three attributes of the control, the payload and bridge, were commanded to move 4-meters. After coming to rest at the desired position, an external disturbance was introduced by pushing on the payload. The performance of the controller, in response to this experiment, is demonstrated in the measured results of Figure 70a. The position of the bridge is shown with the solid green line, while the position of the payload is shown in the dashed blue line. One may observe that the shaped velocity signals of the positioning controller prevented motion-induced oscillations of the payload, while also driving the crane precisely to the 4-meter location. Later, when the external disturbance was introduced, the IPDC eliminated the disruptive oscillations while returning the payload to the desired position.

Another experiment was conducted using the IPDC, in which the crane was again commanded to move 4-meters. While in transit, an external disturbance was introduced into the system. The measured results of this experiment are shown in Figure 70b. Again the IPDC prevented motion-induced oscillations, rejected disturbance-induced oscillations, and precisely positioned the payload.

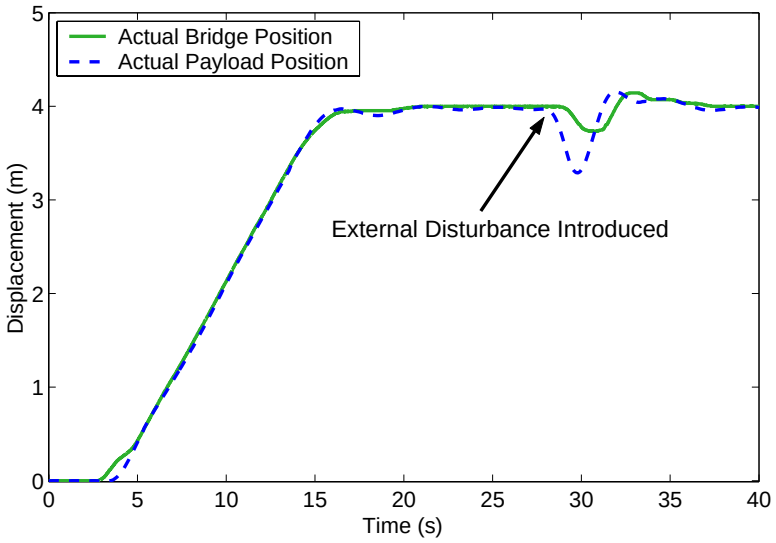

a) Disturbance introduced after crane reached final position.

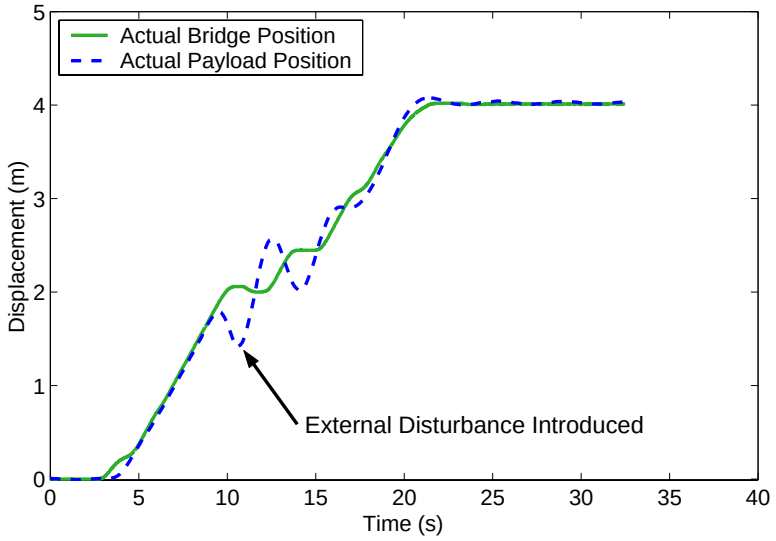

b) Disturbance introduced in transit.

Figure 70: Bridge and payload response under the guidance of the IPDC.

In general, controls engineers are concerned with the stability of a given control scheme, as well as the control effectiveness at accomplishing tasks. The stability of the IPDC is assured for a range of controller gains based on the previous analyses of each of the individual control modules. Furthermore, the experimental results validate the ability of the IPDC to achieve the tertiary objectives of precise positioning, elimination of motion-induced payload oscillations, and disturbance rejection.

4.2.2 Target Tracking

The IPDC relies on sensory feedback of the payload position. The sensor implemented to provide this data is a downward looking machine vision system. One advantage of using a machine vision system in this way is that the potential exists for useful data to be gathered, other than payload coordinate information.

The Siemens vision system used on the 10-ton bridge crane in the MARC has been programmed to actively seek "targets" in addition to its task of sensing hook position. Targets are unique retro-reflective markers that may be placed easily on any surface, such as the top of a potential payload, a vehicle, or the floor. When coordinate information about the targets are sent to the controlling computer, an operator can allow the control to track these targets. The benefit of this feature is that it provides a means by which the crane's hook may be precisely aligned above some non-stationary object, such as a vehicle or potential payload.

An experiment was conducted to demonstrate the effectiveness of IPDC when in a "target tracking" mode of operation. The IPDC was programmed to use coordinate information about a target as the desired reference position. The target was moved around the workspace of the crane. As the crane tracked the target, the position of the payload and bridge were recorded. The measured results of the experiment are shown in Figure 71. Here, the dotted black line represents the moving position of the target. The solid green line and dashed blue line represent the response of the bridge and payload, respectively.

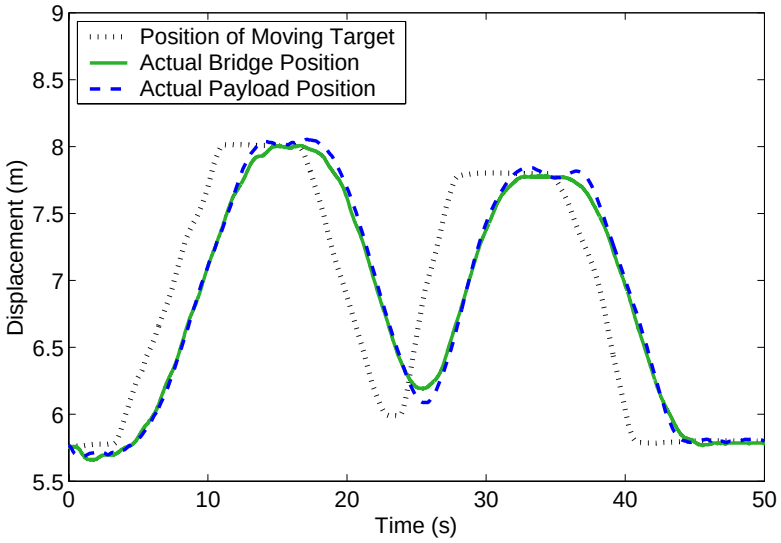

Figure 71: Response of the IPDC to a moving target position.

The ability of the IPDC to follow a non-stationary target is evident from the plot. While tracking the target, the motion-induced and disturbance-induced oscillations are eliminated.

4.3 Interaction between the Control and the Human Operator

Different crane applications may require different operating modes for the IPDC. This section describes manual, partially automatic, and fully automatic modes of operation in which the combined controller may be utilized.

4.3.1 Manual Mode

In cases of infrequent hoisting of irregular objects, where accurate positioning and high efficiency are not essential, a manual mode of operation may be the most appropriate form of control. In manual mode, the position reference signals of the controller are generated when the crane operator depresses the directional buttons of the control pendant. The crane will respond to the operator commands by moving in the direction corresponding to the depressed pendant button. However, because the control is actively input shaping all the operators commands, as well as detecting and correcting external disturbances, the motion of the payload will be free from motion and disturbance-induced oscillations.

4.3.2 Partially Automated Mode

The partially automated control mode is essentially manual operation of the crane that has been enhanced with an automatic positioning feature. This mode of operation may be appropriate, for example, at the Hanford Site in Washington State where radiological packages are regularly stacked in tight matrix formations, requiring positioning accuracy greater than 3 cm. Because of the hazardous content of the payloads, operators often control the cranes remotely, making precise positioning difficult and time consuming.

The partially automated mode allows the motion of the crane to be controlled by the operator's pendent button pushes, just as in manual mode, while the operator attempts to maneuver the crane towards some intended target point. Because of a distant or obstructed view, the operator may have difficulty in driving the crane precisely to the intended destination. Therefore, when the crane is in the proximity of the intended target point, sensors on the crane, such as a machine vision system, will detect coordinate information about the target point. The operator may either continue running the crane in manual mode or use the coordinate information gathered from the sensors as a position reference signal for the control, causing the payload or hook to be driven precisely to the intended destination.

4.3.3 Fully Automated Mode

In fully automated mode, the position set points originate entirely from sensors, a controlling computer, a programmable logic controller, or other programmable or sensing devices. This control mode would be appropriate in highly repetitive tasks or other tasks where the final payload or hook position is known ahead of time. For example, the control could drive the crane to a series of positions that correspond to an array of desired positions programmed into a computer. Once the crane has reached a desired position, it would remain stationary for a programmed period of time (perhaps to conduct hoisting operations) at which time the control would proceed to drive the crane to the next desired position.

CHAPTER 5

CONCLUSIONS AND FUTURE WORK

Bridge and gantry cranes occupy a crucial role within industry. They are used throughout the world in thousands of shipping yards, construction sites, steel mills, warehouses, nuclear power and waste storage facilities, and other industrial complexes. The significant capacity that these systems maintain in the world can hardly be overestimated.

Bridge and gantry cranes are highly flexible in nature, generally responding in an oscillatory manner to external disturbances and motion of the bridge or trolley. In many applications this oscillation has adverse consequences. Swinging of the payload or hook makes precision positioning time consuming and inefficient for an operator. When the payload or surrounding obstacles are of a hazardous or fragile nature, the oscillations may present a safety hazard as well.

The broad usage of bridge and gantry cranes in the last few decades coupled with the need to control unwanted oscillations has impelled a large amount of research pertaining to the control of these structures. Broadly, engineers have sought to control three aspects of crane systems, namely, motion-induced oscillations, disturbance-induced oscillations, and positioning capability. These aspects of crane systems are important because the ease-of-use, efficiency, and safety of crane systems can be significantly improved if controlled successfully. However, the design and implementation of crane control schemes present several challenges to controls engineers. Specifically, the multiple nonlinear behaviors of drives and motors have been difficult to analyze with traditional analysis techniques, and are, therefore, often neglected in controller designs.

Another difficulty has been associated with the use of feedback control. Such a controller is well suited to precisely position the overhead support unit of a crane. If, however, the control must minimize cable sway, in addition to positioning the support unit, the control task becomes much more problematic. Accurate sensing of the payload must be implemented, which is often costly or difficult. When sensing of the payload is available, the control does not respond unless cable sway is present. In this way, the control is inherently *reactive* instead of *anticipatory*.

This thesis has addressed these important design and implementation issues while also developing a control scheme to improve the crane positioning, and sway reduction.

5.1 THESIS CONTRIBUTIONS

A 10-ton bridge crane located in the MARC building at Georgia Tech was used as an experimental test bed for a series of control modules developed throughout this thesis. The hardware modifications, communication network, and programming structure used to implement the various control schemes were described.

This thesis began by considering the dynamics involved with the crane motion. It was shown that motion-induced oscillations of a linear system can be negated through the use of an input shaping control. The physical crane system, however, exhibited nonlinear responses to input signals. A nonlinear model of the crane's drives and motors was developed that contained a nonlinear rate limiter and switching element.

The effects of these hard nonlinearities on the ability of the input shaper to cancel oscillations in the payload were investigated. An analysis technique, based on the deconvolution process, was presented that provided a means by which to gauge the detrimental influences. The technique further serves as a design tool to aid in the selection of input shapers that will be effective, regardless of actuator limitation. For the crane used throughout this thesis, the technique was used to determine that neither the rate limiter, nor the switching element had major negative effects on the oscillation suppression properties of the ZV shaper.

A positioning control module was developed that utilized a bridge-position based strategy, rather than a more difficult payload-position based strategy, to accurately position the crane's payload. An advantage to such a control is the minimum number of sensors required for implementation. The multiple nonlinearities within the controlled system precluded the possibility of a traditional limit cycle analysis. Instead, stability was assured through the use of a BIBO stability analysis, and a simulation/experimental-verification process.

Finally, a disturbance rejection control module was developed. A key feature of the control is the use of plant models. The models provide a means by which the control can distinguish between motion-induced oscillations and oscillations caused by external

disturbances. As a result, the control will attempt to eliminate disruptive disturbance-induced oscillations rather than the desired displacements caused by intended motion.

A control architecture was created in which the input shaping, positioning, and disturbance rejection modules were joined to form one combined controller, the IPDC. It was shown that the IPDC possessed the collective attributes of the individual controllers. Through the analysis of the individual modules, the stability of the IPDC was assured for a range of controller gains. Furthermore, the measured responses of the crane under the guidance of the IPDC validated the ability of the control to achieve the tertiary objectives of precise positioning, elimination of motion-induced oscillations, and disturbance rejection. The control demonstrated a positioning accuracy greater than 13 mm, ability to reduce motion-induced oscillations to less than 5% of the oscillations exhibited during unshaped motion, and eliminate disturbance-induced oscillations.

The implementation of the IPDC affords users different ways to interact with the control, depending on the operational circumstances. A manual mode of operation allows users to guide the crane with the control pendant. At the same time, motion and disturbance induced oscillations will be eliminated. The partially automated mode allows operators with a distant or obstructed view to precisely position the crane within millimeters of a desired location. The fully automated mode of operation allows users to program repetitive trajectories for the crane to follow. Further, the machine vision system employed in sensing the hook/payload position provides the added advantage of capturing coordinate information about targets. When the targets are located on non-stationary objects, such as a vehicle or shipping vessel, the controller has the ability to track these targets. This attribute may enable operators in the future to precisely hoist objects on moving platforms.

5.2 FUTURE WORK

The control developed in this thesis was concerned with controlling planer motion of the crane. By doing so, the nonlinear coupling effects of out-of-plane cable sway were not considered. In addition, the dynamical effects of load hoisting were also neglected. Further research would expand the work presented in this thesis to account for these

aspects of crane motion. Doing so would allow one to determine the modifications to the designed control, if any, needed in order to use the control for general crane motion.

A second area of future research pertains to hard nonlinearities within physical plants. The efforts made in Chapter 3 to understand the effects of two hard nonlinear elements on input shaping were a first step toward a fuller understanding of how input shaping can be more effective on real-world systems. Further work in this area would seek to develop analysis methods, like the *R*-value technique developed in Section 3.1.3.3, for a number of nonlinear elements common to physical systems.

Another area of research that may advance the control of real world systems pertains to the combined positioning and input shaping controller developed in Section 4.1, and shown in Figure 63. This control strategy implemented a shaper-in-the-loop architecture. A negative consequence of this type of architecture is that the control engineer must be concerned with the time-delayed portion of the signal in the feedback loop, as well as the added dynamics caused by the input shaper in the feed forward path. The more traditional method of combining an input shaper and a feedback loop, which avoids both of these pitfalls, is to place the input shaper outside of the feedback loop. This method could not be directly implemented in this control scheme, as shaping of the position reference signal would be ineffectual. However, further work in this area may reveal how a position reference signal may be conditioned to allow the use of an input shaper outside of a feedback loop, like the one employed here.

A final area of advancement is concerned with the effects that the IPDC has on human operators in real world crane operations. Although the IPDC has been shown to be capable of precisely guiding a payload without oscillations, the actual improvements in safety, efficiency, and speed of crane operation will be determined when further work is conducted in union with real operators performing real tasks.

REFERENCES

[1] M. Fliess, J. Levine, and P. Rouchon, "A Simplified Approach of Crane Control Via a Generalized State-Space Model," presented at 30th Conference on Decision and Control, Brighton, England, 1991.

[2] Y. Fang, W. E. Dixon, D. M. Dawson, and E. Zergeroglu, "Nonlinear Coupling Control Laws for a 3-DOF Overhead Crane System," presented at 40th IEEE Conference of Decision and Control, Orlando, Florida, USA, 2001.

[3] A. Piazzi and A. Visioli, "Optimal dynamic-inversion-based control of an overhead crane," *IEE Proc.-Control Theory Appl.*, vol. 149, pp. 405-411, 2002.

[4] Y.-S. Kim, H. Yoshihara, M. Fujioka, and H. Kasahara, "A New Vision-Sensorless Anti-Sway Control System for Container Cranes," presented at 38th IAS Annual Meeting, Industry Applications Conference, 2003.

[5] K. A. F. Moustafa, "Reference Trajectory Tracking of Overhead Cranes," *Journal of Dynamic Systems, Measurement, and Control*, vol. 123, pp. 139-141, 2001.

[6] W. J. O'Connor, "A Gantry Crane Problem Solved," *Journal of Dynamic Systems, Measurement, and Control*, vol. 125, pp. 569-576, 2003.

[7] M. Fliess, "Automatique et Corps Differentiels," *Forum Mathematicum*, vol. 1, pp. 227-238, 1989.

[8] T. Gustafsson and C. Heidenback, "Automatic Control of Unmanned Cranes at the Pasir Panjang Terminal," presented at 2002 IEEE International Conference on Control Applications, Glasgow, Scotland, U.K., 2002.

[9] N. C. Singer and W. P. Seering, "Preshaping Command Inputs to Reduce System Vibration," *J. of Dynamic Sys., Measurement, and Control*, vol. 112, pp. 76-82, 1990.

[10] N. C. Singer, W. E. Singhose, and W. P. Seering, "Comparison of Filtering Methods for Reducing Residual Vibration," *European Journal of Control*, pp. 208-218, 1999.

[11] K. Grosser and W. Singhose, "Command Generation for Reducing Perceived Lag in Flexible Telerobotic Arms," *JSME International Journal*, vol. 43, pp. 755-761, 2000.

[12] L. Pao and W. Singhose, "Unity Magnitude Input Shapers and Their Relation to Time-Optimal Control," presented at IFAC World Congress, San Francisco, CA, 1996.

[13] N. Singer, W. Singhose, and E. Kriikku, "An Input Shaping Controller Enabling Cranes to Move Without Sway," presented at ANS 7th Topical Meeting on Robotics and Remote Systems, Augusta, GA, 1997.

[14] W. Singhose, N. Singer, and W. Seering, "Time-Optimal Negative Input Shapers," *J. of Dynamic Systems, Measurement, and Control*, vol. 119, pp. 198-205, 1997.

[15] W. E. Singhose, W. P. Seering, and N. C. Singer, "Shaping Inputs to Reduce Vibration: A Vector Diagram Approach," presented at IEEE Int. Conf. on Robotics and Automation, Cincinnati, OH, 1990.

[16] A. Khalid, W. Singhose, J. Huey, and J. Lawrence, "Study of Operator Behavior, Learning, and Performance Using an Input-Shaped Bridge Crane," presented at Conference on Control Applications, Taipei, Taiwan, 2004.

[17] N. C. Singer, "Residual Vibration Reduction in Computer Controlled Machines," MIT Artificial Intelligence Lab, Technical Report MIT Artificial Intelligence Laboratory Technical Report Number AITR-1030, February 1989.

[18] W. Singhose, W. Seering, and N. Singer, "Residual Vibration Reduction Using Vector Diagrams to Generate Shaped Inputs," *J. of Mechanical Design*, vol. 116, pp. 654-659, 1994.

[19] W. Singhose, L. Porter, and N. Singer, "Vibration Reduction Using Multi-Hump Extra-Insensitive Input Shapers," presented at American Control Conference, Seattle, WA, 1995.

[20] W. E. Singhose, W. P. Seering, and N. C. Singer, "Input Shaping for Vibration Reduction with Specified Insensitivity to Modeling Errors," presented at Japan-USA Sym. on Flexible Automation, Boston, MA, 1996.

[21] C.-T. Chen, *Linear System Theory and Design*, 3rd ed. New York: Oxford University Press, 1999.

[22] J.-J. E. Slotine and W. Li, *Applied Nonlinear Control*. New Jersey: Prentice-Hall, Inc, 1991.

[23] M. R. Anderson, "Pilot-Induced Oscillations Involving Multiple Nonlinearities," *Journal of guidance, Control, and dynamics*, vol. 21, 1998.

[24] F. Amato, R. Iervolino, M. Pandit, S. Scala, and L. Verde, "Analysis of Pilot-in-the-Loop Oscillations Due to Position and Rate Saturations," presented at Conference on Decision and Control, Sydney, Australia, 2000.

[25] J. R. Huey and W. Singhose, "Stability Analysis of Closed-Loop Input Shaping Control," accepted to the 16th IFAC World Congress, Prague, 2005.